INSTYTUT PROBLEMÓW JĄDROWYCH
im. ANDRZEJA SOŁTANA
ИНСТИТУТ ЯДЕРНЫХ ПРОБЛЕМ им. А.СОЛТАНА
SOLTAN INSTITUTE FOR NUCLEAR STUDIES

RAPORT SINS-2106/A

NUCLEAR AND ATOMIC PHYSICS WITH THE ACCELERATORS OF THE NINETIES

OTWOCK-ŚWIERK

NUCLEAR AND ATOMIC PHYSICS WITH THE ACCELERATORS OF THE NINETIES

Proceedings of the 21st Mikołajki Summer School
on Nuclear Physics held in Mikołajki, Poland,
August 26 - September 5, 1990

SEMINARS

Edited by

Z. SUJKOWSKI
The Soltan Institute for Nuclear Studies

and

G. SZEFLINSKA
Institute of Experimental Physics, Warsaw University

OTWOCK-ŚWIERK, NOVEMBER 1990

Wydaje Instytut Energii Atomowej - OINTEA
Nakład 215 egz. Data złożenia maszynopisu - listopad 1990 r.
Zezwolenie GP.II/441/967/83 z dnia 19 lipca 1983 r.

Abstract :

This volume of the Proceedings of the XXI Masurian Lakes Summer School contains the contributed papers, presented orally or in the form of posters. Vol.1, comprising the invited lectures and the panel discussion, is published by A. Hilger, I.O.P. Publishing Ltd., Bristol, England.

The scope of both volumes is limited to Heavy Ions Physics, nuclear as well as atomic. The inclusion of the latter in the program of our School is no accident. The new generation of heavy ion accelerators ,providing us with beams of ions of nearly any stable or long lived nuclear species with any desired charge, cooled and stored in rings if so wished, has brought about a dynamic growth of a new field : the high energy atomic physics.We expect a continuing healthy cross-fertilization of these two subfields of heavy ion physics.

One of the objectives of the School was to take a "snapshot" of the quickly changing field of nuclear physics at the turn of the decade. We hope that the Proceedings will help the Reader to find at least some answers to the leading question of the Panel Discussion at the end of the School : "Quo Vadis, Nuclear Physics ?"

Резюме :

Предлагаемый вниманию читателей второй том Трудов XXI-й Летней Школы по Ядерной Физике содержит работы представленные участниками в виде докладов на семинарах или стендовых докладов. Доклады прочитанные авторами на Школе а также материалы панельной дискуссии опубликованы в первом томе (A. Hilger, I.O.P. Publishing Ltd., Bristol, England).

Темой Трудов помещенных в обеих томах является Физика Тяжелых Ионов так ядерная как атомная. Включение последней темы не случайно. В настоящее время происходит внедрение акцелераторов новой генерации, которые дают возможность получить почти любые пучки стабильных или долгоживущих ядер, лишенных электронов в любом зарядовом состаянии, накапиваемых

по необходимости в накопительных кольцах, охлаждаемых и ускоряемых до больших энергий. Эти новые технические возможности вызвали динамическое развите нового направления атомной физики высоких энергий. Блиская связь между этими двумя разделами физики тяжелых ионов : ядерной и атомниой физикой, несомненно плодотворна.

Ядерная физика 80-90 годов подвергается необычайно быстрым и глубоким изменениям. Мы надеемся, что Труды нашей Школы помогут читателю найти по крайней мере некоторые ответы на заглавные вопросы заключенные в панельной дискуссии "Quo Vadis, Ядерная Физика ?".

Streszczenie :

Oddawany do rąk Czytelnika tom II Materiałów XXI Letniej Szkoły Fizyki Jądrowej zawiera prace zgłoszone przez uczestników, prezentowane w postaci wygłoszonych seminariów lub też na sesjach plakatowych. Teksty wykładów na zaproszenie oraz materiały dyskusji panelowej zawarte są w Tomie Pierwszym (A.Hilger, I.O.P. Publishing Ltd., Bristol, England).

Przedmiotem prac zawartych w obydwu tomach jest Fizyka Ciężkich Jonów, zarówno jądrowa jak i atomowa. Włączenie tej ostatniej do naszego programu nie jest przypadkowe. Jesteśmy świadkami oddawania do użytku akceleratorów nowej generacji, pozwalających na uzyskiwanie wiązek dowolnych niemal, stabilnych lub długożyciowych jąder atomowych, obdartych z elektronów do dowolnego stanu ładunkowego, gromadzonych w razie potrzeby w pierścieniach zbiorczych, chłodzonych i przyspieszanych do wielkich energii. Te nowe możliwości techniczne spowodowały dynamiczny rozwój nowej dziedziny : fizyki atomowej wysokich energii. Ścisłe związki między tymi dwoma działami fizyki ciężkich jonów : jądrową i atomową są niewątpliwie wzajemnie korzystne.

Fizyka jądrowa na przełomie lat osiemdziesiątych i dziewięćdziesiątych podlega niezwykle szybkim i głębokim przemianom. Mamy nadzieję, że Materiały naszej Szkoły pomogą Czytelnikowi w znalezieniu przynajmniej niektórych odpowiedzi na tytułowe pytanie dyskusji panelowej "Quo Vadis, Fizyko Jądrowa ?".

CONTENTS

We are witnessing a major reorientation of the research in nuclear physics a change of subjects as well as of the working style. Like it or not, "the nineties" are heading towards large scale experiments, large international collaborations, concentrated around few, high energy, heavy ion or electron facilities. There is, hopefully, a lot to be gained in this pursuit. There are also pitfalls of sometimes blindly following the fashion. There may be worthy areas of research unjustly neglected, there is an irreparable loss of the life-style, especially that of individuals working in small teams.

One of the objectives of the XXI Masurian Lakes Summer School (Mikołajki, Poland, August 26 - September 5, 1990) was to take a "snapshot" of the quickly changing field of nuclear physics at the turn of decade. We hope that the Proceedings will help the reader to find at least some answers to the leading question, expressed by the title of the panel discussion at the end of the School: "Quo vadis, nuclear physics?"

The Proceedings are divided into two parts: volume 1, edited by A. Hilger, I.O.P. Publishing Ltd, Bristol., England, comprising the invited lectures and the panel discussion, and this volume, containing the contributed papers, presented during the School orally or in the poster sessions.

The scope of both volumes is limited to heavy ion physics: nuclear as well as atomic. The inclusion of the latter in the program of our School is no accident. The new generation of heavy ion accelerators, providing us with beams of ions of nearly any charge and mass within the periodic table, cooled and stored in rings if so desired, has brought about a dynamic growth of a new field: the high energy atomic physics. We may expect a continuing healthy cross-fertilization of these two subfields of the heavy ion physics.

This School has been sponsored by the Atomic Energy Agency, the Warsaw University and the Soltan Institute for Nuclear Studies. The "Polcolor" TV factory has provided us with a comfortable bus transportation and printed our program.

It is my pleasant duty to acknowledge the help and support of so many colleagues in Poland and abroad: the very gratifying response of the speakers to-be, the enthusiastic work of the organizing committee, the unselfish help during the School of many a School veteran. Last but not least, I want to thank warmly Zdzisław Wilhelmi, the Chairman of the previous 20 Masurian Lakes Summer Schools, for the unfailing support and precious advice during the preparations for this School.

ZIEMOWID SUJKOWSKI

Organizing Committee

Ziemowid Sujkowski (Chairman)

Zdzisław Wilhelmi (Honorary Chairman)

Danka Chmielewska (Scientific Secretary)

Wiktor Kurcewicz

Krzysztof Rusek

List of Participants

Peter Armbruster, Institut Max von Laue - Paul Langevin, Grenoble, France

Witold Augustyniak, Soltan Institute for Nuclear Studies, Warsaw, Poland

Michael Bentley, SERC Daresbury Laboratory, Daresbury, Great Britain

Monique Bernas, Institut de Physique Nucléaire, Orsay, France

Sudeb Bhattacharya, Saha Institute of Nuclear Physics, Calcutta, India

Jan Błocki, Soltan Institute for Nuclear Studies, Świerk, Poland

Gunther Borchert, Institut für Kernphysik Forschungszentrum KFA, Julich, FRG

Janusz Braziewicz, Pedagogical University, Kielce, Poland

Francois Brut, Institut des Sciences Nucleaires, Grenoble, France

Janusz Brzychczyk, Jagiellonian University, Cracow, Poland

Andrzej Budzanowski, Niewodniczański Institute of Nuclear Physics, Cracow, Poland

Peter Butler, University of Liverpool, Liverpool, Great Britain

Martien Carlen, University of Fribourg, Fribourg, Switzerland

Danuta Chmielewska, Soltan Institute for Nuclear Studies, Świerk, Poland

Sławomir Chojnacki, Warsaw University, Warsaw, Poland

Mats Cronqvist, Chalmers University of Technology, Goteborg, Sweden

Tomasz Czosnyka, Warsaw University, Warsaw, Poland

Janusz Dąbrowski, Soltan Institute for Nuclear Studies, Warsaw, Poland

Katarzyna Delegacz, Soltan Institute for Nuclear Studies, Warsaw, Poland

Jose Sant'Ana Dionisio, CSNSM, Orsay, France

Jerzy Dudek, Centre de Recherches Nucleaires, Strasbourg, France

Tibor Fenyes,	Institute of Nuclear Research of the Hungarian Academy of Sciences, Debrecen, Hungary
Bogdan Fornal,	Niewodniczański Institute of Nuclear Physics, Cracow, Poland
Joel Galin,	GANIL, Caen, France
Werner Gast,	Institut für Kernphysik Forschungszentrum KFA, Jülich, FRG
Adrian Gelberg,	Institut für Kernphysik der Universitat zu Köln, Köln, FRG
Lidia Goettig,	Warsaw University, Warsaw, Poland
Walter Greiner,	Institut für Theoretische Physik der Universitat Frankfurt/M, FRG
Kazimierz Grotowski,	Jagiellonian University, Cracow, Poland
Ole Hansen,	Brookhaven National Laboratory, Upton, USA
Joanna Hoszowska,	Soltan Institute for Nuclear Studies, Świerk, Poland
Włodzimierz Iskra,	Soltan Institute for Nuclear Studies, Warsaw, Poland
Jędrzej Iwanicki,	Warsaw University, Warsaw, Poland
Zenon Janas,	Warsaw University, Warsaw, Poland
Jerzy Jastrzębski,	Warsaw University, Warsaw, Poland
Pekka Pauli Jauho,	University of Jyväskylä, Jyväskylä, Finland
Ari Jokinen,	University of Jyväskylä, Jyväskylä, Finland
Waldemar Karczmarczyk,	Warsaw University, Warsaw, Poland
Tomasz Kazimierski,	Warsaw University, Warsaw, Poland
Mohamed Hassan Khalil,	Warsaw University, Warsaw, Poland
Somia Galal,	Cairo, Egypt
Dariusz Klelan,	Soltan Institute for Nuclear Studies, Warsaw, Poland
Kurt Kilian,	Institut für Kernphysik Forschungszentrum KFA, Julich, FRG
Jan Kisiel,	Silesian University, Katowice, Poland
Małgorzata Kistryn,	Jagiellonian University, Cracow, Poland
Hans-Jurgen Kluge,	University of Mainz, Mainz, FRG
Mirosław Kostrubiec,	Silesian University, Katowice, Poland
Jan Kownacki,	Warsaw University, Warsaw, Poland

Beata Kozłowska-Janek, Soltan Institute for Nuclear Studies, Warsaw, Poland

Walentyna Kruszewska, Soltan Institute for Nuclear Studies, Warsaw, Poland

Wiktor Kurcewicz, Warsaw University, Warsaw, Poland

Yvonne Leifels, GSI, Darmstadt, FRG

Volker Lindenstruth, GSI, Darmstadt, FRG

Piotr Lubiński, Warsaw University, Warsaw, Poland

Franco Luccarelli, Universita di Firenze, Florence, Italy

Tomasz Ludziejewski, Soltan Institute for Nuclear Studies, Świerk, Poland

Sergey Lukjanov, Joint Institute for Nuclear Reseach, Dubna, USSR

Ull Lynen, GSI, Darmstadt, FRG

Jerzy Łukasik, Jagiellonian University, Cracow, Poland

Bohdan Marlański, Soltan Institute for Nuclear Studies, Warsaw, Poland

Andrej Matthies, Technische Universitat Dresden, GDR

Tomasz Matulewicz, Warsaw University, Warsaw, Poland

Ralf Steffen Mayer, GSI, Darmstadt, FRG

Władysław Mielczarek, Soltan Institute for Nuclear Studies, Warsaw, Poland

Hannelore Mokler, Darmstadt, FRG

Paul Mokler, GSI, Darmstadt, FRG

Luciano Moretto, Lawrence Berkeley Laboratory, Berkeley, USA

Władysława Nawrocka, Wrocław University, Wrocław, Poland

Thomas Nilsson, Chalmers University of Technology, Goteborg, Sweden

Sławomir Osuch, Warsaw University, Warsaw, Poland

Marcin Palacz, Soltan Institute for Nuclear Studies, Świerk, Poland

Peter Paul, SUNY, Stony Brook, USA

Hekki Tapani Pentilla, University of Jyvaskyla, Jyvaskyla, Finland

Matthias Pfeiffer, University Giessen, Giessen, FRG

Ernest Piasecki, Warsaw University, Warsaw, Poland

Ludwik Pieńkowski, Warsaw University, Warsaw, Poland

Wiesław Pietrzak, Soltan Institute for Nuclear Studies, Warsaw, Poland

Wolfgang Pilz, Technische Universitat Dresden, GDR
Roman Planeta, Jagiellonian University, Cracow, Poland
Weronika Płóciennik, Technical University, Warsaw, Poland
Bożena Pomorska, M. Curie-Skłodowska University, Lublin, Poland
Krzysztof Pomorski, M. Curie-Skłodowska University, Lublin, Poland
Hartmut Reich, Max Planck Institut für Kernphysik, Heidelberg, FRG
Martin Rhein, Institut für Kernphysik, Darmstadt, FRG
Helen Roberts, Glasgow, Great Britain
Grzegorz Rohoziński, Warsaw University, Warsaw, Poland
Jacek Rożynek, Soltan Institute for Nuclear Studies, Warsaw, Poland
Krzysztof Rusek, Soltan Institute for Nuclear Studies, Warsaw, Poland
Krzysztof Rykaczewski, Warsaw University, Warsaw, Poland
Piotr Rymuza, Soltan Institute for Nuclear Studies, Świerk, Poland
Lars Sandberg, University of Stockholm, Stockholm, Sweden
Rudolf Schmidt, GSI, Darmstadt, FRG
Dirk Schwalm, Max Planck Institut für Kernphysik, Heidelberg, FRG
Jacek Semaniak, Pedagogical University, Kielce, Poland
Bruno Sikora, Warsaw University, Warsaw, Poland
Janusz Skalski, Soltan Institute for Nuclear Studies, Warsaw, Poland
Beata Skorupska, M. Curie-Skłodowska University, Lublin, Poland
Wojciech Skulski, Warsaw University, Warsaw, Poland
Arthur Ernest Smith, University of Oxford, Great Britain
Par-Olof Soderman, Uppsala University, Uppsala, Sweden
Zbigniew Sosin, Jagiellonian University, Cracow, Poland
Julian Srebrny, Warsaw University, Warsaw, Poland
Zbigniew Stachura, Niewodniczański Institute of Nuclear Physics, Cracow, Poland
Andrzej Staszczak, M. Curie-Skłodowska University, Lublin, Poland
Elżbieta Stephan, Silesian University, Katowice, Poland
Anna Stonert, Soltan Institute for Nuclear Studies, Warsaw, Poland

Jan Styczen, Niewodniczański Institute of Nuclear Physics, Cracow, Poland

Ziemowid Sujkowski, Soltan Institute for Nuclear Studies, Świerk, Poland

Marek Surała, Warsaw University, Warsaw, Poland

Alicja Surowiec, Silesian University, Katowice, Poland

Grażyna Szeflińska, Warsaw University, Warsaw, Poland

Zygmunt Szeflinski, Warsaw University, Warsaw, Poland

Jerzy Szerypo, Warsaw University, Warsaw, Poland

Władysław Świątecki, Lawrence Berkeley Laboratory, Berkeley, USA

Gurgen Ter-Akopian, Joint Institute for Nuclear Reseach, Dubna, USSR

Rabah Tezkratt, Centre de Recherches Nucleaires, Strasbourg, France

Andrzej Tucholski, Soltan Institute for Nuclear Studies, Swierk, Poland

Garry Tungate, University of Birmingham, Birmingham, Great Britain

Andrzej Turos, Soltan Institute for Nuclear Studies, Warsaw, Poland

Bernd Voss, GSI, Darmstadt, FRG

Wolfgang Wagner, Technical University, Dresden, GDR

Andrzej Warczak, Jagiellonian University, Cracow, Poland

Barbara Warczak, Jagiellonian University, Cracow, Poland

Edmund Wesołowski, Warsaw University, Warsaw, Poland

Andrzej Wieloch, Jagiellonian University, Cracow, Poland

Katarina Wilhelmsen, Chalmers University of Technology, Goteborg, Sweden

Martin Wilpert, Hahn-Meitner Institut fur Kernforschung, West Berlin

Hans Wilschut, Kernfysich Versneller Instituut der Rijksuniversiteit, Groningen, The Netherlands

Andrzej Wojtasiewicz, Warsaw University, Warsaw, Poland

Jacek Wrzesiński, Niewodniczański Institute of Nuclear Physics, Cracow, Poland

Sławomir Wycech, Soltan Institute for Nuclear Studies, Warsaw, Poland

Krystyna Zając	M. Curie-Skłodowska University, Lublin, Poland
Pavel Zarubin,	Joint Institute for Nuclear Reseach, Dubna, USSR
Lucjan Zemło,	Warsaw University, Warsaw, Poland
Wiktor Zipper,	Silesian University, Katowice, Poland
Bogusław Zwięg`.ński,	Soltan Institute for Nuclear Studies, Warsaw, Poland
Zbigniew Żelazny,	Warsaw University, Warsaw, Poland
Jan Żylicz,	Warsaw University, Warsaw, Poland

ON CORRELATIONS BETWEEN FRAGMENT MASS AND EXCITATION ENERGY DIVISION IN THE ^{74}Ge + ^{165}Ho REACTION

P. Planeta[1], J. Toke[2], W.U. Schröder[2] and J.P. Hulzenga[2]

[1] Institute of Physics, Jagellonian University
30 059 Krakow, Reymonta 4, Poland

[2] Department of Chemistry and NSRL
University of Rochester, Rochester, New York 14627

ABSTRACT

Results of alternative analysis of experimental data for ^{74}Ge + ^{165}Ho reaction are presented. Information about the correlation between the excitation energy division and net nucleon transfer is extracted.

The process of dissipation of kinetic energy and its redistribution among the various degrees of freedom in a complex nuclear reaction is of high significance for understanding of the damped reaction mechanism. During the past decade a number of experiments and analyses have been performed which shed light on various aspects of excitation-energy sharing in damped collisions. Several early experiments (see e.g. Ref. [1]) suggest that thermal equilibrium might be achieved very early in the damping process, perhaps as low as E_{loss} = 50 MeV. However, subsequent works [2-5] have indicated that excitation energy is shared nearly equally between the reaction partners in early stages of damping. In addition, some of these studies have also indicated that the partition of excitation energy is dependent

on the not nucleon exchange .

Recent results reported by Płaneta et al. [6] and Kwiatkowski et al. [7] on the ^{74}Ge + ^{165}Ho reaction at 8.5 MeV nucleon have also demonstrate such a dependence on mass. In this experiment mass, A_{PLF}, and charge, Z_{PLF}, of the projectile like fragment (PLF) were identified using a combination of the ΔE-E and time-of-flight techniques. The primary mass of PLF before light particle evaporation, A'_{PLF}, was derived from angular correlation between the PLF and the target-like fragment. Applying statistical model predictions in an iterative event-by-event procedure information on excitation energy of the PLF fragment was extracted from the measured evaporated mass. As shown by Toke et al. [8] in such coincidence measurement instrumental effects may significantly modify experimental results especially for low energy losses.

In order to extract information on the excitation energy division in a way less dependent on experimental conditions the data were reanalyzed using an alternative method. The new approach [9,10] is based on the fact that the mass resolution for secondary fragments is much better than the resolution for the primary reconstructed mass. Additionally resolution for secondary fragments does not dependent on the energy loss.

In the new procedure we were assuming different possible correlations between E^*_{PLF}/E^*_{TOTAL} and A'_{PLF} to be used in the Monte Carlo calculations. The generated mean value of evaporated mass, $\langle \Delta A \rangle = \langle A'_{PLF} - A_{PLF} \rangle$, versus A_{PLF} dependence was than compared to the experimental one. The assumed dependence E^*_{PLF}/E^*_{TOTAL} was linear:

$$E^*_{PLF}/E^*_{TOTAL} = a * A'_{PLF} + b \,, \qquad (1)$$

where A'_{PLF} represents the "true" primary mass of PLF generated in the Monte Carlo procedure. Values of coefficients a and b were treated in our procedure as free parameters. Final result are shown as diamonds in Fig. 1 and a set of straight lines in Fig. 2 representing Eq. 1. The equal excitation energy division limit is represented by a horizontal line. The dotted line indicates the equal temperature limit.

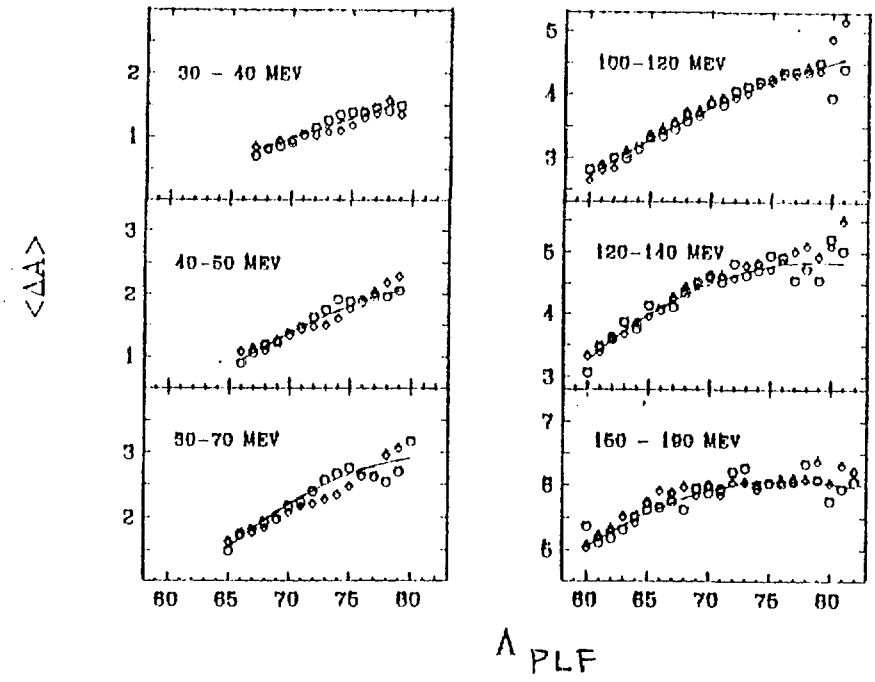

Fig.1 The average evaporated mass versus the secondary mass for energy loss indicated on the picture. Circles represent the experimental data, diamonds results of Monte Carlo simulation. The solid line for each energy loss bin represents the average $\langle \Delta A \rangle$ dependence on secondary mass established in the iterative procedure.

Sensitivity of our method on the primary mass resolution is presented in both parts of Fig. 3. The average evaporated

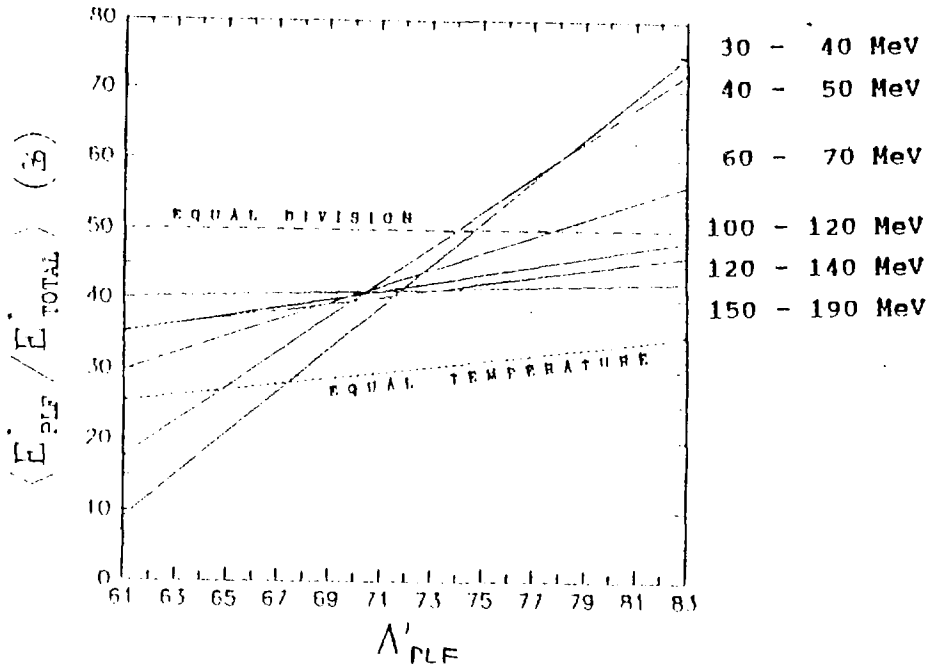

Fig.2 Excitation energy division ratio dependence upon primary mass described by Eq. 1 for energy loss bins indicated on the figure. Additionally the equal excitation energy division limit is represented by a horizontal line. The dotted line indicates the equal temperature limit.

mass is there depicted by circles as a function of the secondary mass (left part) and the reconstructed primary mass (right part). The data are compared with two different Monte Carlo predictions. Diamonds represent simulation for the case where the recoil and experimental angular resolution effects are neglected. The crosses correspond to the full simulation. Comparison between these two different Monte Carlo predictions show that $\langle \Delta A \rangle$ as a function of the secondary mass is practically insensitive to the finite primary mass resolution.

the same quantity presented as a function of A'_{PLF} shows a big discrepancy between both cases.

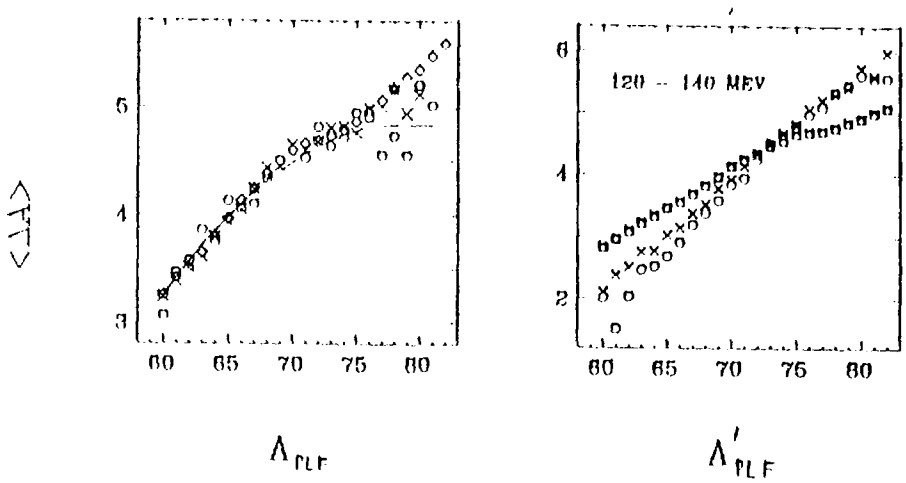

Fig. 3 The dependence of the average evaporated mass upon the secondary mass (left part) and the reconstructed primary mass (right part). The data (circles) are compared with two different Monte Carlo predictions. Diamonds represent simulation for the case where the recoil and experimental angular resolution effects are neglected. The crosses correspond to the full simulation.

In a more transparent fashion the mass dependence of E^*_{PLF}/E^*_{TOTAL} is shown in Fig. 4. Here dependence of the excitation energy division on the PLF primary mass is presented for two representative energy loss windows. Additionally to experimental results (circles) the Monte Carlo simulation ratios are given by diamonds. The dashed line gives the "true" dependence described by Eq. 1. Comparison between dashed lines and diamonds gives for both cases the magnitude of instrumental effects.

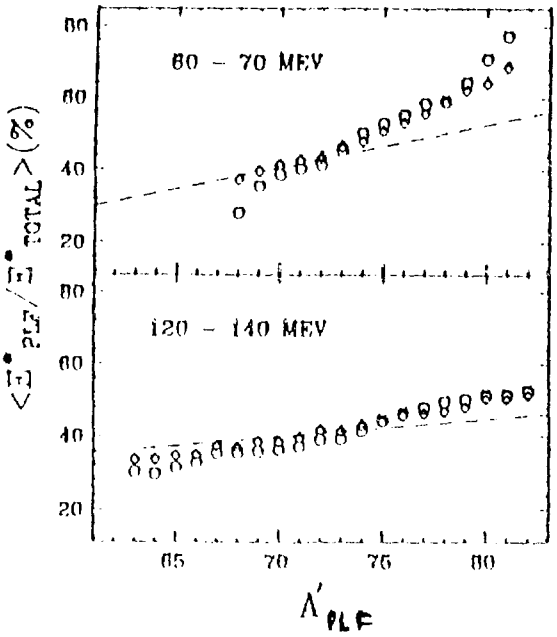

Fig. 4 Dependence of the excitation energy on the PLF primary mass for two representative energy loss windows. The experimental results are given by circles, the Monte Carlo predictions by diamonds. The dashed lines correspond to the "true" dependence described by Eq. 1.

In conclusion, evidence on physical correlations of heat generation mechanisms is presented. At initial stages of the collision, reflected in low total kinetic energy losses, does the heat generated via the nucleon exchange mechanism show a clear acceptor-donor asymmetry.

REFERENCES

1 D. Hilscher et al., Phys. Rev. C20, 576 (1979)

2 T. C. Awes et al., Phys. Rev. Lett. 52, 251 (1984)

3 H. Sohlbach et al., Z. Phys. A328, 205 (1987)

4 R. Vandenbosch et al., Phys. Rev. Lett. 52, 1964 (1984)

5 D. R. Benton et al., Phys. Rev. C38, 1207 (1988)

6 R. Planeta et al., Phys. Rev. C39, 1197 (1989)

7 K. Kwiatkowski et al., Phys. Rev. C41, 958 (1990)

8 J. Toke et al., University of Rochester Report NSRL-339, 1989

9 J. Toke et al., University of Rochester Report NSRL-350, 1989

10 J. Toke et al., Abstract Submitted for the Meeting of the APS, April 16-19, 1990

OPTICAL MODEL WITH CRITICAL ANGULAR MOMENTUM CUT OFF FOR THE FUSION OF LIGHT HEAVY-ION SYSTEMS

J.Czakański, J.Kisiel, M.Kostrubiec, W.Zipper
Intitute of Physics, Silesian University, Uniwersytecka 4,
40-007 Katowice, Poland

P. von Brentano
Institut für Kernphysik der Universität zu Köln,
Zülpicher Str.77, D-5000 Köln 41, Federal Republic of Germany

ABSTRACT.

The extended optical potential model with separate absorptive part for fusion and critical angular momentum cut off was proposed for the calculation of fusion excitation functions. As an example a calculated fusion cross section was presented for the $^{12}C+^{12}C$, $^{12}C+^{14}N$, $^{12}C+^{16}O$ and $^{16}O+^{16}O$ systems for the existing experimental data above Coulomb barrier energy.

The fusion excitation function have been measured for many years for a large number of combinations of colliding ions [1]. The experimental fusion cross section $\sigma_{fus}(E)$ is rather smooth function of energy although for some system the oscillatory structure is observed. For the energies above the Coulomb barrier $\sigma_{fus}(E)$ usually follows the total reaction cross section $\sigma_R(E)$. Above the certian energy $\sigma_{fus}(E)$ becomes considerably smaller than $\sigma_R(E)$ and finally $\sigma_{fus}(E)$ is propotional to the inverse of bombarding energy. Some models were applied for the theoretical description of such behavior

of $\sigma_{fus}(E)$ [2]. Because the fusion cross section is a part of the total reaction cross section it is tempted to use for the fusion the optical model potential $U_{fus}(r)$ which is different form the optical model potential $U_R(r)$ describing the elastic scatterting and the total reaction cross section. Such model with Saxon-Woods form of the potential gives a satisfactory result up to energy region in which $\sigma_{fus}(E)$ decreasing rapidly with increasing energy [3]. We extend this idea by the assumption of a critical angular momentum l_{cr} above which no fusion is possible. This allowed us to describe the fusion cross section in whole energy region starting from the Coulomb barrier energy.

In our model the fusion cross section was calculated according to the formula:

$$\sigma_{fus}(E) = \pi \lambda^2 \sum_{l=0}^{l_{cr}} (2l+1)\, T_{fus}(l,E) \ , \qquad (1)$$

where the fusion transmission coefficients $T_{fus}(l,E)$ were obtained by using the optical model potential $U_{fus}(r)$. As a real part of $U_{fus}(r)$ was taken Satchler-Love microscopic double folded (M3Y) potential $V_s(r)$ which has only one parameter - the renormalizating factor N_s [4]. This potential give a good description of elastic scatterting and the total reaction cross section in a wide energy range. The imaginary part of $U_{fus}(r)$ has a standard Saxon-Woods form. $U_{fus}(r)$ can be writeen as follows

$$U_{fus}(r) = N_s\, V_s(r) + iW_{fus}\, f_{S-W}(r;R_{fus},a_{fus}) \ . \qquad (2)$$

The critical angular momentum l_{cr} was calculated from the inflexion point of the effective real potential curve so it is no a free parameter. The renormalizating factor N_s takes the value 1.0 according to the review paper of Satchler and Love [4] so the real part of the optical models potentials for elastic scattering and fusion are the same. From the fits it was found that $\sigma_{fus}(E)$ depends very weakly on W_{fus} if only W_{fus} is greater than 10MeV. Taking into account the overlap nuclear matter radius the fusion absorption radius r_{fus} has a standard value around 1.0fm [5]. Futhemore for all reported system the same value of $a_{fus} \cong 0.2$fm was obtained from fitting procedure. For more details of the model and discusion of parameters see ref.[6]. The parameters of the optical model potential $U_{fus}(r)$ together with l_{cr} value are presented in table 1.

Table 1.

Reaction	N_s	W_{fus} [MeV]	r_{fus} [fm]	a_{fus} [fm]	l_{cr} [$\hbar$]
$^{12}C + ^{12}C$	1.0	10.0	1.00	0.20	22
$^{12}C + ^{14}N$	1.0	9.8	1.08	0.18	25
$^{12}C + ^{16}O$	1.0	10.0	1.00	0.20	27
$^{16}O + ^{16}O$	1.0	10.0	1.00	0.20	34

The results of the model for $^{12}C+^{12}C$, $^{12}C+^{14}N$, $^{12}C+^{16}O$ and $^{16}O+^{16}O$ systems are shown in fig.1. Cross sections are obtained by using the optical model potential paramaters given in tab.1. The calculated fusion cross sections follow the experimental points in the wide energy range. This good fit was achieved by the using only one parameter a_{fus} which takes the same value

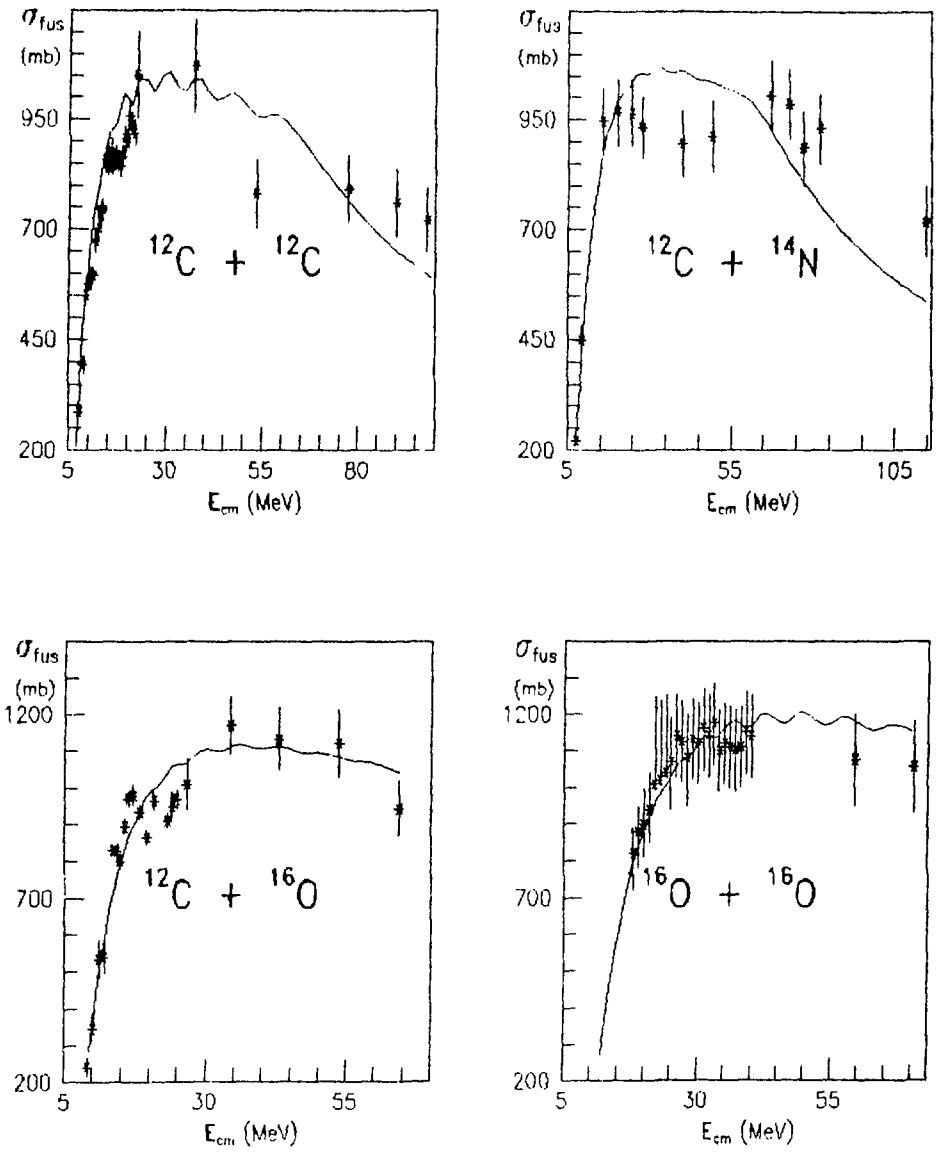

Fig. 1. Comparision of calculated (solid curves) and experimental fusion cross sections for the systems : $^{12}C+^{12}C$ (experimental data from ref. [7]), $^{12}C+^{14}N$ [8], $^{12}C+^{16}O$ [10] and $^{16}O+^{16}O$ [9].

0.2fm for all reactins considered. The extensive experimental data for the fusion excitation functions below Coulomb barrier exist for systems which were taken into account in this contribution. The model presented is verified now for the energy region bellow Coulomb barrier.

This work was partly suppored by the Polish Ministry of National Education under contract CPBP 01.09 and by the BMFT under contract No 06OK143.

References

[1] Q.Haider and F.B.Malik, Atomic Data and Nuclear Data Tables 31,185 (1984)

[2] For a review: Ch.Ngo, Prog.in Particle and Nuclear Physics (ed.A.Faessler), Vol.16 Pergamon,Oxford

[3] K.Hatogai at al., Prog.Theor.Phys.68,2014 (1982)

[4] G.R.Satchler and W.G.Love, Phys.Rep.55,183 (1979)

[5] J.Galin at al., Phys.Rev.C9,1018 (1974)

[6] W.Zipper at al., (to be published in Z.Phys.A)

[7] M.N.Namboodiri at al., Nucl.Phys.A263,491 (1976)
D.G.Kovar at al., Phys.Rev.C20,1305 (1979)

[8] R.G.Stokstad at al., Phys.Rev.Lett.36,1529 (1976)
J.Gommez del Campo at al. Phys.Rev.C19,2170 (1979)
Z.E.Switkowski at al., Nucl.Phys.A279,502 (1977)

[9] D.G.Kovar at al., Phys.Rev.C20,1305 (1979)
C.Beck at al., Phys.Rev.C29,1942 (1984)
Y.Eyal at al., Phys.Rev.C13,1527 (1976)

[10] B.Fernandez at al., Nucl.Phys.A306,259 (1978)
F.Saint-Laurent at al., Nucl.Phys.A327,517 (1979)

COMPETITION BETWEEN pn AND d EMISSION IN $\alpha+^{51}V, ^{54}Fe$ REACTIONS AT 26.5 MeV.

P. Bednarczyk, E. Bozek, B. Fornal, M. Lach, A. Maj, W. Meczynski, T. Pawlat, J. Styczen.

H. Niewodniczanski Institute of Nuclear Physics, Cracow, Poland

ABSTRACT

The competition between pn and d evaporated from compound nuclei created in the fusion of 26.5 MeV α-particles on ^{51}V and ^{54}Fe was studied. The nuclear level density parameter a=A/9.3 for excited nuclei populated in these reactions was extracted.

In a compound nucleus decay the same evaporation residuum may often be reached by different sequences of emitted particles. For example, emission of np or pn as well as emission of deuterons leads to the same residuum with $A_{RES}=A_{CN}-2$, $Z_{RES}=Z_{CN}-1$. The difference is that the cascades of np or pn pass through an "intermediate nucleus" $[A_{CN}-1, Z_{CN}]$ or $[A_{CN}-1, Z_{CN}-1]$, respectively, whereas d-evaporation brings the decaying system directly to the final nucleus. Because in both cases the evaporation residuum is the same, one might expect that the competition between these two processes (np and pn or d-evaporation) would reflect the structure of the "intermediate nuclei".

Two nuclear reactions were chosen to look at the pn and d competition. The 26.5 MeV α-beam from U-120 Cracow cyclotron was focused on the ^{51}V and ^{54}Fe metallic foils. During two, long runs the coincidences between γ-rays and light charged particles were recorded event by event on the magnetic tape. γ-rays were measured in the Ge(Li) detector whereas p, d, t and α's were detected in the ΔE-E silicon telescope. The telescope was placed at the backward angle $\theta_{LAB}=140^{\circ}$ to select only particles evaporated from the CN. Particle spectra associated with different reaction channels were generated off-line requiring the coincidence with characteristic γ-rays.

Fig. 1 shows proton-spectra for particular evaporation channels after $\alpha+^{54}Fe$ fusion reaction. Protons emitted in the (α, p) channel are in average much more energetic. In fact, being followed only by γ-ray cascades they have to bring the decaying system close to the yrast line, where the

competition between particle and γ-ray starts to be significant. Deviations between proton-spectra for (α,pn) and $(\alpha,2p)$ channels reflect the fact, that protons in (α,pn) channel are emitted prevalently in the second step of the cascade where the emitting system has much lower excitation energy. In the $(\alpha,2p)$ case one deals with protons evaporated in both steps: the first at a high excitation energy and the second with much lower excitation energy.

The deuteron-spectra from (α,d) channel are too poor for presentation due to a very low counting rate of d-γ coincidences. Nevertheless, the statistics in the coincidence γ-spectra was good enough that the σ_{pn} to σ_{d} ratio in the two cases of $\alpha+^{51}V$ and $\alpha+^{54}Fe$ could be easily calculated (Fig.2).

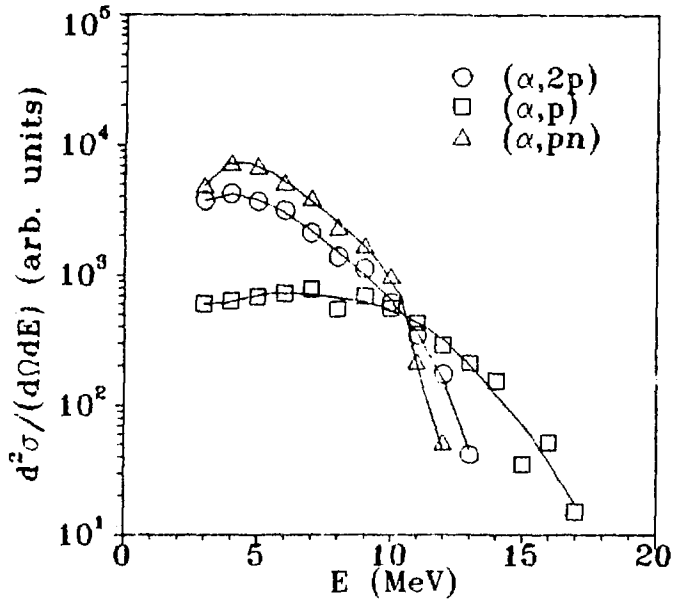

Fig.1. Spectra of protons emitted in particular channels of $\alpha+^{54}Fe$ reaction. The solid lines are drawn to guide the eye.

It is rather well established that the CN decay, at the excitation energy considered here, can nicely be described in the frame of the statistical model. Therefore, the calculations we report here were performed with the evaporation code CASCADE [1]. They included the emission of four particles n,p,d,α and γ-decay. In Fig.2 we show the predictions of the statistical model with standard input parameters (the level density parameter a=A/8) for the σ_{pn}/σ_{d}. It is seen that they overestimate the experimental values by a factor of 2.

In order to understand this result a number of additional CASCADE calculations have been performed. It turns out that the calculated σ_{pn}/σ_{d} ratio is insensitive neither to changes of the level density parameter nor to variations of other statistical model parameters which characterize

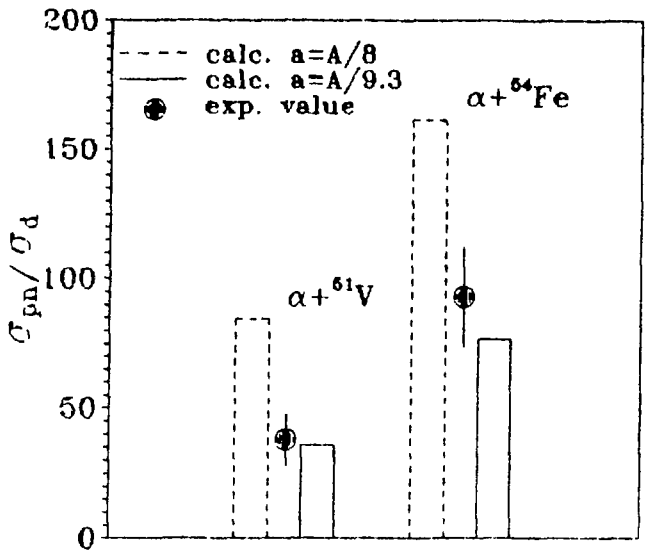

Fig.2. The σ_{pn}/σ_d ratios obtained from experiment and CASCADE calculations for $\alpha+^{51}V$, ^{54}Fe reactions.

the evaporation residuum $[A_{CN}-2,Z_{CN}-1]$. Noticeable changes of the σ_{pn}/σ_d ratio can be achieved exlusively by varying the level density in the "intermediate nucleus" i.e. $[A_{CN}-1,Z_{CN}]$ or $[A_{CN}-1,Z_{CN}-1]$. In fact, the calculations with the level density parameter a=A/9.3 are able to account for the measured pn to d ratios as shown in Fig.2.

Similar conclusion regarding the leveldensity parameter has been drawn in Ref. [2], where the value a-A/9.5 is necessary to describe the GDR γ-ray spectrum from hot ^{63}Cu system, neighboring to the systems studied in the present work.

As a conclusion, the pn and d competition seems to be very sensitive to the nuclear level density of decaying equilibrated systems and can be used as an easily measurable probe for this quantity at excitation energes of about 20 MeV.

REFERENCES

1. F.Puhlhofer, Nucl. Phys. **A280 (1977) 267.**

2. M.Kicl ska-Habior et al., Phys. Rev. **C36 (1987) 612.**

ANALYZING POWER OF THE $^{34}S(p,t)^{32}S$ REACTION AT 30 AND 40 MeV

M. Siemiński, A. Saganek, E. Wesołowski, Z. Wilhelmi
Warsaw University
S. Takami, K. Hatori
Institute for Atomic Energy, Rikkyo University
T. Hasegawa, M. Yasue
Institute for Nuclear Study, Tokyo University
T. Nakagawa, J. Takamatsu
Tohoku University

Abstract

The analyzing power angular distributions for the $^{34}S(p,t)^{32}S(gs,0^+)$ reaction, measured at 30 and 40 MeV of protons, are compared with predictions of the finite-range DWBA model. The experimental results can be reproduced correctly, without including the sequential transfer process.

A mechanism of the (p,t) reaction, used, among other things, for an investigation of the neutron pair correlations in nuclei, is still not fully understood [1]. Predictions of the simple model of mechanism as a one- step transfer of the two neutron pair coupled to a spin equal to zero can not fit properly the measured total cross-sections nor the excitation functions.

Theoretical estimations show, that a refinement of the model (by accounting for the s' and d states of triton, the tensor forces, the excitation of both the target nucleus before transfer and the final nucleus after transfer of a neutron pair does not change the total cross section very much. Only the mechanism of the sequential transfer of neutrons may influence the reaction cross section significantly [2].

In general the analyzing power of the (p,t) reaction depends on two factors: the intrinsic structures of the target and final nuclei and the mechanism of transfer of two neutrons.

According to the final range DWBA calculations, in our case of $0^+ - 0^+$ transfer on the ^{34}S nuclei, the analyzing power practically does not depend on the intrinsic structure of the neutron pair wave function. Differences in analyzing power calculated with the wave function of Wildenthal [3]:

$$\Psi = \alpha(2s_{1/2})^2 + \beta(1d_{3/2})^2 + \gamma(1d_{5/2})^2$$

in which amplitudes of $2s_{1/2}$, $1d_{3/2}$ and $1d_{5/2}$ components are set consecutively zero, are insignificant (see Fig. 1).

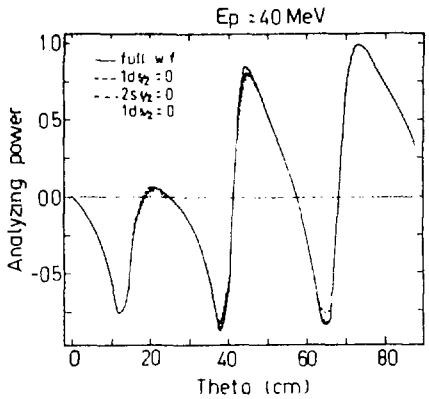

Fig. 1

In case of the one-step transfer of a spin zero neutron pair between states with spins 0^+, the analyzing power is produced by the spin-orbit interaction in the entrance and exit channels. The l-s interaction in the

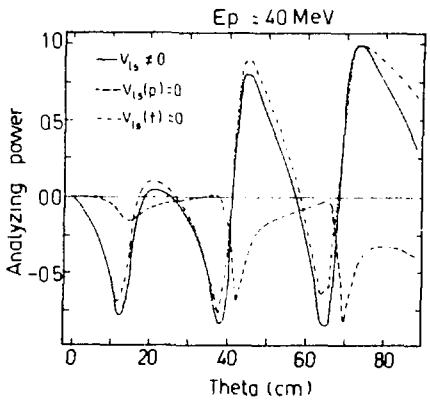

Fig. 2

proton channel is much stronger, so it has a dominant influence on the analyzing power. This is depicted in Fig.2 in which the angular distributions of the analyzing powers for three cases: 1) $V_{ls}(p) \neq 0$, $V_{ls}(t) \neq 0$; 2) $V_{ls}(p)=0$, $V_{ls}(t) \neq 0$; 3) $V_{ls}(p) \neq 0$, $V_{ls}(t)=0$ are shown.

On the other hand, in case of the sequential transfer of two neutrons the spin-orbit interaction in an intermediate stage of the reaction may cause changing of the angular distribution shape of the analyzing power, which could be observed when the contribution of this process is significant. According to Igarashi [2], the analyzing powers for these two mechanisms have opposite sign at small angles.

An analysis of the proton energy dependence of the reaction differential cross section [4] shows, that for proton energies up to about 20 MeV, the cross section of the sequential mechanism is comparable, or even predominates the one-step transfer cross section. With increasing the energy of protons the sequential transfer contribution decreases, and at 80 MeV of proton energy the one-step transfer prevails (over 80% of total cross section). However, similarity of shapes of the cross section angular distribution for both the one-step and the sequential transfer processes makes that the conclusions drawn from cross section experiments are doubtful.

A few years ago, the attention was drawn to the possibility of determination of the one-step and sequential transfer mechanism contributions from the measured analyzing power. Some drastic changes in a shape of the analyzing power observed in certain region of incident energy [5] were interpreted as being a result of opening of the sequential reaction channel or at least a predominance of this channel over the one-step process.

In the present work we make an attempt to observe an effect of a variation of contributions of both processes on the reaction analyzing power. The $^{34}S(p,t)^{32}S(gs.,0^+)$ reaction was chosen for investigation. The analyzing power measured at proton energy of 30 and 40 MeV is shown in Figs 3 and 4.

The experiment was performed using the beam of the INS cyclotron of Tokyo University. In Figs 3 and 4 the solid lines represent the results of the finite range DWBA calculations (DWUCK 5, [6]), in which one-step transfer of a neutron pair is assumed.

Results of calculations fit pretty well the angular distributions of analyzing power for angles greater than 20 deg. In the range of small

angles the experimental results taken at proton energy of 40 MeV show minimum around 10 deg., which feature is predicted correctly by one step model. In case of the experiment at 30 MeV such minimum is not observed at theses angles. It is not

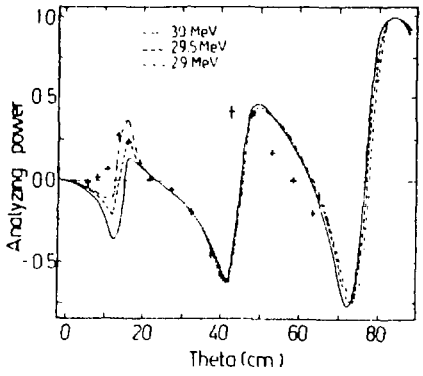

Fig. 3

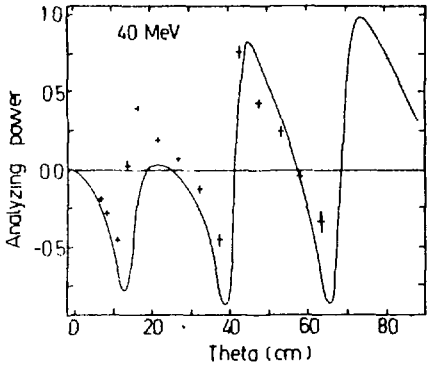

Fig. 4

reproduced by calculations. This disagreement between calculations and the experiment may be a result of 'kinematic effect'.

In Fig. 3 the calculated angular distributions of analyzing power as a function of the incident proton energy are given. Our calculations reproduce the experimental distributions at 30 MeV pretty well if the incident proton energy is shifted slightly down by about 0.5 - 1.0 MeV. The quite similar effect can be obtained by slightly changing the Q-value of the reaction. We conclude, that the quasi-resonant behavior of positive bump of analyzing power is caused mainly by variation of the kinetic energy in the reaction exit channel.

The differences in the shapes of analyzing power of the $^{34}S(p,t)^{32}S(gs.,0^+)$ at 30 and 40 MeV do not give any reason that a new mechanism of the reaction, the sequential transfer, should be included in calculations.

It must be noticed that a similar quasi-resonant positive bump in the analyzing power distributions of the reaction can be reproduced in the zero range DWBA calculations, but the incident proton energy must be shifted nearly by 5 MeV.

In conclusion, the analyzing power angular distributions measured can be reproduced successfully by calculations in a frame of the one-step transfer model, without any contribution of the sequential transfer.

Unfortunately, the cross section predicted is 5 to 8 times smaller than the measured one, while the zero range DWBA calculations with semi empirical constant $D_o=22*10^4$ fm^3/MeV^2 differ no more than a factor of two. It remains still a serious, well known drawback of the finite range DWBA calculations of the (p,t) reaction.

In order to make our conclusion more convinced we intend to expand our measurements over smaller and higher proton energy regions.

---

1. W.T. Pinkston, Comments Nucl.Part.Phys.Rev.12(1984)133

2. M. Igarashi, Thesis, Department of Physics, Tokyo Medical College, 1988

3. H. Nann and B.H. Wildenthal, Phys.Rev. C13(1976)1009

4. H. Wienke et al, Nucl.Phys. A442(1985)397

5. H. Iida et al, Phys.Rev. C29(1984)328

6. P.D. Kuntz, Colorado University, 1985, unpublished.

MULTIPOLE DECOMPOSITION OF DOUBLY DIFFERENTIAL CROSS SECTIONS - A MODEL INDEPENDENT ANALYSIS

S.Osuch, G.Szeflińska, Z.Szeflński, Z.Wilhelmi
Nuclear Physics Laboratory, Institute of Experimental Physics
Warsaw University, Hoża 69, 00-681 Warsaw, Poland

INTRODUCTION

We propose here a new, model independent method which can be used to analyze high quality data from inelastic scattering or charge exchange reactions. Such data contain resonances observed as bumps superimposed on a smooth continuum generally assumed to be background (see fig.1). The major problem in these studies is the decomposition of data into bumps originating from nuclear excitations and the underlying continuum.

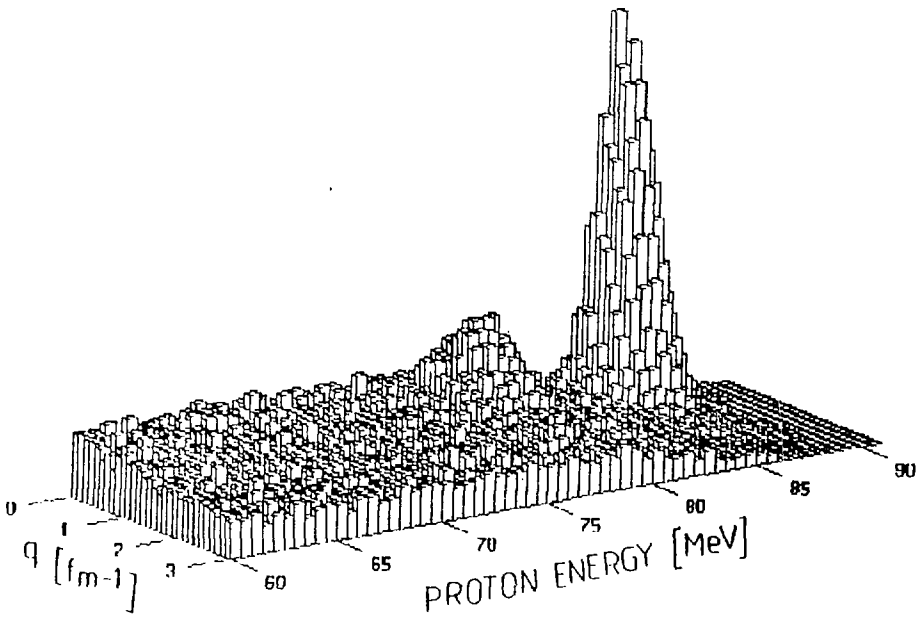

Fig.1 Simulated doubly differential cross section from $^{12}C(n,p)^{12}B$ reaction at E_n=100 MeV.

Additionally, the resonance part of the spectrum should be disentangled into multipole components. We have prepared a method of data treatment, which in a model independent way extracts strengths and angular distributions of successive giant resonances.

Our approach is exclusively based on measured quantity i.e. doubly differential cross section. The analysis makes no explicit assumptions on the shapes of the resonances contributing to the cross section, allowing all shapes with no functional form to be assumed.

MULTIPOLE DECOMPOSITION OF EXPERIMENTAL DATA

In order to unfold doubly differential cross section $\frac{d^2\sigma}{dq\,dE}$ into multipole components a matrix method have been developed. In this method the experimental data are represented by a two dimensional array. One dimension provides the energy intervals and the other the momentum transfer intervals.

Assuming factorization of the cross section, the experimental doubly differential cross section data can be treated as a fold of several multipole strength distributions and corresponding momentum transfer distributions. As the first step in our method we establish the number of components that contribute to the input data (i.e. background and a number of multipoles). We test the hypothesis concerning the lowest acceptable value of the rank of the double differential cross section matrix (equal to the number of components).

In the next step the continuous background is subtracted. We fit the smooth function describing two dimensional surface in order to determine continuous part of the spectra. Extracted in that way the continuous background is subtracted from input data to get the resonance part R_{ij}. The correctness of this procedure can be tested as after subtracting the background correctly, the number of components of remaining double differential cross section should be lower by one than the initial number of components.

Finally the partition of the remaining - resonant part R_{ij} into individual multipoles is performed. If we denote the energy dependence of the strength distribution of multipole λ by $S_\lambda(E)$, and the momentum transfer distribution of outgoing particles exciting a giant resonance of multpolarity λ by $T_\lambda(q)$, then the matrix R_{ij} is decomposed into λ_{max} matrices to fulfill the equation:

$$R_{ij} = \sum_{\lambda=1}^{\lambda_{max}} S_{i\lambda} \; T_{\lambda j} \qquad (1)$$

The matrix R_{ij} consists of $i_{max} \times j_{max}$ data points where i_{max} denotes number of energy bins and j_{max} number of momentum transfer bins. $S_{i\lambda}$ and $T_{i\lambda}$ are two-dimensional matrices dimensioned $i_{max} \times \lambda_{max}$ and $j_{max} \times \lambda_{max}$ respectively. In our approach the matrix elements $S_{i\lambda}$ and $T_{i\lambda}$ are unknown quantities. The necessity condition to obtain solution is

$$\lambda_{max} \times (j_{max} + i_{max}) < j_{max} \times i_{max} \qquad (2)$$

Generally, decomposition of R_{ij} into multipole components R^{λ}_{ij} is non-unique. In order to obtain reasonable (physical) solution an additional assumption is introduced, namely that the distributions of multipole strength, $S_{i\lambda}$ and momentum transfer $T_{\lambda j}$ are non negative for every subscript λ, i and j. A similar idea [1], was used to analyze the inelastic scattering (e,e'p) and (e,e'α) data leading to excitation of giant resonances.

In order to find unknown matrices $S_{i\lambda}$ and $T_{\lambda j}$, a model independent method was developed, which solve eq. 1 by iterative procedure. To start decomposition, zero approximation for both, the strength and momentum transfer distribution should be assumed. Reasonable zero approximation can be obtained by assignment of selected rows in R_{ij} to $S_{i\lambda}$, and columns to $T_{\lambda j}$. The first approximation of the solution is obtained by solving set of overdetermined linear equations finding by least-squares method $T^{(1)}_{\lambda j}$. Having $T^{(1)}_{\lambda j}$ we can solve once more the set of linear equations finding now $S^{(1)}_{i\lambda}$.

Generally, having k^{th} approximation of the solution $S_{i\lambda}^{(k)}$ and $T_{\lambda j}^{(k)}$, we must solve two successive sets of linear equations in order to obtain $(k+1)^{th}$ approximation of the solution

$$\sum_{\lambda=1}^{\lambda_{max}} S_{i\lambda}^{(k)} \; T_{\lambda j}^{(k+1)} = R_{i,j}$$

$$\sum_{\lambda=1}^{\lambda_{max}} S_{i\lambda}^{(k+1)} \; T_{\lambda j}^{(k+1)} = R_{ij} \qquad (3)$$

If, in successive iterations, the desired degree of convergence is obtained, the procedure is stopped after the n-th iteration. The matrices $S_{i\lambda}^{(n)}$ and $T_{\lambda j}^{(n)}$ are accepted to be solutions of matrix equation (1). The output at this stage are the energy and momentum transfer spectra of each individual multipole, which can be compared with theory to extract the physical information.

ANALYSIS

Prior to applying the method to experimental data, it was subjected to a computer test. The experimental matrix was generated (see Fig. 1), and then unfolded by iterative procedure in order to find distribution of strength $S_\lambda(E)$ and momentum transfer $T_\lambda(q)$. In the simulation of experimental data two giant resonances were assumed to have a concentrated gaussian distribution located on the continuous background. Momentum transfer distributions were formed to have Bessel function dependence $J_0^2(q)$, and $J_1^2(q)$ respectively. Matrix R was folded as a product of S and T and randomly disturbed by statistical errors of Poisson distribution. The simulation was performed in order to generate matrix R of dimension 32x30 (32 channels in energy spectrum and 30 channels in momentum transfer distribution). The solutions were found using the method described above and compared to generated functions $T_\lambda(q)$ and $S_\lambda(E)$ in order to check validity of the method. Ten iterations leads to the solution of eq. (1) shown in Figs. 2 and 3.

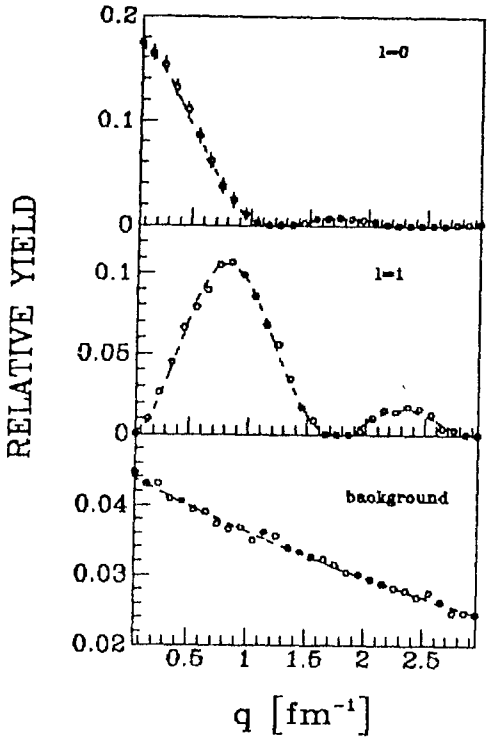

Fig.2 Unfolded momentum transfer distribution of two multipole components and the background. The circles represent the solutions and assumed input distributions are denoted by dashed lines.

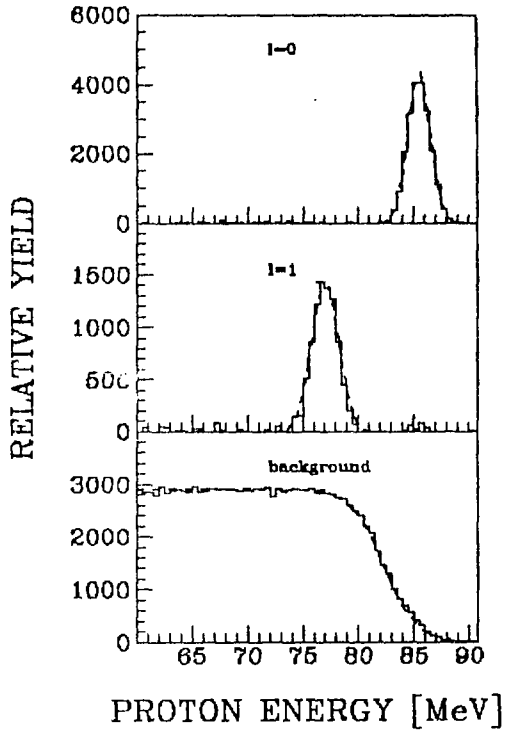

Fig.3 Unfolded strength distribution of two multipole components and the background. The solutions are denoted by histograms and the assumed input distributions by dashed lines.

The generated functions describing strength and momentum transfer distributions are denoted by dashed lines in Figs.2 and 3 while the solutions are denoted by circles and histograms respectively. The energy distributions and momentum transfer distribution functions are very close to input functions. As we see the reproduction of strength widths and positions of extracted distributions are good. Even in the case of the unfavorable conditions (i.e., statistical fluctuations in the data or zero approximation far from the minimum), the procedure applied to the Monte-Carlo generated data was found to work very well.

CONCLUSIONS

Our model independent method of unfolding the measured doubly differential cross section was demonstrated to work properly even in the case of overlapping resonances and very weak strength. It was found that the result of the decomposition does not depend on the assumed zero approximation solutions needed to start iterations. Our method of data decomposition allows us to analyze the differential cross section measured over the full angular range of the first diffraction peak. It means that various giant resonances can be studied using this approach. Moreover, the method allows to avoid many problems which faced the "traditional approach" of data decomposition. The method is to be applied to the (n,p) experiments, like $^{12}C(n,p)$ reaction at E_n=100 MeV [2].

This work has been supported by the National Research Program CPBP 01.09.

REFERENCES

1. Th.Kihm, K.T.Knöpfle, H.Riedesel, P.Voruganti, H.J.Emmrich, G.Fricke, R.Neuhausen, and R.K.M.Schneider, Phys. Rev. Lett. 56(1986)2789

2. H.Condé, S.Hultqvist, N.Olsson, T.Rönnqvist, R.Zorro, J.Blomgren, G.Tibell, A.Håkansson, O.Jonsson, A.Lindholm, L.Nilsson, P.-U.Renberg, A.Brockstedt, P.Ekström, M.Österlund, F.P.Brady, Z.Szeflińskl., Nucl. Instr. and Meth. A292(1990)121

Nuclear Charge Distribution in Symmetric and Asymmetric Fission Induced by Light Charged Particles

Pekka P. Jauho*
Department of Physics, University of Jyväskylä
40100 Jyväskylä, Finland

We have studied the charge dispersion by determining the yields of elements in isobaric mass chains at A= 80, 82, 84, 110, 112, 114, 116, 118, 120 using proton and deuteron induced fission of ^{238}U. There have been extensive studies of independent fission yields using thermal neutron induced (asymmetric) fission [1], but little is known about yields in the case of nearly symmetric fission studied in this work.

The (p,f)-studies were performed using 20 MeV protons from the MC-20 cyclotron in Jyväskylä. The (d,f)-reaction was studied at the Louvain-la-Neuve K= 120 heavy ion cyclotron using 18, 25, and 41 MeV deuteron energies and continuous beam. We used the IGISOL facility in Jyväskylä and the Louvain-la-Neuve LIGISOL to separate the mass chains. The IGISOL method is fast since no ion source is needed. The efficiency is also practically independent of the chemical properties of nuclides making the method well suited for charge dispersion studies. Standard spectroscopic methods were used to determine the level structure of isotopes in the mass chains. In Jyväskylä we have measured γ-abundances, i.e. γ-intensities per 100 β-decays, by resolving exponential components in time spectra when the beam is in pulsed mode. For this purpose we detected γ-singles, β-singles (with β-telescope) and γ(β)-coincidences simultaneously in the same setup.

Our experimental values for the mean isobaric charge Z and the standard deviation σ_Z and the relative merits of the (d,f)- and (p,f)- reactions as means of producing extremely neutron rich isotopes in this mass region will be discussed.

[1] A.C. Wahl, Atomic Data and Nuclear Data Tables 39, 1 (1988)

This work has been supported by the Academy of Finland.

* in collaboration with M.E. Leino[1], P. Decrock[2], P. Dendooven[2], P. Van Duppen[2], K. Eskola[1], M. Huyse[2], A. Jokinen, J.M. Parmonen, H. Penttilä, G. Reusen[2], P. Taskinen, J. Wauters[2], J. Äystö

1) Department of Physics, University of Helsinki, Finland
2) LISOL, I.K.S., K.U. Leuven, Belgium

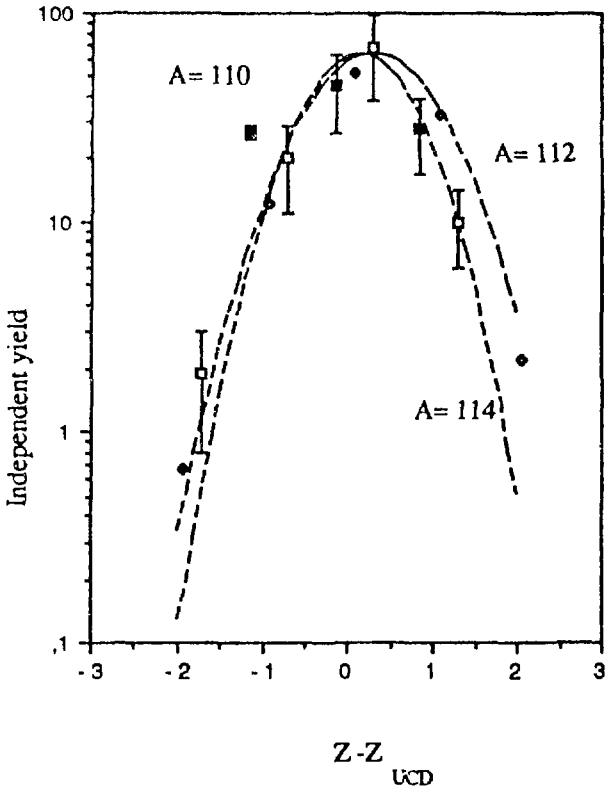

Figure 1. Independent yields Y (Z -Z_{UCD}, A) of fission products in the isobaric mass chains A= 110, 112, 114 in the reaction ^{238}U (p, f), Ep= 20 MeV. Z_{UCD} is taken from the unchanged charge distribution hypothesis:
$Z_{UCD}= (Z_F /A_F)(A +\nu(A))$, where $\nu(A)$ is the mean number of prompt neutrons evaporated.

Table 1. Average charge numbers Z_{ave} (mea) and variances σ^2_Z(mea) have been calculated on the data shown in figure 1. The values for thermal neutron induced fission (Wahl) are represented for comparison (ref. 1).

A	Z_{ave}(mea)	σ_Z(mea)	Z_{ave}(Wahl)	σ_Z(Wahl)	Z_{UCD}	Z_{ave}(mea) -Z_{UCD}
110	44.01+-0.20	-	43.16	0.58	44.16	-0.15
112	45.24	0.71	44.21	0.62	44.94	0.30
114	45.86	0.60	45.17	0.60	45.72	0.14

The Mean-Square Charge Radii of Ba Isotopes*

B. Nerlo-Pomorska, K. Pomorski, B. Skorupska
Department of Theoretical Physics, University M.C.S., Lublin, Poland

Abstract

The microscopic calculations of the mean-square charge radii and the quadrupole moments of Ba isotopes where done. It was shown that the pairing mean field deformation Δ influences strongly the magnitude of the isotopic shift of $< r^2 >$.

The newest development of the measurement techniques of nuclear mean-square charge radii of nuclei gives us more accurate data [1] demanding a theoretical effort in order to explain diversing nuclear sizes and shapes mechanisms.

The microscopic calculation of $< r^2 >$ was done for the neutron deficient nuclei with $50 < Z, N < 82$. The deformed single-particle Nilsson potential with the universal set of the parameters [2] was used. The calculations were performed using the generator coordinate method (GCM) and assuming the extended gaussian overlap approximation (GOA). The BCS wave function depending on quadrupole (ε) and hexadecapole (ε_4) deformation was taken as the generator function. The expectation value of the r^2 operator between the ground state wave function of the collective GCM+GOA hamiltonian gives the theoretical estimate of $< r^2 >$ [3].

The results of the calculation for Ba isotopes are compared with the experimental data in Fig. 1. The absolute values of $< r^2 >$ are not given by experiment, so we have assumed the radius of the magic isotope ^{138}Ba to be equal to the size of the spherical liquid drop.

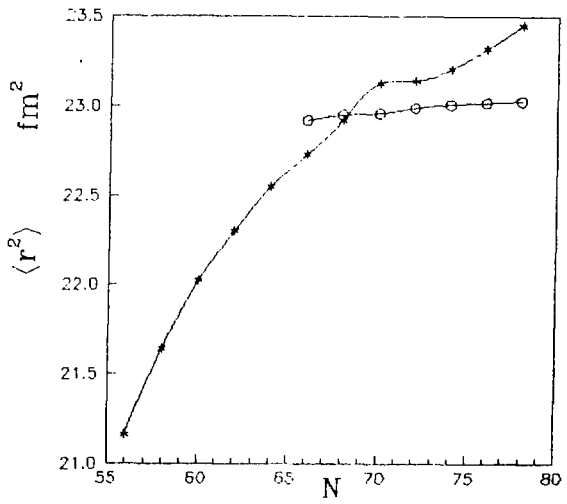

Figure 1: The microscopic estimates of $< r^2 >$ for Ba isotopes compared with the experimental data(c).

*Paper supported by the Polish Ministry of Education, project CPBP-01.09 .

The slopes(so called isotopic shift) of the theoretical curve are larger than that from measurement.In order to explain this discrepancy we performed the analysis of the influence of some parameters on the value of the mean-square charge radius of nuclei. The dependences of $< r^2 >$ for ^{126}Ba isotope on ϵ, ϵ_4 and Δ are plotted in Fig.2 a, b and c correspondingly. All dependencies are taken around the equilibrium point which is marked by arrows on the plots.

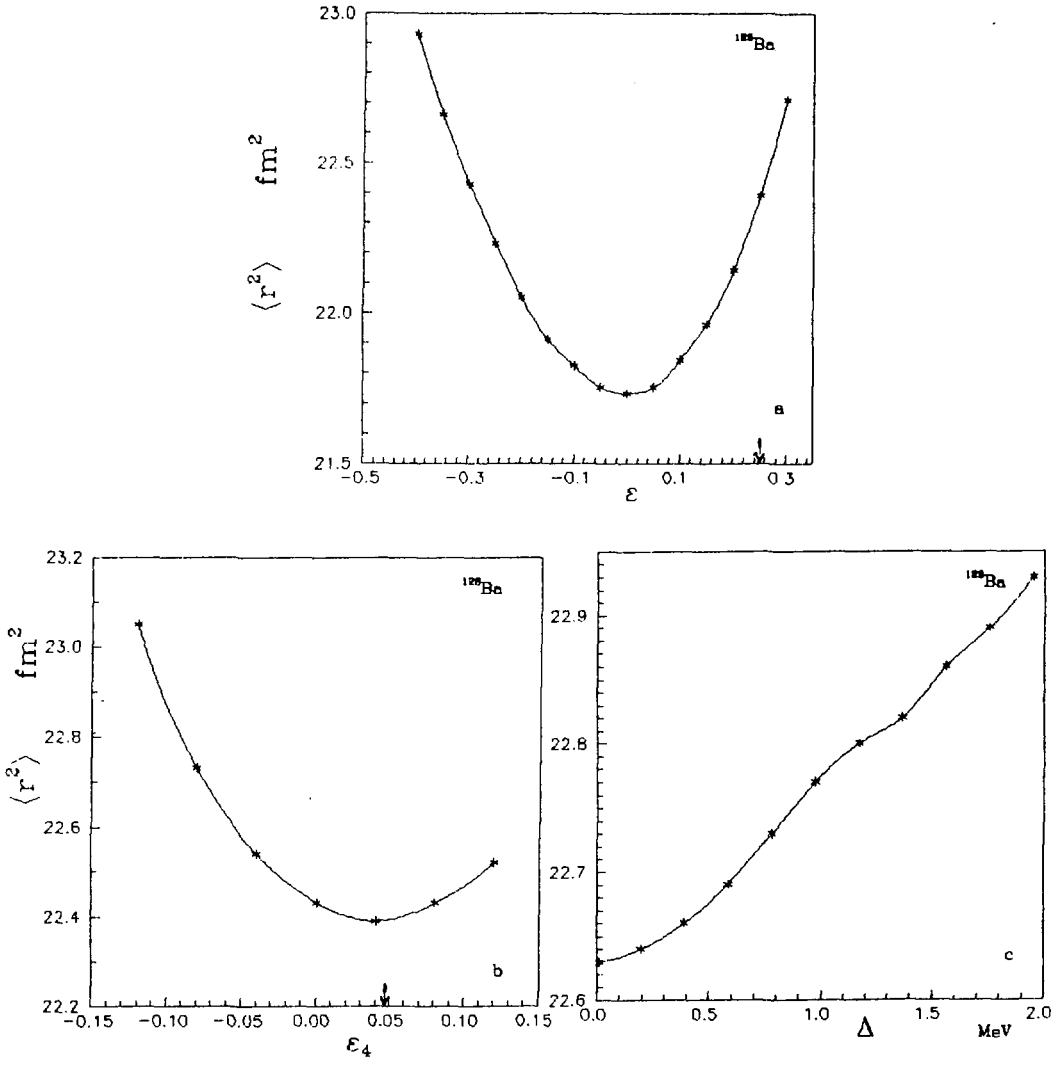

Figure 2: The dependences of $< r^2 >$ for ^{126}Ba isotope on ϵ (a), ϵ_4 (b) and Δ (c).

It is seen that the change of $< r^2 >$ with respect to ϵ_4 or Δ is similar.It means that the pairing gap Δ is as important parameter as the hexadecapole deformation ϵ_4.

Assuming that the experimental value of quadrupole moment Q_{20} establishes well the quadrupole deformation ϵ we can estimate ϵ_4. Namely, we have evaluated within the deformed liquid drop model the values of quadrupole (ϵ^{LD}) and hexadecapole (ϵ_4^{LD}) deformations which reproduce the experimental [1] $< r^2 >$ and Q_{20} and compared them

with the microscopic equilibrium deformations ($\epsilon^{eq}, \epsilon_4^{eq}$). In Fig. 3 we can see that they differ much from each other especially for the heaviest Ba isotopes.

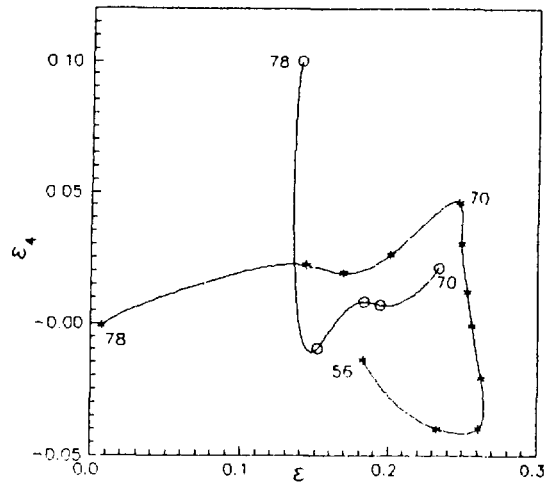

Figure 3: The microscopic equilibrium points (*) and their estimates deduced from the experimental values of $< r^2 >$ and Q_{20} (o).

This discrepancy means that the other factors in spite of ε , and ϵ_4 deformations could be important.

For the next investigation we took the quadrupole deformation of the Nilsson potential (ε) and the pairing gap (Δ) and we vary them free in order to reproduce in microscopic calculation the experimental values of $< r^2 >$ and Q_{20}. The results of this analysis on ε and Δ plane are plotted in Fig. 4 for Ba isotopes.

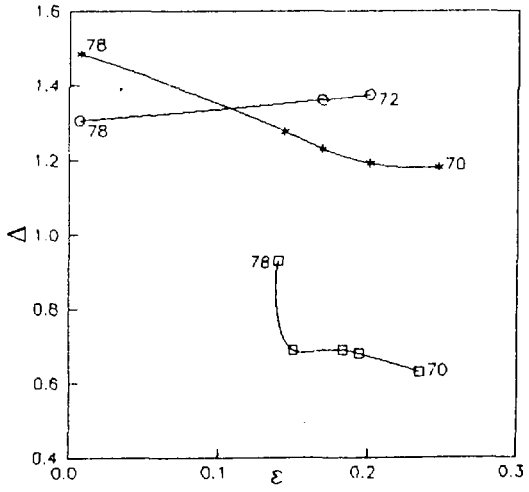

Figure 4: The quadrupole deformations and energy gaps obtained microscopically (*) and from experimental masses (o) and extracted from $< r^2 >$ and Q_{20} ($\sqcap$) .

The equilibrium values ($\varepsilon^{eq}, \Delta^{eq}$) as well as the estimates of Δ^{exp} obtained from the experimental masses [4] are marked. The values of Δ which reproduce the experi-

mental $< r^2 >$ and Q^{20} are almost half of their estimates from masses. This result could be understood in the dynamical pairing model [5] in which the most probable Δ is much smaller as that corresponding to the minimum of the BCS energy.

The following conclusion can be drawn from our investigation. The quadrupole and hexadecapole deformations should be taken into account in order to reproduce the experimental isotopic shifts of $< r^2 >$ of the neutron deficient nuclei. But the deformation ε and ε^4 can not alone explain the experimental data. The dependence of $< r^2 >$ on Δ is also important. The more careful dynamical treatment of pairing degrees of freedom is necessary.

Further improvement of the single particle scheme and probably taking into account the quadrupole-pairing term are planned.

References:

1. P. Aufmuth, K. Heilig, S. Steudel, Atomic Data and Nuclear Data Tables 37, 455-490 (1987)

2. T. Seo, Z. Phys. **A324** (1986) 1

3. B. Nerlo-Pomorska, K. Pomorski, M. Brack, E. Werner, Nucl. Phys, **A552** (1986) 252
   B. Nerlo-Pomorska, K. Pomorski, B. Skorupska, Proc. of the XXV School in Zakopane, 5-12 May 1990

4. P. Möller, J. R. Nix, Atomic Data and Nucl. Data Tables, November 7, 1986

5. A. Goźdź, K. Pomorski, M. Brack, E. Werner, Nucl. Phys. **A442** (1985) 50

BETA-DECAY HALF-LIVES OF VERY NEUTRON RICH Ni, Co, Fe ISOTOPES PRODUCED BY THERMAL FISSION OF ^{235}U AND ^{239}Pu

M. Bernas*, P. Armbruster, J.P. Bocquet**, R. Brissot**, H. Faust, S. Czajkowski* and J.L. Sida*

Institut Laue-Langevin, Grenoble, France
*Institut de Physique Nucléaire, Orsay, France
**Institut des Sciences Nucléaires, Grenoble, France

- Introduction

Thermal neutron or low energy fission has long been the unique way to produce neutron rich isotopes. On the extremely light side of the light fission products, we have identified unambiguously several new n-rich isotopes of Nickel and Copper in the thermal neutron fission of ^{235}U at the ILL high flux reactor in Grenoble [1]. These isotopes, the lightest masses ever observed in binary thermal fission, have a significant neutron excess since they profit from the large neutron to proton ratio of the fissioning ^{236}U parent nucleus, but they are produced with low rates. Identified in the focal plane of the Lohengrin spectrometer, the isotopes are well separated, but rare compared to other fission products. Therefore, facing this experimental challenge, we developed a novel method to determine β^- decay half-lives out of a few events.

Previous studies of β^- -decay of light fission products have already been extended down to ^{80}Zn [2,3]. More recently half-lives and $\beta \cdot \gamma$ decay schemes have also been reported for ^{74}Cu [4,5], ^{75}Cu [4,6], ^{76}Cu and ^{78}Cu [4]. In all these cases, on-line mass separator techniques were applied. With the available ion sources, the study of Ni isotopes is still difficult since this element can not be efficiently extracted. However, ^{69}Ni, the heaviest Ni isotope for which the half-life is known, was indeed separated by this technique [7]. The heaviest Ni isotopes, ^{67}Ni [8] and ^{68}Ni [9] for which mass excess and spectroscopic features are known, were studied by quasi-elastic transfer reactions.

Using time correlations, we remeasured the half-life of ^{74}Cu and ^{75}Cu to validate our method and to confirm the only result published for ^{75}Cu at that time [4]. This method was extended to the new isotopes of ^{71}Ni, ^{72}Ni, ^{73}Ni, ^{74}Ni, ^{69}Co, ^{68}Co and ^{68}Fe and the results are presented here.

I - Analysis and identification of the ions

The fragments are produced by thermal fission of ^{235}U or ^{239}Pu induced by the neutrons of the high flux reactor. They cover wide ranges of mass A (69 to 168), of kinetic energy E (50 to 115 MeV) and of charge state q (15 to 25). They are separated by the recoil spectrometer Lohengrin [10] which combines electrostatic and magnetic deflections in perpendicular planes. Many fragments appear with similar discrete values of A/q and equal values of E/q, and thus a detector has to provide a complementary separation. If the energies are measured in an ionization chamber (I.C.), the few charge states can be separated and the mass lines well identified. Using a narrow slit of 4mm on the target, an A/q ratio can be selected with a resolution of 800. However, when the fragments of interest are

produced with extremely low yields (e.c. 10^{-8} fragments/fission), even this good resolution could not prevent a potential contamination from the tails of neighboring high yield A/q distributions. The slit defining the velocity range has a length of 70 mm, which introduces an energy spread of 1%. It is the main contribution to the energy definition of the I.C. system. This definition is sufficient to separate the charge states and consequently the A lines. In order to identify the few isobars populating an A line, the energy loss ΔE is accurately measured [11] (fig.1). The resolution achieved for the isotopes investigated is $Z/\Delta Z = 32$.

The Z value is determined by extrapolation from the isobars in a well known mass line, like A=82. Along the line A=72 (E = 90 MeV, q = 19) shown in fig.1, the group with the smallest ΔE is attributed to ^{72}Ni and the next one to ^{72}Cu.

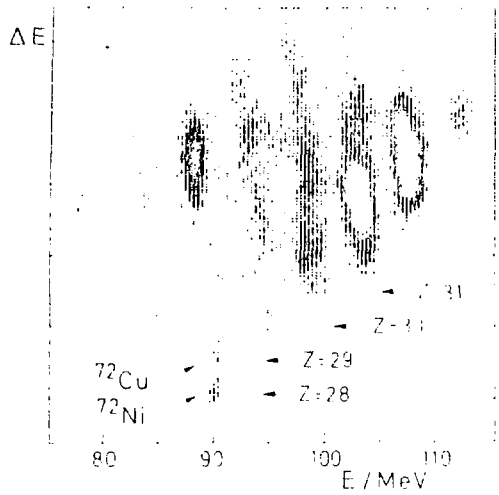

fig. 1 - Example of $\Delta E - E$ scatter plot (A=72). The isotopes of A=72 q=19 are indicated. The large number of contaminants are due either to different q-values combining with fitting mass values (below the hatched line) or to ions having suffered charge changing collisions in the rest gas between the magnetic and electric deflectors (above the hatched line).

We took advantage of the large n-odd even effect on the yields to measure the half-lives of the even Ni on the ^{235}U target. In a second experiment, a ^{239}Pu source was used, which provided the isotopes under study with larger yields and a smaller n-odd even effect.

II - How to measure the β decay half-lives?

Only a few relevant fragments per hour reach the detector together with a large number of contaminant fission products. Each of those emits 2 to 3 β particles, which, together with a considerable background due to the high radiation field close to the beam tubes of the high flux reactor, makes this measurement somewhat a challenge. Furthermore, the half-lives for the new neutron rich isotopes are predicted as relatively long $\sim$ 1 s.

β delayed neutron counting, one of the most efficient methods, could not be used since estimated neutron emission probabilities, Pn, are lower than 0.3% for the Ni isotopes under study. With the very low count rate expected β-delayed γ ray spectroscopy is excluded, even with a multitude of high-efficiency Ge(Li) counters. We applied a method of time correlation between the fragment of interest and the detection of a subsequent β particle.

The ions are implanted close to the end of their trajectories into one of 8 decoupled small (10 10 mm), thin (0.5 mm) solid state detectors where the subsequent β is also detected. The energy loss of a minimum ionizing electron amounts to 170 kev in a 0.5 mm Si detector where the energy resolution is 12 kev. The energy threshold was kept above 40 kev.(see fig.2).

All the signals which are not affiliated with the fragments under study constitute the background.

They may come from β decays of any other fission fragment or rare gas isotopes flowing to the entrance window of the I.C., or they may be due to X-rays produced in the condenser. The rate of β events due to the decay of the fragment under study is negligible compared to the total β rate. Therefore the background rate b is simply the β counting rate, which was measured accurately and checked to stay constant over each irradiatiation.

Correlating the position of the implanted ion with the position of the subsequent electron detected leads to a division of the random events.

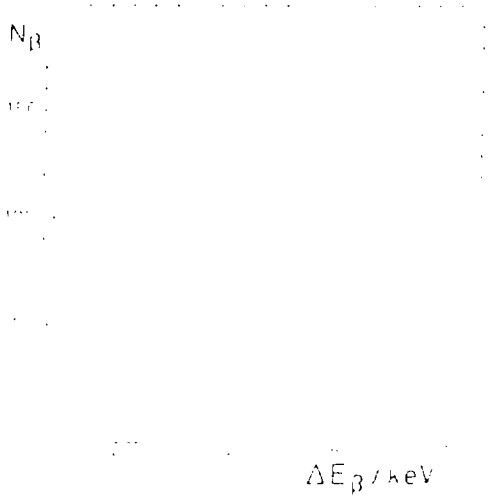

fig. 2 - Typical energy loss spectrum of β's in one of the Si detectors

III - Analysis of time correlations

1) Probability functions

- The spectrum of time intervals between the arrival of a relevant ion and the following β's detected within a critical time t_c, summed over the detectors, is a function of λ, with $\lambda = \ln 2/T_{1/2}$. The time t_c is chosen as 2 to 5 times the value expected for the half-life $T_{1/2}$. Superimposed on a constant background rate, the β's emitted by the fragments are found at the shorter time intervals. This spectrum is calculated with the expression :

$$\Delta N_{F\beta}(t) = N_F \times \rho(\lambda, t)\Delta t$$

where $N_F = n_i T$ is the number of separated fragments summed over the 8 detectors and $\rho(\lambda, t)$ is the probability density for counting a β in one of the detectors per unit of time. This density ρ may be written as

$$\rho(\lambda, t) = b + \varepsilon\lambda e^{-\lambda t} \qquad (1)$$

The spectrum of the first β detected after each fragment, summed over the detectors, can also be analysed. If there were no β-decay, the probability would be given by $\rho(t) = b \times \exp(-bt)$. Time intervals between the last β occuring before a fragment and the fragment are providing this purely statistical distribution. For each measurement reported here, this logarithmic time spectrum was evaluated and shown to be a unique straight line of slope b, ensuring that β counting rates were stable.

The first β detected after a fragment comes either from the fragment decay or from background. Since the two processes are independent, the probability for having **not** detected a β at time t is the product of the two probabilities, one for having not counted a background β, e^{-bt}, and the other for having **not** detected the β of the decay, $1 - \varepsilon(1 - e^{-\lambda t})$

that is to say:

$$\left(1-\varepsilon(1-e^{-\lambda t})\right)\times e^{-bt}$$

The probability density of detecting the first β at time t is given by the first derivative of this product:

$$\rho_1(\lambda,t)=\varepsilon(b+\lambda)e^{-(b+\lambda)t}+(1-\varepsilon)be^{-bt} \tag{2}$$

which is normalised to one, and the probability spectrum of time intervals between the fragments and the first β particle detected is given by $\Delta N_{1\beta}(t)=N_F\rho_1(\lambda,t)\Delta t$

The expressions for 2β - chain decays have been derived long ago and expressions 1 and 2 become :

$$\rho(\lambda,t)=b+\varepsilon\lambda e^{-\lambda t}+\varepsilon\,\frac{\lambda\lambda'}{\lambda-\lambda'}\left(e^{-\lambda' t}-e^{-\lambda t}\right) \tag{1'}$$

$$\begin{aligned}\rho_1(\lambda,t)=&(1-\varepsilon)^2be^{-bt}\\&+\varepsilon\left(1-(1-\varepsilon)\frac{\lambda'}{\lambda-\lambda'}\right)(b+\lambda)e^{-(b+\lambda)t}\\&+\varepsilon(1-\varepsilon)\,\frac{\lambda}{\lambda-\lambda'}(b+\lambda')e^{-(b+\lambda')t}\end{aligned} \tag{2'}$$

They must be used whenever λ' is not negligible compared to λ.

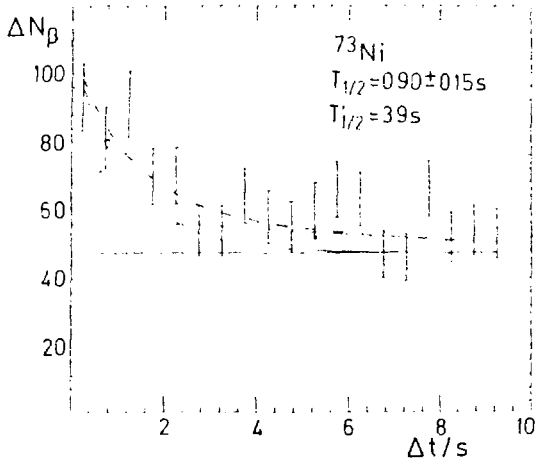

fig. 3- ^{73}Ni fitted spectrum of time correlations for β's detected in a time t_r in order to illustrate the second method. The decay under study, the background, and the filiation are indicated

2) χ^2 minimisation

Chosing an appropriate time interval $\delta t = T_{1/2}/10$ the spectra for time intervals Δt, $\Delta N_{F\beta}=f(\Delta t)$ can be reproduced by a χ^2 minimization in terms of $\rho(\lambda,t)$ or $\rho_1(\lambda,t)$ (when considering only the first β) in order to obtain the parameter λ. The uncertainty on the value of λ is associated to a variation of 1 on χ^2 .

3) Maximum likelyhood (MLH)

The least square method is simple to apply, but it fails to properly estimate parameters when the number of events becomes small. In that case, one seeks to maximize the information content of the data by utilizing the occurence time t_i of each individual event.

Suppose that after the arrival of an ion the β events occur with a probability $\rho(\lambda, t)$ per unit of time. For a Poisson distribution, the probability for ℓ events to occur between $t = 0$ and $t = t_c$ is $e^{-m} m^{\ell} / |\ell\ell|$ where

$m = \int_0^{t_c} \rho(\lambda, t) dt$, is the mean value of the number of events in this time interval. Given a sequence of ℓ independent events occuring at the times $t_1, \ldots t_{i-1}, t_i \ldots$, up to t_c the probability of finding this sequence is the product of the probabilities to find no events between the event times t_{i-1} and t_i and one event between time t_i and $t_i + \Delta t_i$. It is written as

$$\exp\left(-\int_0^{t_1} \rho(t)dt\right)\rho(t_1)\Delta t_1 \times \exp\left(-\int_{t_1}^{t_2} \rho(t)dt\right)\rho(t_2)\Delta t_2 \times \ldots \times \exp\left(-\int_{t_\ell}^{t_c} \rho(t)dt\right)$$

$$= e^{-m} \prod_{i=1}^{\ell} \rho(t_i)\Delta t_i$$

and there exists a value of λ which makes the total probability maximum. It is found as the maximum of a likelyhood function, $\mathcal{L}$, which is defined for each fragment as follows :

$$\mathcal{L} = e^{-m} \prod_{i=1}^{\ell} \rho(t_i)$$

where t_i is the time sequence of the β's detected after a fragment over a time t_c, m is the mean number of β's per fragment and l, the number of β's detected over this time t_c.

For N_F fragments, the N_F likelyhood functions are multiplied ; m becomes the mean value of the number of β's expected in the time $N_F \times t_c$ and l the total number of β's counted within this same time. Instead of finding the maximum of $\mathcal{L}$, it is equal but simpler to minimize

$$-\ln \mathcal{L} = m - \sum_{i=1}^{\ell} \ln \rho(\lambda, t_i)$$

The standard deviation σ is given to a good accuracy by $\sigma = 1/\sqrt{F}$ where $F = \dfrac{\partial^2 |-\ln \mathcal{L}|}{\partial \lambda^2}$

With $\rho(t)$ given by equation 1 we obtain

$$-\ln \mathcal{L} = N_F \left[bt_c + \varepsilon(1 - e^{-\lambda t_c}) \right] - \sum_{i=1}^{\ell} \ln(b + \varepsilon\lambda e^{-\lambda t_i})$$

$$F = \varepsilon N_F t_c^2 e^{-\lambda t_c} + \sum_{i=1}^{\ell} \frac{\varepsilon^2 + \varepsilon t_i b e^{\lambda t_i}(2 - \lambda t_i)}{(be^{\lambda t_i} + \varepsilon\lambda)^2}$$

When the filiation of decay constant λ' had to be included in the analysis, the expression 1' was used for $\rho(\lambda, t)$ and the corresponding expression for F - more complicated - has been similarly derived.

The time sequences of the first β detected after a registered fragment can be analysed in the frame of M.L.H. using the probability law $\rho_1(\lambda, t)$. The formulae are given in ref. [13].

IV - Measurements and results

1) Test of the methods

The time correlations depend on λ, on ε, and on b. Since those three quantities are correlated in the analysis, we chose to accurately determine the last two quantities in order to constrain the search to the first unknown parameter λ. The isobaric chain A=96 was used to test our methods, since the

production yield for this mass is one of the largest. At intermediate ΔE, the $Sr(Z = 38)$, $T_{1/2} = 1$ s is the main component with $\eta_{2\beta} = 65\%$.

To determine the efficiency a high flux of fragments was chosen and then, in the absence of contaminants, the β background can be neglected. The cumulative yield in the β chain is well known (1.67), thus the ratio of counted β's compared to mass 96 ions directly provides the β efficiency *in situ*.

On the contrary, a small flux of fragments was used to check the practicability of the correlation methods. Although the three isobars could not be well separated, a ΔE-E window was set on the scatter plot narrow enough to select the ^{96}Sr fragments. The counting rate was adjusted by setting a diaphragm at the entrance of the magnetic field of Lohengrin in order to obtain a frequency of 8 fragments/hour per detector, a value small enough - compared to the decay constant $\lambda = 0.7/s$ - to be neglected. The time correlation spectrum of β's counted within a time t_c could be analysed either to deduce the decay constant λ, or to extract both parameters λ and ϵ (see fig.5) since the statistics were sufficient and the background frequency b was low enough, 0.19/s.

The values deduced for $T_{1/2}$, 1.05 ± 0.15 s and, in case of a 2 parameter analysis, for $T_{1/2}$ and ϵ, 1.00 ± 0.13 s and 0.53, respectively, show the achievement of the method, since the published value is 1.06 ± 0.04 s [4].

2) Application to Ni Co and Fe isotopes

Fragment kinetic energies E and charge states q were selected in order to optimize the counting rate of studied fragments and to keep the background rate compatible with the half-life. The proportion of selected fragments versus contaminants is indeed very low (table I).

Fissionning source	Isotope	Rate of all fragments / hour	Rate of the relevant isotopes / hour	Background rate/ detector/s. (b)	Factor of "practicability" ($\epsilon\lambda$/b)
^{235}U	^{72}Ni	1000	3	0.192	0.77
	^{74}Ni	1700	1.3	0.216	1.31
^{239}Pu	^{71}Ni	540	13	0.169	0.71
	^{72}Ni	2200	17.2	0.213	0.57
	^{73}Ni	3000	4.6	0.251	1.12
	^{69}Co	1620	1.52	0.31	3.71
	^{68}Co	3800	0.38	0.42	3.20
	^{68}Fe		0.15		5.75

TABLE I

Both analysis, i) the χ^2 minimisations of time spectra and ii)the maximum likelyhood (M.L.H.) analysis of time distributions up to 10 seconds were performed for two sets of data: a) time intervals between the fragments and the next β arrival and b) time intervals between fragments and consecutive β's. The optimum time interval δt for the first analysis is chosen between 0.1 s and 0.4 s. The four values obtained for each half-life are statistically compatible, but scattered. No systematic deviation can be observed, but the M.L.H. procedures lead to less scattered values. The improvement due to the M.L.H. analysis becomes even more obvious for a very small number of correlations.

Both type of methods a and b can be compared. With the first one the time data is truncated, but a notion of sequence (the first) is exploited. With the second one, in principle, all the detected β's (ϵN_F are indeed included in the evaluation, however the sequence of the β's occuring after each fragment is not accounted for, only the product of independent probabilities is exploited. We have extended the

time distribution analysis of the first β to the second β, at the price of a more complex calculation in order to analyse the 2β-chains which coud be observed in the ^{68}Fe decay. This will be discussed in [15]

V - Calculated and measured half-lives

Systematic comparisons of experimental values with calculated ones are relevant in order to test the validity of nuclear and β-decay models and to provide a basis for chosing a reliable type of extrapolation. In fact, more half-life of n-rich nuclei are required for a complete r-process calculation. Local maxima in the solar A abundancies are related to the existence of waiting-points around A=80, 130 and 195. In those regions, the n-shell closure provides a limit to the r-process, beyond which the n-capture is hampered by the sudden drop in S_n to values smaller than 2 Mev. They are unambiguous foot-prints of this process and the concerned isotopes can more easily be measured, since they are closer to the stability valley. Predictions of half-life and β-decay scheme of isotopes flooded by the high neutron flux before the waiting points are also of importance in order to reproduce the relative yields and the elemental composition in the waiting point peak abundances.

The calculation of a half-life requires the knowledge of many features of the decay, the final states quantum number, the initial and final state nuclear configurations and the β decay interaction. Since the final states and the energy gaps are not known, drastic approximations are needed for which a few methods have been developped.

1° - The "Gross theory", (G.T.) of β-decay fulfills the sum rules and uses a spreading width of collective states as the only free parameter. The model has been improved recently [16]. The values we use in the following (A on table II) were calculated with the G.T. distribution width parameter of 50 Mev and an intermediate "bottom raising" of the ground-state Q_β-value due to the fact that transitions to low-lying states may be forbidden. This evaluation is labeled (1b) in ref [16].

2° - The "microscopic approach", developped by Klapdor [17] is a shell model calculation which makes use of the Tamm-Dancoff approximation. It is labelled B in the following. This calculation has recently been ameliorated by using the Q.R.P.A. [18]. Only the half-lives of the most n-rich isotopes (C) are predicted.

The ratios of measured half-lives over the calculated ones, [16, 17, 18] are plotted in fig. 4. Measured values are taken from references [4] to [7] and from the present results with their experimental uncertainties. The main discrepancies occur for isotopes before the proton shell closure at Z<28, for which half-lives are consistently overestimated by almost one order of magnitude. K.L.Kratz attributed the origin of such a failure [19] to the sensitivity of predictions to the changes in deformations (quadrupole moment) of the decaying isotopes. Predictions of half-lives of n-rich nickel are in very good agreement with each other and with the measured values, but they decrease slightly too fast with the excess of neutrons. In the case of copper isotopes there is a clear difference between both predictions : Gross theory predictions are scattered and too large by a factor of about 2, while microscopic calculations reproduce the variation of half-lives in terms of the neutron excess, but they are too small by the same factor. This trend may also reflect a defect in the assumptions made when crossing the Z=28 shell closure.

A similar over-estimation of half-lives calculated with the same models was found by J.Äystö [20] for n-rich isotopes just before the Z=50 proton shell closure. It was explained by similar arguments. In rapid neutron-capture process (n,γ) scenario, these n-rich isotopes would be less effective, since they β-decay too rapidly [19]. It will therefore modify the relative importance of the waiting-point abundancies maxima at A=80 as well as its elemental composition. The calculated mass position of the peak would also be shifted. Even with their rather large experimental uncertainties, the present results allows one to appppreciate the performances and the limits of theories for β- decay and for nuclear structure. With further results they will help to solve the r-process puzzle.

Isotope	Total number of relevant fissions	Present values of $T_{1/2}$ (s.)	Calculated half life (s.)
^{71}Ni	652	1.95 ± 0.38	2.18 A 3.03 B 5.44 C
^{72}Ni	625	2.05 ± 0.35	2.48 2.08 1.56
^{73}Ni	405	0.86 ± 0.15	0.69 0.88 0.81
^{74}Ni	73	1.07 ± 0.50	0.57 0.8 0.46
^{69}Co	175	0.27 ± 0.05	0.73 0.68 0.07
^{68}Co	80	0.18 ± 0.10	0.80 0.81 0.29
^{69}Fe	29	0.10 ± 0.06	0.37 0.42 0.16

TABLE II

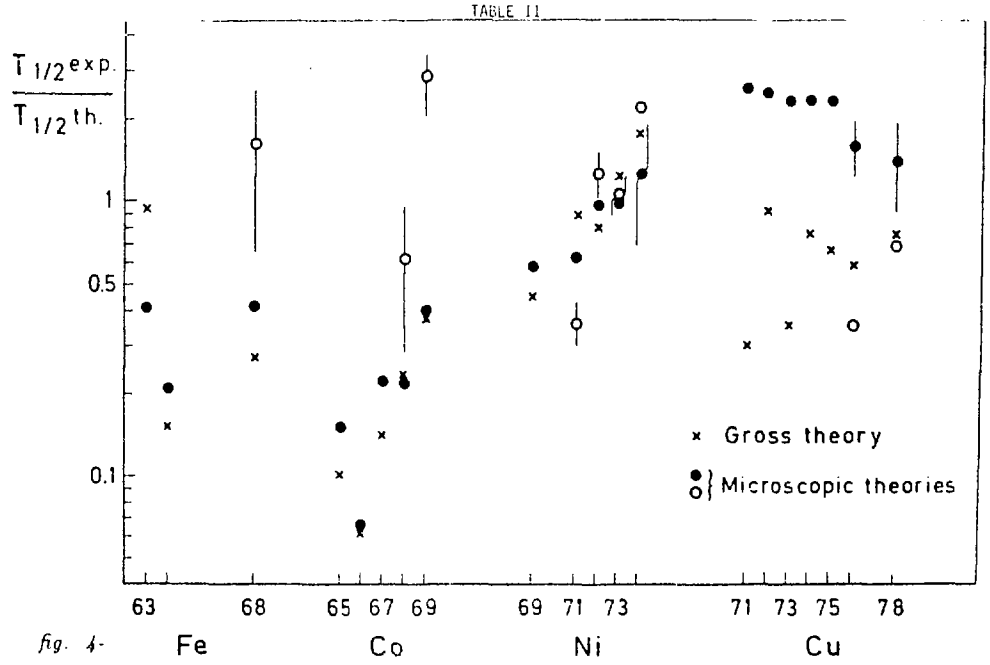

fig. 4-

Conclusion

The present method could be applied to other sources of exotic isotopes. It is appropriate for half-life measurements of new isotopes occuring with low rates, when other subsequent particles (γ or n) are not measurable and when contaminant ions are not rejected well enough by electrostatic or magnetic filters. A first step has thus been achieved towards the doubly magic isotope of ^{78}Ni which is one of the most fascinating objects still to be reached far from stability. The knowledge of half-lives in this region provide a significant test of nuclear models along the line of proton shell closure ($Z = 28$) far apart from stability and of β decay theory. Further, their values enter as ingredients into the r-process calculations aimed at reproducing the relative mass abundances of nuclei beyond iron as they are found in the solar system.

REFERENCES

[1] P. Armbruster, M. Bernas, J.P. Bocquet, R. Brissot, H R. Faust and P. Roussel
Europhysics Letters 4 7 p793 (1987)

[2] E. Lund, K. Aleklett, B. Fogelberg, A. Sangariyavanish,
Proc. Int. Conf. AMCO7, ed. O.Klepper, T.H. Darmstadt p102 (1984)

[3] R.L. Gill, R.F. Casten, D.D. Warner, A. Piotrowski, H. Mach, J.C. Hill, F.K. Wohn, J.A. Winger, R. Moreh Phys. Rev. Lett. 56 p1874 (1986)

[4] E. Lund, B. Ekström, B. Fogelberg and G. Rudstam
Fifth International Conference on Nuclei far from Stability, Rosseau Lake, Ontario, ed I.S.Towner p578 (1987)

[5] J.A. Winger, John C. Hill, F.K. Wohn, E. K. Warburton, R.L. Gill, A. Piotrowski and D.S. Brenner, Phys. Rev. C39 p1976 (1989)

[6] P.L. Reeder, R.A. Warner, R.M. Liebsch, R.L. Gill and A. Piotrowski
Phys. Rev. C 31 p1029 (1985)

[7] U. Bosch, W.D. Schmidt-Ott, P. Tidemand-Petersson, E. Runte, W. Hillebrandt, M. Lechle, F.K. Thielemann, R. Kirchner, O. Klepper, E. Roeckl, R. Kyraczewski, D. Schardt, N. Kaffrell, M. Bernas, Ph. Dessagne and W. Kurcewicz, Phys. Lett. 164B p22 (1985) and references therein

[8] Ph. Dessagne, M. Bernas, M. Langevin, G.C. Morrison, J. Payet, F. Pougheon and P. Roussel
Nucl Phys. A426 p399 (1984)

[9] M Girod, Ph Dessagne, M. Bernas, M. Langevin, F. Pougheon and P. Roussel
Phys. Rev. C 37, p2600 (1988)

[10] E. Moll, H. Schrader, G. Siegert, M. Asghar, J.P. Bocquet, G.Bailleul, J.P.Gautheron, J. Greif, G.I.Crawford, C.Chauvin, H.Ewald, H.Wollnik, P.Armbruster, G.Fiebig, H.Lawin and K.Sistemich,
Nucl. Instr. and Meth. 123 p615 (1975)

[11] J.P. Bocquet, R. Brissot, H.R. Faust Nucl. Instr. and Meth.A 267 p466 (1988)

[12] B.T. Cleveland Nucl. Instr. and Meth. 214 p451 (1983)

[13] M. Bernas, P. Armbruster, J. P. Bocquet, R. Brissot, H. Faust, Ch. Kozhuharov and J. L. Sida
Z. für Phys A336 p41 (1990)

[14] G. Bailleul, J.P. Bocquet, H Schrader, R. Stippler, B. Pfeiffer, M. Asghar, C. Chauvin, J.P Gautheron, J. Greif, G. Siegert, P. Armbruster, H. Ewald, J. Blachot, E. Monnand and F. Schussler
Z. für Phys A273 p283 (1975)

[15] M. Bernas, P. Armbruster, S. Czajkowski, H. Faust and J. P. Bocquet to be published

[16] T. Tachibana, M. Yamada and K. Nakata
Report of Sciences and Engineering Research Laboratory, Wasada University (1988)

[17] H.V. Klapdor, J. Metzinger, T. Oda Atomic Data and Nuclear Data Tables 31 p81 (1984)

[18] A. Staudt, E. Bender, K. Muto and H. V. Klapdor
Atomic Data and Nuclear Data Tables 44 p79 (1990)

[19] K.L. Kratz, B. Pfeiffer, A. Wöhr and P. Möller, Z. für Phys. A, 332 p419 (1989)

[20] J. Äystö and P. Taskinen,
Contribution to the XX Summer School on Nucl. Struct. Studies by means of Nuclear Reactions, (Sept. 1988) Mikołajki, Poland

SUPERDEFORMED STRUCTURES IN THE ^{145,146}Gd ISOTOPES

OSIRIS–COLLABORATION (KFA Jülich, HMI Berlin, Univ. Bonn, Univ. Köln)
ESSA 30–COLLABORATION (Univ. Bonn, Daresbury Lab., KFA Jülich,
Univ. Köln, Univ. Liverpool)
presented by W. Gast, Institut für Kernpyhsi, KFA Jülich
D-5170 Jülich, W.-Germany

The intrinsic configuration of specific structures like superdeformed (SD) bands in rotating nuclei can be investigated by studying their proton or (and) neutron dependence. For the A ≈ 150 region discrete superdeformed bands are already known in the ^{148}Gd [1], ^{149}Gd [2] and ^{150}Gd [3] isotopes. In our work we extend these investigations to lighter isotopes.

A first indication for the existence of discrete superdeformed bands in ^{145,146}Gd we obtain from an experiment done at Daresbury using the ESSA 30 spectrometer. By bombarding a stack of ^{102}Ru targets with a ^{48}Ca beam of 205 MeV we populated Gd and collected 600 Mio. double– and 80 Mio. triple events. The big number of triples allowed us to perform an off–line analysis where we make use of the pronounced

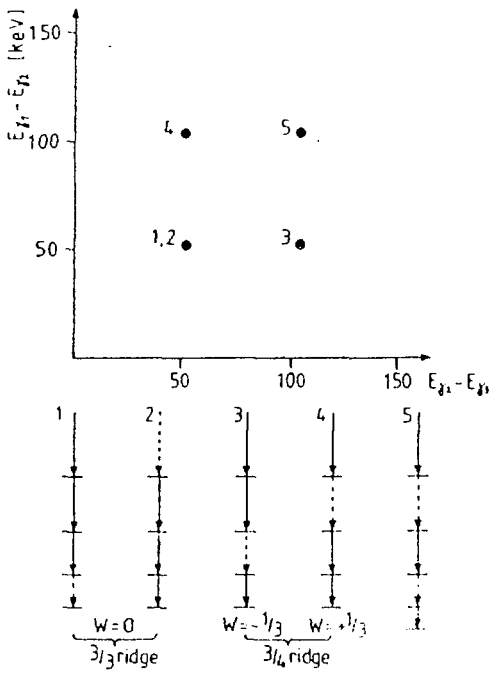

Fig. 1:
Schematic correlation matrix of energy differences of triple events from the decay of a SD band and definition of a dimensionless parameter W characterizing rotational sequences in a 3–fold coincidence space (c.f. ref. 9). Dashed lines denote unobserved transitions. For $E\gamma_1 > E\gamma_2 > E\gamma_3$

$$W = \frac{(E\gamma_1 - E\gamma_2) - (E\gamma_2 - E\gamma_3)}{(E\gamma_1 - E\gamma_2) + (E\gamma_2 - E\gamma_3)}$$

energy correlations of SD bands. That is, if we rearrange in our triple events the energy parameters in such a way that parameter 1 always contains the lowest and parameter 3 the highest energy, we can construct a correlation matrix from energy differences instead from absolute energies. In such a matrix superdeformed structures should be enhanced since in SD bands the energy difference between neighbouring transitions is nearly constant and hence they are accumulated at fixed positions (c.f. Fig. 1). Transitions following this SD pattern can easily be projected out of this matrix by putting 2-dim. gates on the correlation peaks and sorting the corresponding energies into an 1-dim. spectrum. The result of such an analysis for our data is shown in Fig. 2). Indeed one observes several sequences of transitions which show the expected behaviour, three of them are marked by their energies. However, in order to establish these sequences as SD bands one has to prove that the transitions are fast and in coincidence with each other. Unfortunately, the low statistics of the triples data did not allow to prove the individual coincidence relations and the 2-fold coincidences were too much contaminated by strong low multiplicity transitions, which could not be suppressed due to the missing multiplicity filter detector of the ESSA 30 setup.

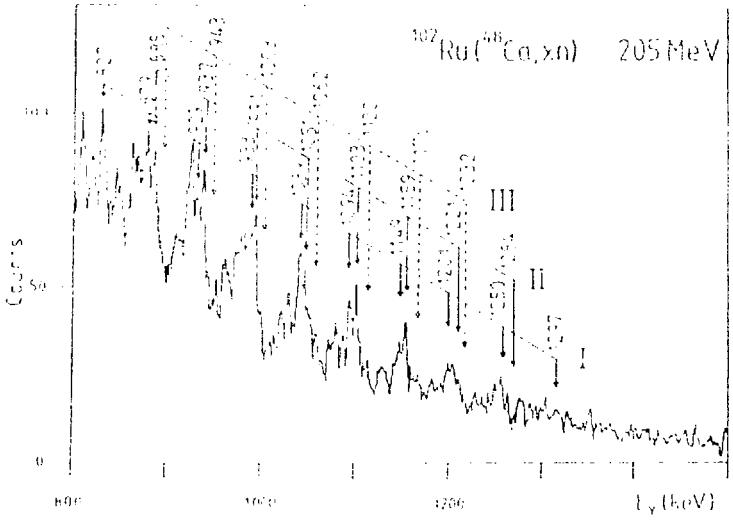

Fig. 2:
Projection of γ-transitions gated on the 2-dim. correlation peaks of superdeformed structures observed in the correlation matrix of energy differences in triple events.

Therefore we repeated the experiment at the VICKSI accelerator of the HMI, Berlin, using the ^{100}Pd (^{40}Ar,xn) reaction. The γ-radiation was measured with the OSIRIS spectrometer consisting of 12 Compton-suppressed Ge detectors and an inner ball of 48 bismuth germanate (BGO) scintillators acting as a γ-ray multipli-

city and sum–energy filter. We carried out two experiments:

(i) To study the coincidence correlations of the fast SD transitions with optimal energy resolution we bombarded two self–supporting Pd foils of 0.5 mg/cm² thickness with a 175 MeV Ar beam. We stopped the recoiling nuclei 15 mm downstream from the target in a ^{197}Au foil of 8 mg/cm² to detect the prompt and delayed γ–radiation with the BGO filter but only prompt radiation with the Ge detectors. In this way we obtained the correct γ–ray multiplicity and sum–energy information despite the isomers existing in Gd [4] but reduced the background in the Ge detectors. From the analysis of the 250 Mio. double and 10 Mio. triple events we could establish at least one discrete band consisting of 13 approximately equally spaced transitions between 826.7 and 1448.3 keV. The resulting sum spectrum which corresponds to sequence I of Fig. 2) is shown in Fig. 3). From individual coincidence spectra we could prove that each transition up to that of 1345.7 keV is in coincidence with the other members of the band The last two transitions have been assigned from the sum spectrum.

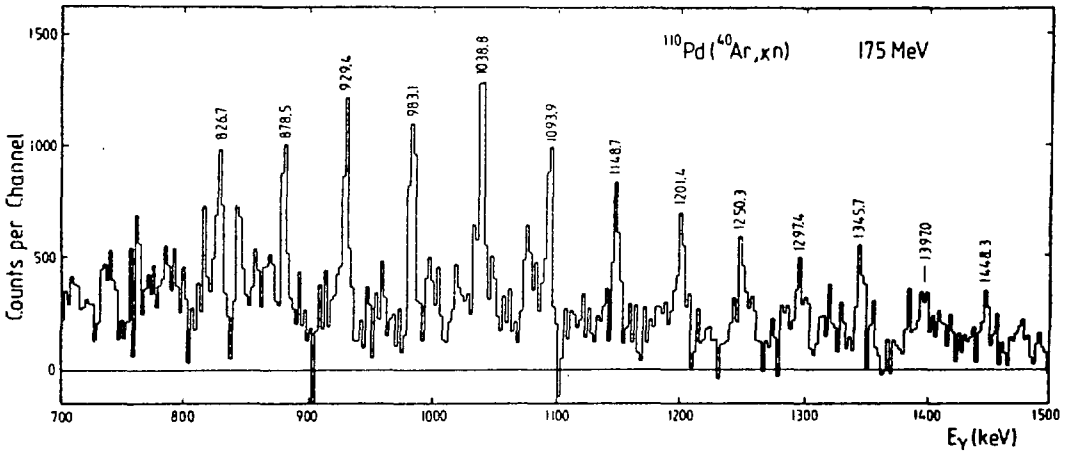

Fig. 3:
Gamma–ray spectrum obtained from the ^{110}Pd(^{40}Ar,xn) reaction at 175 MeV beam energy by summation of spectra gated on ten members of the SD band.

ii) Lifetime information for this band was obtained from an experiment with a backed target at a beam energy of 180 MeV. The target consisted of a 1.2 mg/cm² thick Pd foil backed by a layer of 18 m/cm² ^{197}Au. Using the DSA method [5] the fractions of full Doppler shift $F = v/v_0$, with an initial recoil

velocity of $v_0 = 0.026c$, were extracted from the data up to the 1297.4 keV transition. The F factor of the 1345.7 keV transition could be determined from the thin–target experiment. The F factor has been converted to the effective lifetime utilizing a velocity distribution of the recoiling nuclei which was calculated by a Monte Carlo method [6]. The effective lifetimes are increasing smoothly with decreasing transition energy as expected for a SD band. To determine the average quadrupole moment theoretical F factors have been calculated [7] assuming a constant quadrupole moment and prompt side feeding into the seven high–spin members of the band taking into account the experimental intensity distribution (Fig. 4a). A comparision with the experimental results (cf. Fig. 4b) yields a quadrupole moment of $Q_0 = 12 \pm 2$ eb. [8].

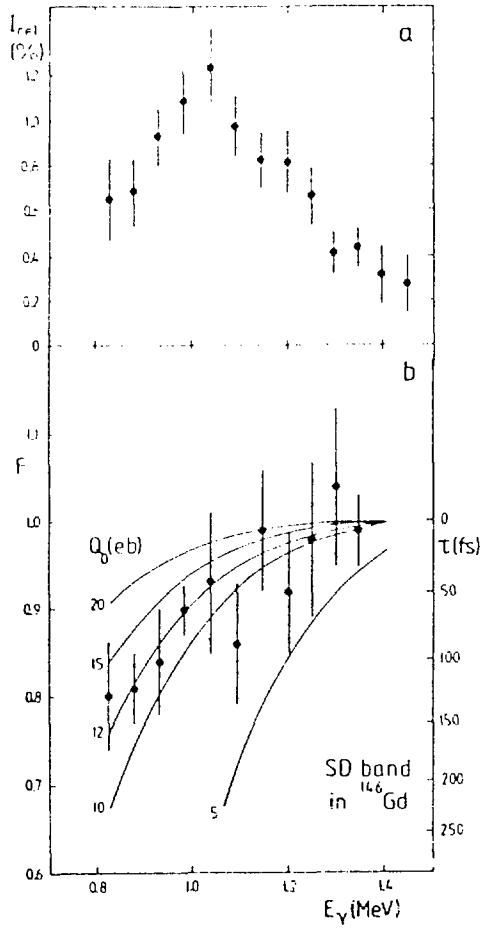

Fig. 4:

a) Relative intensities of SD transitions normalized to the ground–state transition of ^{146}Gd.

b) Experimental fractions of full Doppler shift for the SD transitions. Calculated values are given as solid lines for various quadrupole moments.

After we successfully established one of the sequences showing up in the triples data as superdeformed band we started a search for the other sequences. But, although some of them are of comparable intensity in the triples projection (cf. Fig. 2), we were not able to prove their SD band structure from the data discussed up to now. However, meanwhile we performed two further experiments to study superdeformation in Gd where we used the same targets and the same setup, but increased the bombarding energy for the thin target to 190 MeV and for the backed target to 200 MeV. The data analysis is still in progress but preliminary results indicate that at least two of the additional sequences, denoted as II and III in Fig. 2 are populated in these experiments. The corresponding sum spectra are shown in Fig. 5 together with some individual coincidence spectra by which we prove that they indeed form bands. From the DSA analysis of the backed target experiment we hope to be able to extract the lifetime information.

In summary, we established a discrete SD band in Gd consisting of 13 transitions with a quadrupole moment of $Q_0 = 12 \pm 2$ eb. Indications for at least two additional sequences of SD structure have been observed. We have shown that the triples analysis presented at the beginning is a very powerful and sensitive method to detect SD collective correlations in nuclei. However, with regard to the quality of the spectra presented here, which is not untypical for many experiments of this type using state of the art spectrometers, we have also shown, that we are approaching the limits of our present day technology. We have to sharpen our spectroscopic tools to be able to explore this new exciting field of nuclear spectroscopy in secondary minima. Actually this is one of the ideas leading to the establishment of the EUROBALL collaboration.

REFERENCES

[1] M.A. Deleplanque et al., Phys. Rev. Lett. 60 (1988) 1626

[2] B. Haas et al., Phys. Rev. Lett. 60 (1988) 503

[3] P. Fallon et al., Phys. Lett. B218 (1989) 137

[4] R. Broda et al., Z. Phys. A285 (1978) 423

[5] P.J. Nolan and J.F. Sharpey-Schäfer, Rep. Prog. Phys. 42 (1979) 1

[6] J. Bacelar, private communication

[7] G. Hebbinghaus et al., Phys. Rev. Lett. 59 (1987) 2024

[8] G. Hebbinghaus et al. Phys. Lett. B240 (1990) 311

[9] B. Mottelson, Contribution to the Workshop On Nuclear Structure, Kopenhagen (1988)

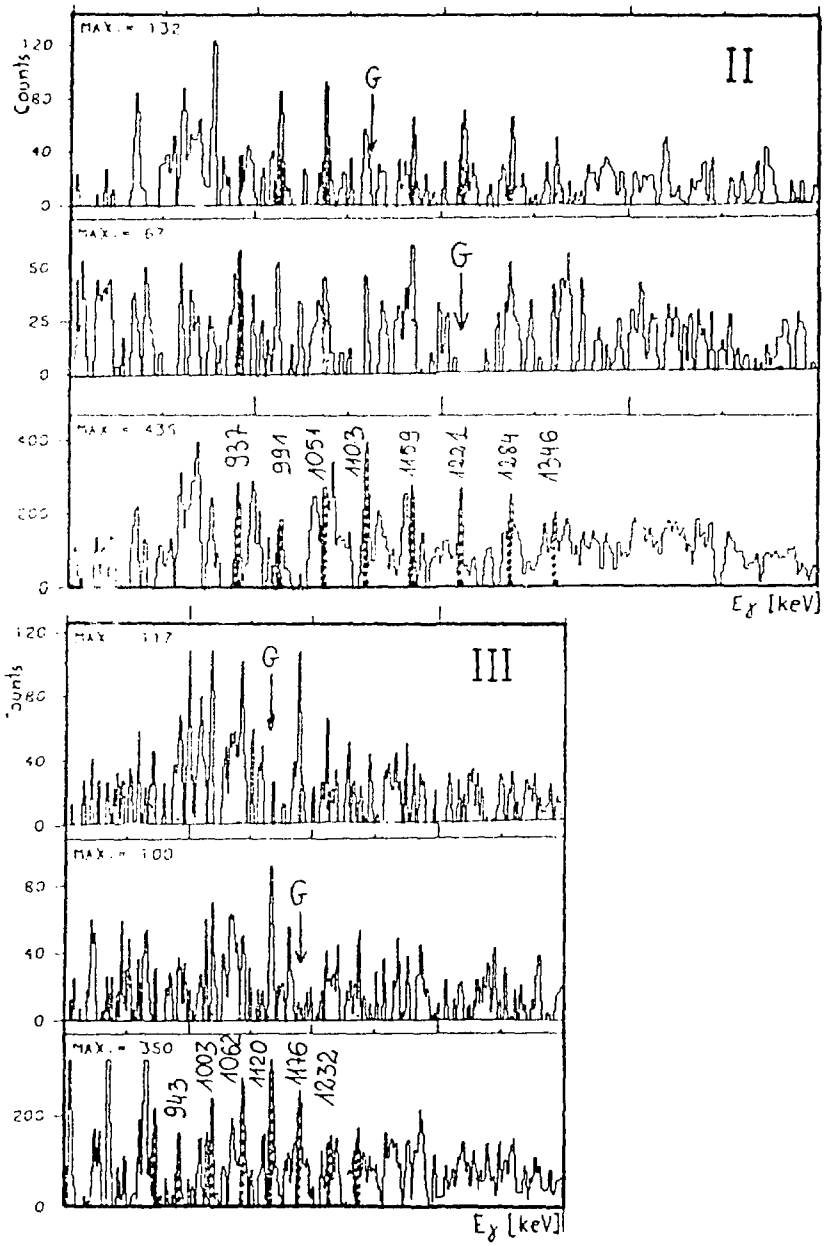

Fig. 5:
Sum–spectra of cuts on SD structures observed in the $^{110}Pd(^{40}Ar,xn)$ reaction at 190 MeV beam energy together with some representative spectra gated on individual transitions.

STRUCTURE OF ODD-ODD Sb AND In NUCLEI

T. Fényes, Zs. Dombrádi and Z. Gácsi
Institute of Nuclear Research of the Hungarian Academy of Sciences, Debrecen, Hungary

ABSTRACT

The level structure of ^{118,116}Sb and ^{114,112,110}In, ^{108,106}In nuclei was studied with complex γ- and e$^-$-spectroscopic methods via (p,nγ) and in some cases (α,nγ) reactions at different bombarding particle energies between 5 and 17 MeV. Large amount of spectroscopic information has been obtained and significantly extended level schemes have been deduced.

The energy spectra and electromagnetic properties of ^{116}Sb, ^{116,114,112,110,108,106}In nuclei were calculated in the framework of the interacting boson-fermion-fermion / odd-odd truncated quadrupole phonon model (IBFFM/OTQM). Numerous p-n multiplet members have been identified. The main systematic trends and observed nuclear structure anomalies have been reasonably described by the theory.

1. EXPERIMENTAL TECHNIQUES

Enriched stable isotopes of Ag, Cd, In, and Sn were bombarded with p and α beams of small size isochronous cyclotrons. γ-ray spectra (E_γ, I_p), γγ coincidences, internal conversion electron spectra, γ-ray angular distributions, lifetimes of excited levels, and relative reaction cross sections [$\sigma_{rel}(E_{LEV})$] were measured at different bombarding particle energies. Ge(HP), Ge(LEPS), and Si(Li) detectors, superconducting and conventional magnetic lens, as well as miniorange electron spectrometers were used in the experiments. Level schemes, energies (E_{LEV}), spins, parities, γ-branching ratios, and γ-mixing ratios have been deduced. The spins have been determined on the basis of Hauser-Feshbach analysis, internal conversion coefficients of transitions, and γ-ray angular distribution data.

2. EXPERIMENTAL AND THEORETICAL RESULTS: Sb NUCLEI

The level scheme of ^{116}Sb is compared with the results of parabolic rule calculations in fig. 1. The experimental data in column (d) are given on the basis of our (p,nγ) and (α,nγ) reaction results [1,2], with the exception of configurations. The latters are based on the (^{3}He,d) proton transfer reaction study of Kamermans et al. [3]; only components having large spectroscopic factors are shown.

The parabolic rule [4] predicts the energy splitting of proton-neutron multiplets as a function of J(J+1), where J is the spin of the state. Using $\alpha_2^0 \approx 5.4$ MeV quadrupole and $\alpha_1^0 \approx 15/A = 0.13$ MeV spin-vibrational interaction strengths, as well as occupation probabilities (V^2) of subshells taken from the systematics of experimental data, the energy splitting of more than six p-n multiplets could be described reasonably well. At each multiplet we used one overall normalization term, which pushed up (or down) all members of the given multiplet with the same energy.

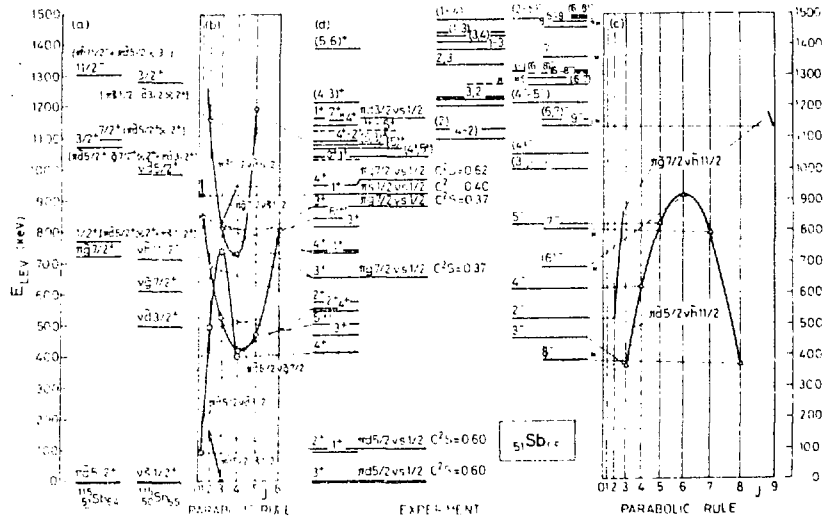

Fig. 1. p-n multiplet states in ^{116}Sb. (a) Experimental level energies and configurations of the low-lying states of ^{115}Sb and ^{115}Sn nuclei. (b) and (c) Results of the parabolic rule calculation. (d) Experimental results on ^{116}Sb.* indicates the members of high-spin level scheme based on the 8^- isomeric state.

Between the neighbouring J and J+1 members of the same p-n multiplet one can expect M1 transitions. The majority of them have been observed experimentally.

As seen in fig. 1 many members of the $\pi\tilde{d}_{5/2}\nu\tilde{s}_{1/2}$, $\pi\tilde{d}_{5/2}\nu\tilde{d}_{3/2}$, $\pi\tilde{d}_{5/2}\nu\tilde{g}_{7/2}$, $\pi\tilde{g}_{7/2}\nu\tilde{s}_{1/2}$, $\pi\tilde{d}_{5/2}\nu\tilde{d}_{5/2}$, $\pi\tilde{s}_{1/2}\nu\tilde{s}_{1/2}$, $\pi\tilde{d}_{5/2}\nu\tilde{h}_{11/2}$, $\pi\tilde{g}_{7/2}\nu\tilde{h}_{11/2}$ multiplets could be identified. In the 3_3^+ and 3_5^+ states the $\pi\tilde{g}_{7/2}\nu\tilde{s}_{1/2}$ and $\pi\tilde{d}_{5/2}\nu\tilde{d}_{3/2}$ components are strongly mixed.

In order to get a deeper insight into the structure of the low-lying states of ^{116}Sb we have calculated the energies and electromagnetic properties of the states on the basis of truncated quadrupole phonon model for odd-odd nuclei [5]. This model is equivalent with the interactig boson-fermion-fermion model on phenomenological level.

The Hamiltonian of the model is

$$H_{OTQM} = H_{TQM} + \sum_{i=p,n} H^i + \sum_{i=p,n} H^i_{PVI} + H^{pn}_{EFF},$$

where H_{OTQM} is the SU(6) quadrupole phonon Hamiltonian of the even-even core, H^i denotes the Hamiltonian of the odd proton and odd neutron in a spherical potential, and H^i_{PVI} is the Hamiltonian of the particle-vibration interaction. It contains three terms, the monopole, dynamical and exchange interactions. H^{pn}_{EFF} is the Hamiltonian of the effective p-n interaction. We have considered only central delta force and spin-spin interaction of the form

$$H^{pn}_{EFF} = 4\pi\delta(\vec{r}_p - \vec{r}_n)\,[v_D + v_S\boldsymbol{\sigma}_p.\boldsymbol{\sigma}_n] + V_{\sigma\sigma}(\boldsymbol{\sigma}_p.\boldsymbol{\sigma}_n).$$

The OTQM Hamiltonian was diagonalized in the proton-quasineutron weak coupling basis $|(j_p j_n)I, NR; J\rangle$, where I is the resulting angular momentum of j_p and j_n states, R is the angular momentum of the N-phonon state, and J is the total angular momentum.

The computer code IBFFM/OTQM used in the calculations was written by Brant, Paar and Vretenar [6].

Details of calculation are described in ref. [2].

The experimental and theoretical level schemes of the low-lying positive parity states of ^{116}Sb are shown in fig. 2.

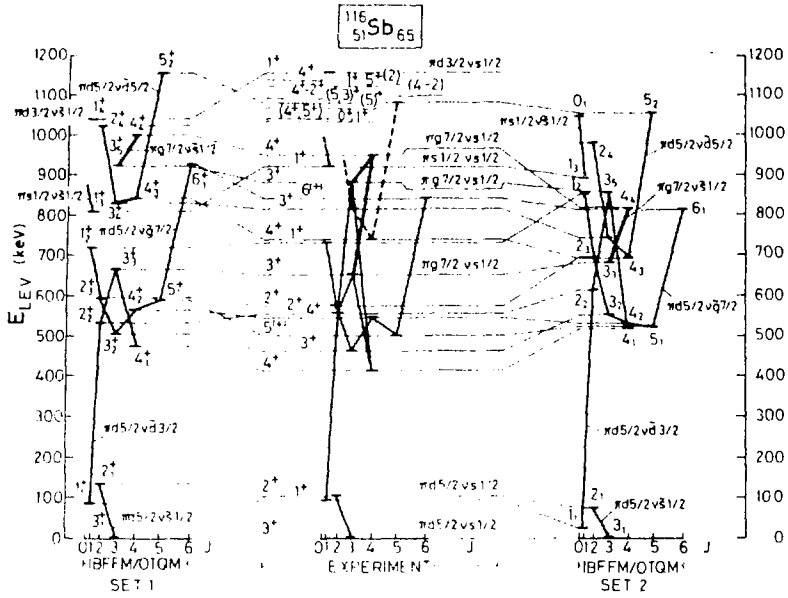

Fig. 2. IBFFM/OTQM theoretical level spectrum of ^{116}Sb in comparison with experimental data. The solid lines connect the members of the given multiplet. Set 1 and Set 2 refer to different parametrizations.

The IBFFM/OTQM calculations preserved the approximate classification of the parabolic rule. For example the 2_1^+ and 3_1^+ states are dominated by components with $\pi d_{5/2}\nu\tilde{s}_{1/2}$ configuration, the 1_2^+, 2_3^+, 3_2^+, 4_2^+, 5_1^+, 6_1^+ states by components with $\pi d_{5/2}\nu\tilde{g}_{7/2}$ configuration etc.

The magnetic dipole moments are known for the 3_1^+ ground and 1_1^+ excited states: $|\mu_{exp}(3_1^+)| = 2.715(9)\mu_N$ and $\mu_{exp}(1_1^+) = +\ 2.47(9)\mu_N$ [7]. The corresponding theoretical values (for set 1 calculations) are $\mu_{IBFFM}(3_1^+) = +\ 2.79\ \mu_N$ and $\mu_{IBFFM}(1_1^+) = +\ 2.30\ \mu_N$, they agree with the experimental ones within 7 %.

The γ-branching ratios and γ-mixing ratios have also been calculated, they show also reasonable agreement with the corresponding experimental values [2].

From (p,nγ) and (α,nγ) reactions we have obtained preliminary level schemes for ^{118}Sb, too [8].

3. EXPERIMENTAL AND THEORETICAL RESULTS: In NUCLEI

The results obtained on odd-odd In nuclei have been published in the following papers: ^{116}In [9], ^{114}In [10], ^{112}In [11], ^{110}In [12, 13], ^{108}In [14], and ^{106}In [15].

The energy splitting of two p-n multiplets of the odd-odd In nuclei is shown in fig. 3.

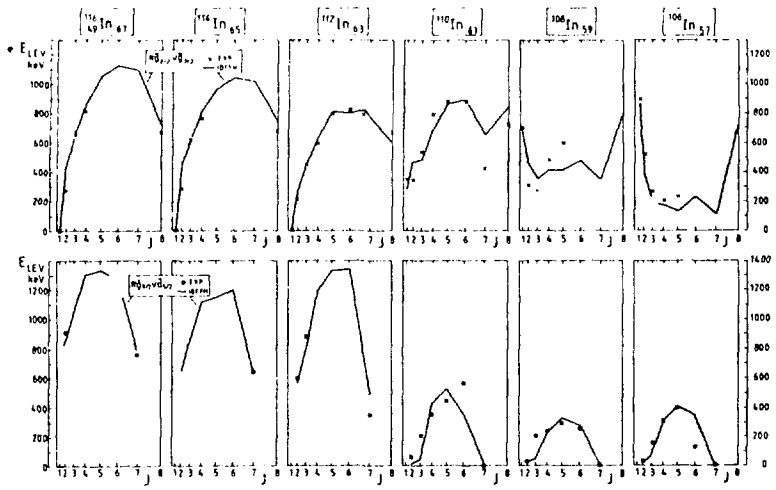

Fig. 3. The energy splitting of the $\pi g_{9/2}\nu\tilde{g}_{7/2}$ and $\pi g_{9/2}\nu\tilde{d}_{5/2}$ multiplets in the odd-odd In nuclei, as a function of J(J+1), where J is the spin of the state.

It is interesting that the shape of energy-splitting of the $\pi g_{9/2}\nu\tilde{g}_{7/2}$ multiplet changes from an open-down parabola in $^{116, 114, 112}$In, through a W-like pattern in ^{108}In, to a (distorted) open-up parabola in ^{106}In. The IBFFM/OTQM calculations could give a resonable description of this change. The inversion is caused by the fact, that the $\tilde{g}_{7/2}$ quasineutron is hole-like in ^{116}In and particle-like in ^{106}In. The W-like distorsion of the parabola is caused by the exchange interaction. The dynamical interaction is strong near $V_\nu^2 = 0$ or 1, and weak near $V_\nu^2 = 0.5$; while the exchange interaction plays an important role only around Fermi level ($V_\nu^2 = 0.5$). The increased strength of exchange interaction points out the increased role of Pauli principle in $^{110, 108}$In.

The experimental magnetic dipole and electric quadrupole moments are compared in fig. 4. The sign of the moments was properly reproduced in all cases. The μ_{exp} and μ_{IBFFM} values agree within a few %. The IBFFM calculations show that the contribution of the collective electromagnetic operator is relatively small to the magnetic dipole moments, and is significant to the Q values.

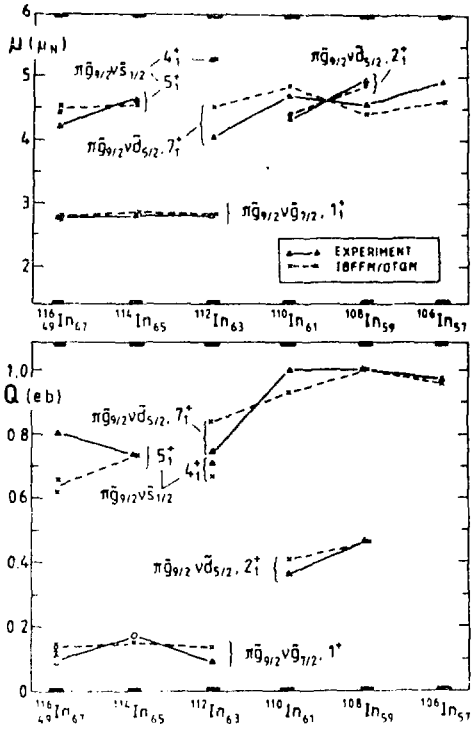

Fig. 4. Experimental [7] and IBFFM/OTQM electromagnetic moments of odd-odd $^{116-106}$In nuclei.

REFERENCES

[1] Z. Gácsi et al., to be published in Phys. Rev. C
[2] Z. Gácsi et al., to be published in Phys. Rev. C
[3] R. Kamermans et al., Phys. Rev. C 17 (1978) 1555
[4] V. Paar, Nucl. Phys. A331 (1979) 16
[5] V. Paar, in In-Beam Nuclear Spectroscopy, ed. Zs. Dombrádi and T. Fényes, vol. 2, p. 675 (Akad. Kiadó, Budapest, 1984)
[6] S. Brant, V. Paar, and D. Vretenar, IKP Jülich, 1985, unpublished
[7] P. Raghavan, Atomic Data and Nuclear Data Tables 42 (1989) 189
[8] J. Gulyás et al., unpublished
[9] T. Fényes and Zs. Dombrádi, Acta Phys. Hung. 65 (1989) 295
[10] J. Timár et al., Nucl. Phys. A455 (1986) 477
[11] T. Kibédi et al., Phys. Rev. C 37 (1988) 2391
[12] A. Krasznahorkay et al., Nucl. Phys. A473 (1987) 471
[13] A. Krasznahorkay et al., Nucl. Phys. A503 (1989) 113
[14] A. Krasznahorkay et al., Nucl. Phys. A499 (1989) 453
[15] J. Gulyás et al., Nucl. Phys. A506 (1990) 196

ARE THERE β- and γ-BANDS IN TRANSITIONAL NUCLEI?

A. Gelberg[1,2], D. Lieberz[1], W. Lieberz[1], P. von Brentano[1], T. Otsuka[3] and M. Sugita[2]

[1] Institut für Kernphysik der Universität zu Köln, D-5000 Köln, Fed. Rep. Germany
[2] Japan Atomic Energy Research Institute, Tokai, Ibaraki 319-11, Japan
[3] Department of Physics, University of Tokyo, Bunkyo-ku, Tokyo 113, Japan

Abstract: A comparison of the O(6)-limit of the IBM and of the triaxial rotor model with β-vibration has been carried out for the nucleus ^{126}Xe. The comparison has been extended to include the Rotation Vibration model. In conclusion it was found that the 0_2^+ and 2_2^+ states in transitional nuclei can not be interpreted as β- and γ-band heads respectively.

The Interacting Boson Model (IBM) [1] provides an algebraic description of collective nuclear motion. It is the object of this talk to examine some properties of the O(6) dynamic symmetry as applied to the mass region around A=130 and to carry out a comparison with collective geometric models, in particular with the Triaxial Rotor Model (TRM) [2,3]. We will address the question whether it is appropriate to talk about quasi-β- and quasi-γ-bands in this region.
It has been observed in ref. [4] that the O(6)-limit of IBM is able to describe important experimental features of Xe, Ba and Ce nuclei around A=130.
The O(6) dynamic symmetry is based on the group chain

$$\begin{array}{ccccccc} U(6) & \supset & O(6) & \supset & O(5) & \supset & O(3) \\ N & & \sigma & & \tau & & L \end{array} \qquad (1)$$

The quantum numbers written under each group label the irreps. N is the total boson number; σ and τ label the irrep. of U(6) and O(5) respectively. L is the total angular momentum. Only s- and d-bosons are considered.
The energy eigenvalues can be expressed as a sum of Casimir operators leading to

$$E = \frac{1}{4}A(N-\sigma)(N+\sigma+4) + \frac{1}{6}B\tau(\tau+3) + CL(L+1) \qquad (2)$$

The E2 transition operator has the form

$$T(E2) = q\{(d^\dagger\tilde{s} + s^\dagger\tilde{d}) + \chi[d^\dagger\tilde{d}]^{(2)}\} \qquad (3)$$

Following P. van Isacker [5] we relax the condition χ=0 imposed in ref. [1]. If χ=0 only transitions with $\Delta\tau=\pm1$, $\Delta\sigma=0$ are allowed. The second term of (3) generates transitions which follow the selection rule $\Delta\tau=0,\pm2$. These transitions are generally weaker ("O(6) forbidden transitions").

A comparison of excitation energies in ^{126}Xe with those calculated from (2) is shown in fig. 1 [6]. States belonging to the O(6) irreps. σ=N and σ=N-2 can be recognized. Experimental and theoretical B(E2) ratios are given in table 1. A more extensive comparison can be found in ref. [6]. At large boson number the B(E2) ratios inside the σ=N irrep. are identical to those of the γ-soft rotor of L. Wilets and M. Jean [7,8,9]. The connexion to geometric models can be investigated by introducing an intrinsic boson [10].

$$b_c^\dagger(\beta,\gamma) = (1+\beta^2)^{-1}[\beta\cos\gamma d_0^\dagger + \frac{1}{\sqrt{2}}\beta\sin\gamma(d_2^\dagger + d_{-2}^\dagger) + s^\dagger] \tag{4}$$

and an intrinsic state (boson condensate)

$$|c;\beta\gamma> = (N!)^{-1/2}(b_c^\dagger)^N|0> \tag{5}$$

where β and γ are the deformation parameters. An energy surface can be defined

$$E_N(\beta,\gamma) = < c;\beta\gamma|H|c;\beta\gamma> \tag{6}$$

where H is the IBM Hamiltonian.
If an O(6) type Hamiltonian is chosen, $E_N(\beta,\gamma)$ is independent of γ, hence the similarity to the γ-soft rotor becomes obvious; in this case β=1.
However, if the average in (6) is taken in an angular momentum projected state [11], e.g. in the ground state, E_N has a rather shallow minimum at 30°. If a "slice" with γ=30° is cut out of the wave function the analogue of a rigid triaxial rotor is created [12]. At small boson number, e.g. N$\leq$10, this object has a good overlap with the correct O(6) eigenstate. On the contrary, for large N$\geq$20, the overlap decreases. The energy spectrum at large N becomes identical to that of the Davydov-Filippov rigid triaxial rotor. Therefore we can consider the latter as being similar to the classical limit of an O(6) nucleus in which a value γ=30° has been cut out of the interval $0° \leq \gamma \leq 60°$. Therefore we can expect an analogy between O(6) and triaxial rotor with γ=30° but certainly no identity [13].
While the rigid triaxial rotor has no excited 0^+ state, a version including β vibrations has been developed by Davydov and Chaban [3]. We tried to fit the levels in ^{126}Xe by this model. As one can see from table 1, some branching ratios which are correctly obtained from O(6)-IBM are in disagreement with the TRM calculation. In particular, the 0_2^+ state of the TRM should decay to the ground state 2_1^+. In reality the former decays to the 2_2^+ state and the IBM correctly reproduces this feature. Therefore the 0_2^+ state is not the quasi-β-band head.
In the IBM this state belongs to the lowest O(6) irrep. with σ=N, and it is characterized by τ=3, ν_Δ=1, where the latter counts the number of boson triplets coupled to L=0. This state can be obtained by angular momentum projection from the intrinsic state (5); as a matter of fact all states with N=σ can be obtained in this wav. From the viewpoint of the IBM, the 0_2^+ state in transitional nuclei is not an intrinsic excitation, but a collective one (see A. Leviatan [14]).
The β- and γ-intrinsic excitations can be described by introducing nonspherical bosons [14]. In particular in the O(6) case one can use

$$b_\beta^\dagger = \frac{1}{\sqrt{2}}(d_0^\dagger - s^\dagger) \tag{7}$$

If the O(6)-paired bosons are introduced through

$$S^+ = \frac{1}{2}[d^\dagger d^\dagger - (s^\dagger)^2] \equiv (S^-)^\dagger, \tag{8}$$

It can be shown [14] that an intrinsic state containing β-bosons has the form

$$|\mathrm{N n_\beta}> = N_{\mathrm{N n_\beta}}(S^+)^{\mathrm{n_\beta}}(b_c)^{\mathrm{N-2n_\beta}}|0> \tag{9}$$

where $N_{\mathrm{N n_\beta}}$ is a normalization factor and

$$\mathrm{n_\beta} = \frac{\mathrm{N} - \sigma}{2} \tag{10}$$

In the large N limit is $S^+ \approx b_c^\dagger b_\beta^\dagger$ and

$$|\mathrm{N n_\beta}> = N_{\mathrm{N n_\beta}}(b_c^\dagger)^{\mathrm{N-n_\beta}}(b_\beta^\dagger)^{\mathrm{n_\beta}}|0> \tag{11}$$

i.e. $\mathrm{n_\beta}$ condensate bosons have been replaced by β-bosons.
According to (11) one can expect the σ=N-2, τ=0, 0_3^+ state to have the properties of the β-band head. The 0_3^+ state has been observed in ^{128}Xe but only in a transfer reaction and its decay properties are unknown. On the contrary there is no intrinsic γ-excitation in the O(6) limit [14]. In this case the nonspherical γ-boson represents a spurious excitation. The absence of a γ-vibration is a consequence of the γ-independence of the potential. This means that we must consider the band based on 2_2^+ as a collective and not an intrinsic excitation. It would be correct to call it an O(5) rotation. This excitation appears as soon as the axial symmetry is removed.
A comparison was carried out with a model whose potential included harmonic vibrational terms in the β and γ variables, viz. the Rotation Vibration Model (RVM) [15] of A. Fässler and W. Greiner. The model Hamiltonian is diagonalized on a basis with quantum numbers K, $\mathrm{n_\beta}$ and $\mathrm{n_2}$, the latter is related to γ-vibrations [15]. A fit of energy levels is shown in fig. 2. The quality of the fit is comparable to that of the IBM. One can notice that also in this model it is the 0_3^+ state which has one β-phonon. One can also compare the quantum numbers of the two models. We noticed that the values of ν_Δ on one hand and $\mathrm{n_2}$ on the other hand are the same. There is a qualitative explanation to this coincidence. As a consequence of the O(5) symmetry, the γ dependence of the wave function of L = 0 states is given by a Legendre polynomial $\mathrm{P}_{\nu_\Delta}(\cos 3\gamma)$ [12,16]. Therefore ν_Δ actually counts the number of nodes in the $0° \leq \gamma \leq 60°$ interval. Since $\mathrm{n_2}$ plays the role of a radial quantum number in the RVM, it also determines the number of nodes.

The authors would like to thank S.G. Rohoziński and J. Srebrny for interesting discussions. This work was funded by the BMFT under contract No. 06OK272. One of the authors (A.G.) would like to thank the Physics Department of JAERI for support.

References

[1] F. Iachello and A. Arima, the Interacting Boson Model, Cambridge University Press, 1987
[2] A.S. Davydov and G.F. Filippov, Nucl. Phys. 8, 237 (1958)
[3] A.S. Davydov and A.S. Chaban, Nucl. Phys. 20, 499 (1960)
[4] R.F. Casten and P. von Brentano, Phys. Lett. B152, 22 (1985)
[5] P. van Isacker, Nucl. Phys. A465, 497 (1987)
[6] W. Lieberz et al., Phys. Lett. B240, 38 (1990)
[7] L. Wilets and M. Jean, Phys. Rev. 102, 788 (1956)
[8] J. Meyer-Ter-Vehn, Phys. Lett. B84, 10 (1979)
[9] R.F. Casten and J.A. Cizewski Nucl. Phys. A309, 477 (1978)
[10] J. Ginocchio and M. Kirson, Nucl. Phys. A350, 31 (1980)
[11] J. Dobes, Phys. Lett. B158, 97 (1985)
[12] T. Otsuka and M. Sugita, Phys. Rev. Lett. 59, 1541 (1987)
[13] M. Sugita, T. Otsuka and A. Gelberg, Nucl. Phys. A493, 350 (1989)
[14] A. Leviatan, Ann. Phys. 179, 201 (1987)
[15] J.M.Eisenberg and W. Greiner, Nuclear Models, Vol. 1 (North Holland, Amsterdam 1987)
[16] E. Chacon, M. Moshinsky and R.T. Sharp, J. Math. Phys. 17, 668 (1976)

Table 1: "B(E2)"-ratios in ^{126}Xe. The experimental ratios based on the intensities divided by E_γ^5, so that these ratios are B(E2)-ratios in the strict sense only if either no M1-parts are involved or are taken into account (marked with [a]). Any undetected M1-portion will lower the experimental ratios (exception: 4_3^+). [b]: B(E2)-ratios of the ARM within the band build on the one β-phonon excited 0^+-state, assuming that this band corresponds to the experimental "K=0"-band. B(E2)'s of $O(6)_\chi$ are calculated with $\chi = -0.5$ in (3).

			"B(E2)"-ratios					
level	spin	transition	exp.		O(6)	$O(6)_\chi$	ARM	RVM
879.9	2_2^+	$491.3 \rightarrow 2_1^+$	100	[a]	100	100	100	100
		$879.9 \rightarrow 0_1^+$	1.5 ± 0.4	[a]	0	1.5	1.9	8.6
1317.7	3_1^+	$375.7 \rightarrow 4_1^+$	34^{+10}_{-34}	[a]	40	40	39	31
		$437.8 \rightarrow 2_2^+$	100	[a]	100	100	100	100
		$929.0 \rightarrow 2_1^+$	$2.0^{+0.6}_{-1.7}$	[a]	0	2.0	2.1	8.3
1488.4	4_2^+	$546.4 \rightarrow 4_1^+$	76 ± 22	[a]	91	91	70	52
		$608.5 \rightarrow 2_2^+$	100	[a]	100	100	100	100
		$1099.8 \rightarrow 2_1^+$	0.4 ± 0.1	[a]	0	2.0	5.9	0.03
1903.5	5_1^+	$268.5 \rightarrow 6_1^+$	75 ± 23		45	45	58	31
		$415.1 \rightarrow 4_2^+$	76 ± 21		45	45	105	63
		$585.8 \rightarrow 3_1^+$	100	[a]	100	100	100	100
		$961.6 \rightarrow 4_1^+$	2.9 ± 0.8		0	2.0	0.02	2.8
1313.9	0_2^+	$434.0 \rightarrow 2_2^+$	100	[a]	100	100	100 [b]	100
		$925.3 \rightarrow 2_1^+$	7.7 ± 2.2	[a]	0	2.0	567 [b]	0.3
1678.5	2_3^+	$360.8 \rightarrow 3_1^+$	67 ± 25		125	125	5.5 [b]	69
		$364.2 \rightarrow 0_2^+$	100	[a]	100	100	100 [b]	100
		$736.4 \rightarrow 4_1^+$	2.0 ± 0.8	[a]	0	1.1	20 [b]	0.4
		$798.8 \rightarrow 2_2^+$	2.2 ± 1.0		0	3.5	5.6 [b]	11
		$1290.0 \rightarrow 2_1^+$	0.14 ± 0.06		0	0	6.9 [b]	0.04
		$1678.2 \rightarrow 0_1^+$	0.13 ± 0.04	[a]	0	0	4.4 [b]	0
2042.1	4_4^+	$363.4 \rightarrow 2_3^+$	100	[a]	100	100	100 [b]	100
		$1100.2 \rightarrow 4_1^+$	7.9 ± 3.4		0	0	3.4 [b]	0.08
		$1653.5 \rightarrow 2_1^+$	0.9 ± 0.4	[a]	0	0	3.4 [b]	0.02
1903.1	4_3^+	$414.8 \rightarrow 4_2^+$	100		100	100	100	100
		$585.3 \rightarrow 3_1^+$	43 ± 13		115	115	150	159
		$961.2 \rightarrow 4_1^+$	4.5 ± 1.4		0	0.4	12	24
		$1023.2 \rightarrow 2_2^+$	2.8 ± 0.9		0	2.5	75	4.3

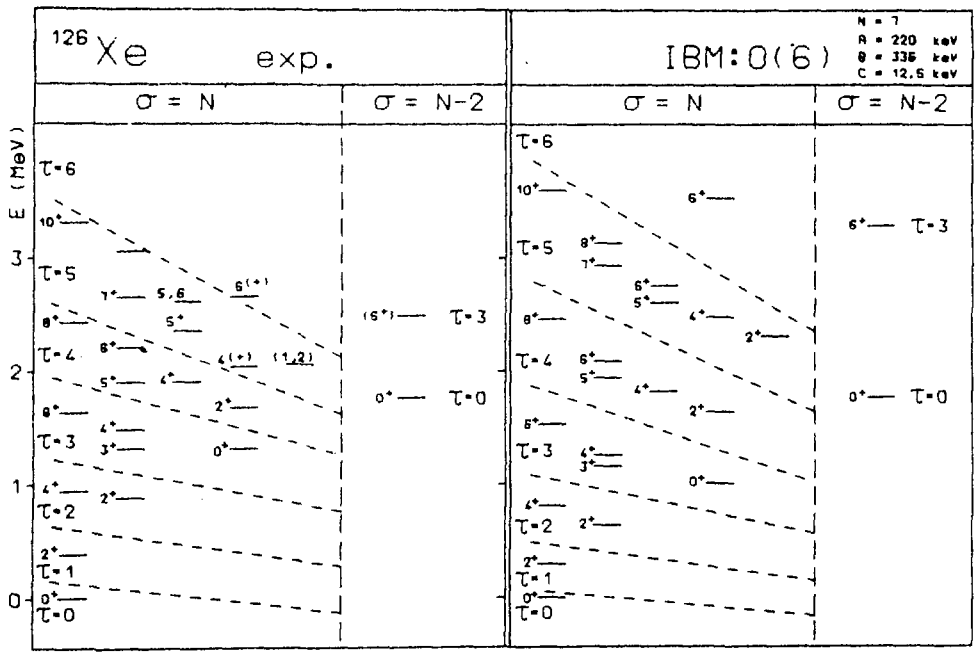

Fig. 1: Excitation energies in ^{126}Xe

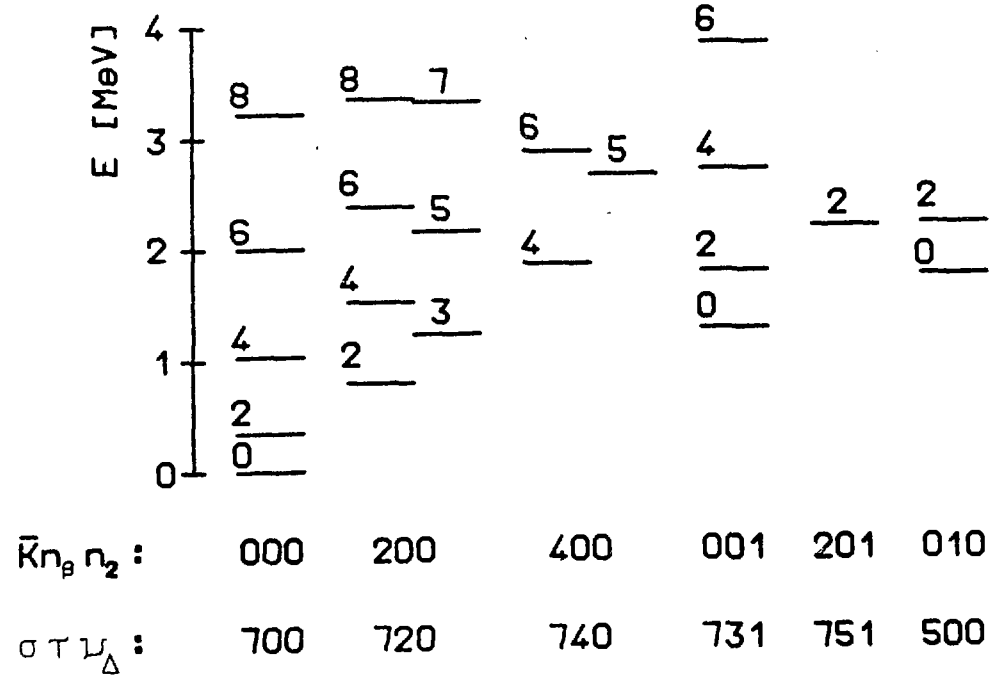

Fig. 2: Excitation energies in ^{126}Xe calculated with the RVM. The quantum numbers are given to bandheads.

HIGH SPIN STATES IN ^{131}Ce

M. PALACZ[1], Z. SUJKOWSKI[1], J. NYBERG[2],
J. BACELAR[3], J. JONGMAN[3], W. URBAN[3],
W. HESSELINK[4], J. NASSER[4], A. PLOMPEN[4]

[1] Soltan Institute for Nuclear Studies, Świerk, Poland
[2] The Niels Bohr Institute, University of Copenhagen, Denmark
[3] K.V.I, Groningen, The Netherlands
[4] V. U. Amsterdam, The Netherlands

Abstract. Gamma ray spectra from the ^{117}Sn(^{18}O,4n)^{131}Ce reaction have been studied with the NORDBALL array of 15 Compton-suppressed Ge detectors. States up to $I = 51/2\ \hbar$, $E \approx 8\ MeV$ are populated. Evidence is presented for bands built on three- and possibly five- quasiparticle configurations resulting from the alignment of $h_{11/2}$ neutrons.

Nuclei in the $A \sim 130$ region exhibit a variety of coexisting shapes at relatively low excitation energy and spin values. In particular strongly collective bands (SD bands) with $Q = 8 - 10\ eb$ and $\beta_2 \sim 0.4$ have recently been observed throughout the region [GOD, WAD87]. In spite of the relatively strong population of these bands there is as yet no firmly established link to the underlying less strongly deformed states. This suggests an effective fragmentation of the strength in the decay mode of the SD bands. A detailed knowledge of the "normal" band structures is needed to locate this strength.

One candidate for such an analysis is ^{131}Ce, where a strongly populated SD band of 14 transitions has been observed in the (^{36}S,5n) reaction [LUO87]. The band is also strongly fed in the (^{18}O,4n) reaction [NYB], even though the feeding occurs at lower spins. The quadrupole moment of this band has been determined to be $Q_0 \sim 6.0\ eb$ [HE90]. The band seems to depopulate mostly to the states with $I = (19/2 - 21/2)\ \hbar^-$ and $I = (15/2 - 17/2)\ \hbar^-$, $\beta_2 \sim 0.2$, but no transitions linking this band with less deformed states have been found.

Low lying states of both the positive and negative parity bands have earlier been established in ^{131}Ce up to $I = 27/2\ \hbar$ and $23/2\ \hbar$ respectively [GIZ77]. An extension of some of these bands to higher spins can be found in refs. [NOL82, NOL83].

The present work reports on the study of the ^{117}Sn(^{18}O,4n)^{131}Ce reaction done at the Tandem Accelerator Laboratory of the Niels Bohr Institute. A stack of three thin ($\sim 0.4\ mg/cm^2$) self supporting ^{117}Sn foils was bombarded with 85 MeV ^{18}O beam. The NORDBALL array of 15 Compton suppressed Ge spectrometers with a γ-ray multiplicity filter of 10 BaF_2 detectors was used [SLE89]. Coincidence events with at least two Ge and one BaF_2 detector firing were recorded in a list mode. About 10^8 events were collected. The quality of the data is illustrated in fig. 1 with examples of the gated γ-ray spectra, corrected for efficiency and for the Doppler shifts.

Fig. 2 presents the level scheme based on the coincidence relationships and on the earlier parity and spin assignments [GIZ79] of the lowest states. The levels are arranged into five bands of positive (II, III, IV) and negative (I, V) parity. There is evidence for linking transitions between systems of positive and negative parity; the linking chains are, however, incomplete. Likewise, there is a relatively strong cascade of transitions

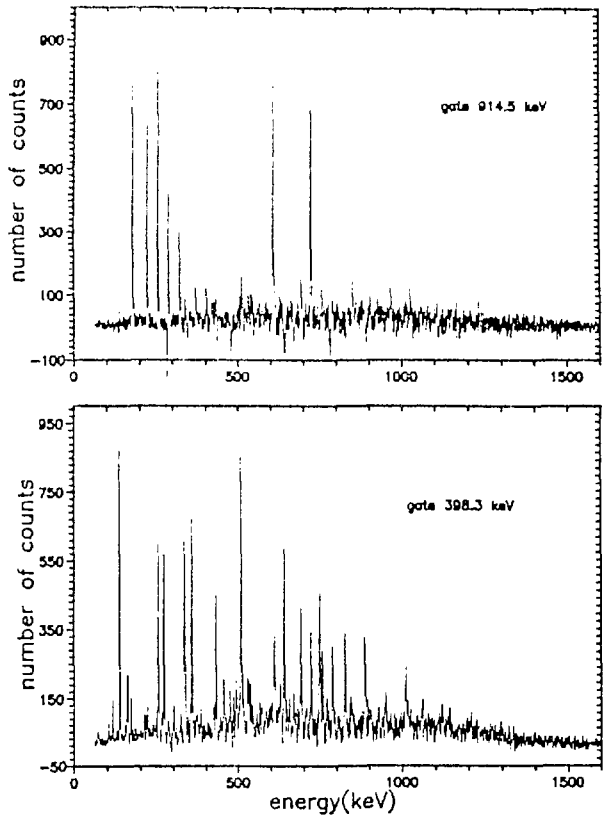

Fig. 1 Examples of the efficiency corrected $\gamma-\gamma$ coincidence spectra.

depopulating the lowest states of bands III, which by-pass the known levels and whose energies do not add up to the excitation energies of the levels in question. Transitions linking band V to band I do not support all the strength of band V, either. The incomplete depopulation paths are marked with dashed "hanging" arrows in fig. 2

In order to interpret the observed bands in terms of quasiparticle configurations the experimental alignments and routhians were calculated for bands I, II, III, IV, V. This was done using the method given by Bengtsson and Frauendorf [BEN79]. Harris parameters $J_0 = 13.4\ \hbar^2 MeV^{-1}$ and $J_1 = 39.1\ \hbar^4 MeV^{-3}$ were used. The K-value was assumed to be 7/2 for bands II, III, IV, V and 3/2 for band I. The results of calculations are shown in fig. 3, together with the proposed assignments of quasi-particle configurations.

In the negative parity part of decay scheme, the lowest, yrast cascade is typical for $\nu h_{11/2}$ orbital with large triaxiality ($\gamma \sim -20^\circ$) causing large signature splitting. Similar bands have been observed throughout the region [ARY84, MA87, NYA89]. At the frequency within the interval 0.37-0.41 a band crossing is observed and is interpreted as due to alignment of the pair of $h_{11/2}$ protons. The influence of the aligned protons on the shape of the nucleus is different than that of the neutron. The neutron, which lies in the lower part of $h_{11/2}$ shell, drives the nucleus to negative gamma values (triaxiality), whereas protons, lying in the upper part of the shell, change the shape of the nucleus

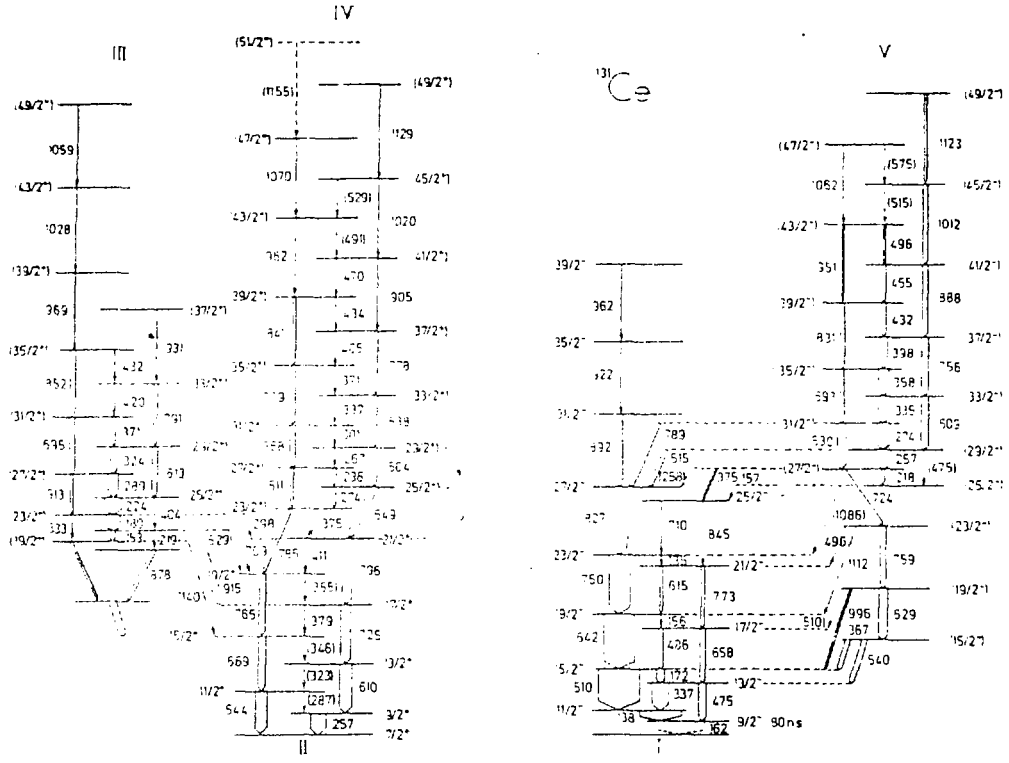

Fig.2 Level scheme of ^{131}Ce. Super-deformed band of 14 transitions is not shown on the picture. The widths of the arrows are proportional to transition intensities.

to the prolate one. The lack of signature splitting in the $\nu h_{11/2} \otimes (\pi h_{11/2})^2$ band is consistent with the prolate shape.

The ground state band is extended to higher spins above the point corresponding to decoupling of protons. This band continuation shows rapid increase of alignment and is interpreted as the beginning of the band built on $(\nu h_{11/2})^3$ configuration. Two additional aligned $h_{11/2}$ neutrons would drive the nucleus to more negative gamma values, so the nucleus would have collective oblate shape ($\gamma \sim -60°$)

For $N = 73$ and β_2 deformation around 0.2 the lowest positive parity band is probably built on one decoupled $g_{7/2}$ neutron. This band is crossed by two 3-quasiparticle bands at nearly the same frequency (0.31 MeV). One of these bands is built on the $\nu g_{7/2} \otimes (\pi h_{11/2})^2$ configuration, the other one, probably, on $\nu h_{11/2} \otimes \pi h_{11/2} \otimes \pi g_{7/2}$. If one chooses the assignment shown in fig 3b, then the increase of alignment in high spin/frequency part of $\nu h_{11/2} \otimes \pi h_{11/2} \otimes \pi g_{7/2}$ band may be due to decoupling of the second pair of nucleons, namely $h_{11/2}$ neutrons. This would thus indicate the appearence of 5-quasiparticle configuration. The lack of the crossing of the second 3-qp band with

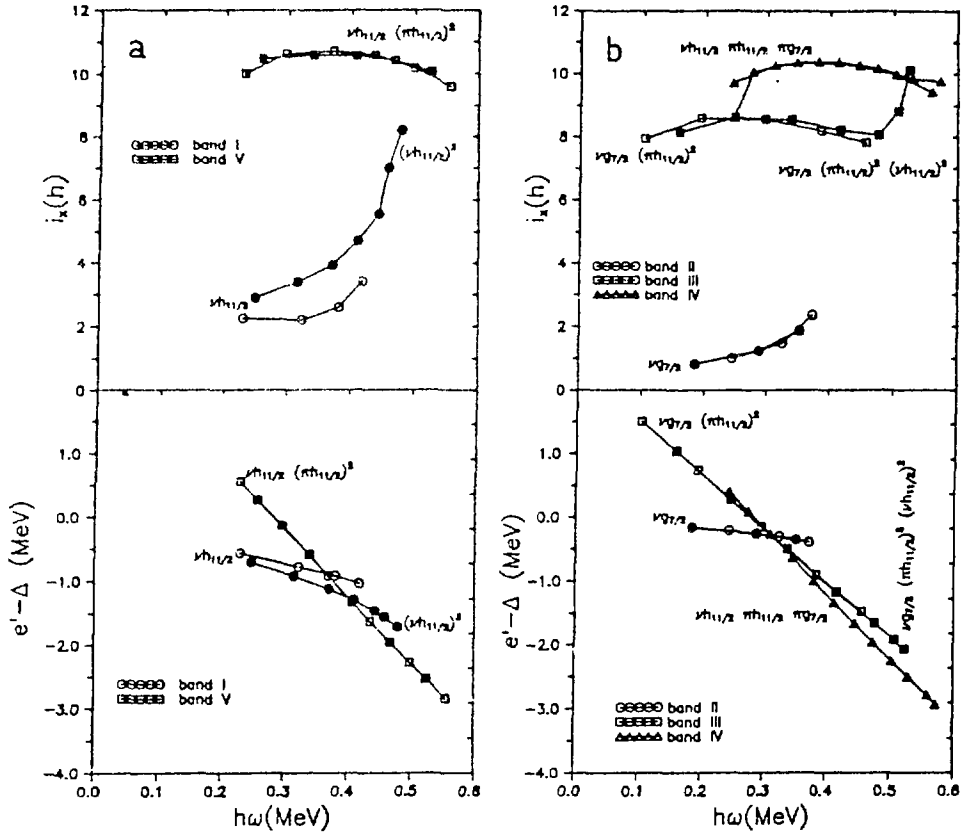

Fig.3 Alignments (i_x) and routhians (e') for bands of negative (a) and positive (b) parity.

alignment of neutrons and protons is already blocked in this band.

Conclusion: We have expanded ^{131}Ce decay scheme up to relatively high spins and excitation energies. Besides the previously reported bands built on $\nu h_{11/2}$, $\nu g_{7/2}$ and $\nu h_{11/2} \otimes (\pi h_{11/2})^2$ configurations, we have observed two bands with presumably 3-qp character: $\nu g_{7/2} \otimes (\pi h_{11/2})^2$ and $\nu h_{11/2} \otimes \pi h_{11/2} \otimes \pi g_{7/2}$. We also propose the assignment for two others bands oserved as being due to alignment of the pair of the $h_{11/2}$ neutrons, that is one built on 3-qp $(\nu h_{11/2})^3$ configuration and one on 5-qp $\nu g_{7/2} \otimes (\pi h_{11/2})^2 \otimes (\nu h_{11/2})^2$ configuration.

Acknowledgment: The authors are indebted to Witek Nazarewicz for inspiring discussions.

References:

[GOD] M. J. Godfrey et al. University of Liverpool preprint
[WAD87] J. Phys. G: Nucl. Phys. **13** (1987) L207
[LUO87] Y-X. Luo et al., Z. Phys. **A329**, (1987), 125
[NYB] J. Nyberg et al., to be published
[HE90] Y. He et al., J.Phys. G: Nucl. Part. Phys. **16** (1990) 657

[GIZ77] J. Gizon et al., Nucl. Phys. **A290** (1977) 272
[NOL82] P. J. Nolan et al., Phys. Lett. **109B** (1982) 269
[NOL83] P.J. Nolan et al., "Workshop on Nuclear Structure at High Spin", The Niels Bohr Institute, Tandem Accelerator Laboratory, May 24-27, 1983, slide report
[SLE89] Sletten et al., Proc. The Intern. Conf. on the Spectroscopy of Heavy Nuclei, 25-30 June 1989, Crete, IOP Publishing, Bristol UK
[BEN79] R. Bengtsson, S. Frauendorf, Nucl. Phys. **A327** (1979) 139
[ARY84] R. Aryaeinejad et al., J. Phys. G: Nucl. Phys. **10** (1984) 955-967
[MA87] R. Ma et al., Phys. Rev **C36** (1987) 2322-2329
[NYA89] B.M. Nyako et al. Z. Phys. A - Atomic Nuclei **334** (1989) 513-514
[WYS89] R. Wyss et al., Nucl. Phys. **A505** (1989) 337
[ARY84] R. Aryaeinejad et al., J. Phys. G: Nucl. Phys. **10** (1984) 955

The Dependence of Delta Electrons Accompanying Deep Inelastic And Transfer Reactions on Nuclear Contact Times

J. HOSZOWSKA, T. ŁUKASIEWICZ, Z. SUJKOWSKI

Soltan Institute For Nuclear Studies, 05-400 Swierk, Poland

ABSTRACT: Discussion of the applicability of δ electron spectroscopy to the study of the time evolution of heavy ion collisions at intermediate bombarding energies is presented. The dependence of delta electron spectra on nuclear contact time is analysed for Xe+Sn, Xe+Pb and U+U reactions at 20 MeV/u and 40 MeV/u beam energies.

1. INTRODUCTION

The analysis of delta electron spectra offers a capability to test various models of *time evolution of deep inelastic and transfer reactions* [Re79].

Delta electrons are emitted due to a rapidly changing Coulomb potential during the time when the nuclei form a quasi molecule. For Rutherford trajectories, the energy spectrum of delta electrons is a monotonically decreasing function of electron energy. If a simple model of H.I. reaction is assumed, where the nuclei stick together for a time T during which its relative distance is constant, in the delta electron spectrum pronounced oscillations are expected. The period of these oscillations is related to the nuclear sticking time $\Delta E=h/T$

In a more realistic model, a number of effects have to be considered which wash out the oscillatory pattern. In a deep inelastic (DIC) reaction the finite resolution of the measured energy loss corresponds to a certain interval of nuclear contact times. Statistical fluctuations can also play a significant role in wiping out the oscillations. Even for a single impact parameter, one is dealing with a distribution of different trajectories and interaction times [Fr90]. This distribution smears out the oscillatory structure. The effect of nuclear contact, nevertheless, is still considerable and is observable as a change in the shape of delta electron spectra, especially at high electron energies.

Applying the fitting procedure to the measured delta electron spectra,a mean collision trajectory can be obtained and in consequence the information about the mean interaction time and the width of the time distribution. The procedure for obtaining internuclear distance R(t) is model independent within the limits of its applicability [Kr88].

The idea to use δ electrons as an atomic clock for the time scale of deep inelastic reactions has been verified experimentally at low ion energies ($\leq$10 MeV/u). The experimentalists centered their interest on super heavy systems, in which apart from the delta electron emission the production of positrons is particularly interesting from the point of view of quantum electrodynamics.

The purpose of the present note is to analyse the applicability of δ–electrons as a probe for nuclear reaction dynamics at intermediate energies and for medium heavy and heavy systems

2. RESULTS OF MODEL CALCULATIONS.

The energy differential electron emission probability dP/dE calculated in the framework of the time dependent perturbation theory is given by:

$$\frac{dP}{dE_{e^-}} = |a(\omega)|^2 \qquad \text{where}$$

$$(2.1) \qquad a(\omega) = \int_{-\infty}^{+\infty} \left(\frac{M}{\omega}\right) \frac{\dot{R}}{R} \exp(i\omega t) dt \quad \text{and} \quad \hbar\omega = E_{e^-} + E_{bind}$$

R - is the internuclear distance and $\dot{R}(t)$ its derivative. (Discussion of limits of its applicability of eqs.(2.1) is presented in the APPENDIX)

The model that we adopted (time dependent perturbation theory) is not capable of reproducing the absolute values of the ionization probability. However, because the matrix element depends weakly on R ,we can compare relative δ-electron probabilities for various trajectories. The aim of our model calculations is to test to what extent the proposed method is sensitive to nuclear sticking time. We present the results of our calculations for U + Xe, Sn, Xe + Pb and U + U systems.

Equation (2.1) shows, that the transition amplitude $a(\omega)$ is essentialy the Fourier transform of the quantity $(d\dot{R}/dt)/R$. For the calculations of the nuclear trajectories we choose a realistic model of HI collisions [Bo78]. The nuclear motion is calculated from macroscopic equations, using parameter-free prescriptions for the conservative and friction forces. The conservative forces are derived from liquid drop potential energies (Coulomb + surface terms) and proximity potential of J.Blocki [Bl77]. For the friction, the proximity "window formula" of Randrup [Ra77] with a flux correction is used. An exchange of particles across the window is also taken into account. The numerical calculations of R(t) are performed with a code written by M.Dworzecka and modified by H.Feldmeier and J.Blocki.

A comparison of the delta electron spectra for Xe + Sn and U + U reactions at 20 MeV/u and also for U + U at 40 MeV/u bombarding energy is shown in fig.1. The curves represent the spectra calculated for dissipative collisions in different T.K.E.L. windows and for a quasielastic reaction. Effects of finite resolution and statistical fluctuations are accounted for by weighting the spectrum with a wide Gaussian distribution of impact parameters (indicated as insets in the figure). One can recognize the increasing effect of nuclear contact with increasing energy loss, and the corresponding change of shape of the spectra. In fig.2 a comparison of the ratios of inelastic to elastic δ-electron emission probabilities vs electron energy for different nuclear contact times is shown as an illustration.

One of our objectives was to determine up to what value of beam energy the delta electron spectrum is sensitive to prolonged nuclear nuclear contact. Due to a faster deceleration at higher beam energies the time variation of the two-center Coulomb potential is greater when the nuclei approach each other. Thus, the contribution to the total production amplitude from the initial phase becomes dominant (see fig.3). This effect and the decrease of nuclear contact times, contribute additionaly to the destruction of the inteference pattern in the delta electron spectra at higher incident energies. A comparison of delta electron spectra for one impact parameter and four different beam energies is shown in fig.4. The influence of nuclear contact time on the spectra diminishes for higher energies.

However, the heavier the system the longer are nuclear contact times (fig.5).Also, due to relativistic contraction of the electronic wave function with decreasing internuclear distance, an increase in the emission probability of the high energy delta electrons is expected for heavier systems.

Thus, our model calculations show that the δ-electron spectra of high Z united systems at bombarding energies in the region of Fermi velocities (40 Mev/u), remain only weakly sensitive to the time evolution of nuclear reaction.

An observable ex deficione left out of the present analysis is that of the angular distribution of delta electrons. This could possibly be used for more asymmetric systems, where the monopole approximation breaks down (see Appendix).

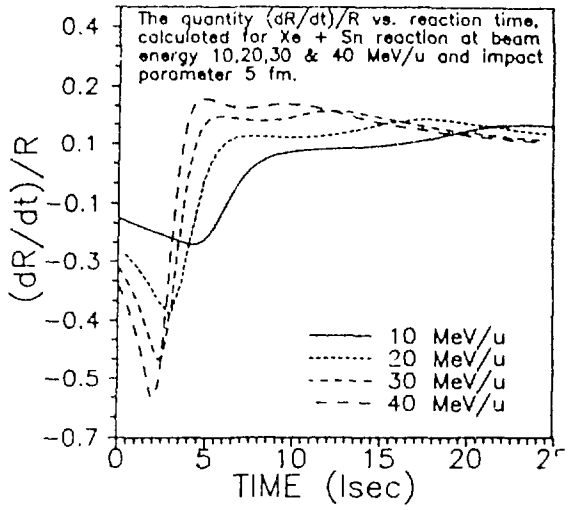

Fig.3

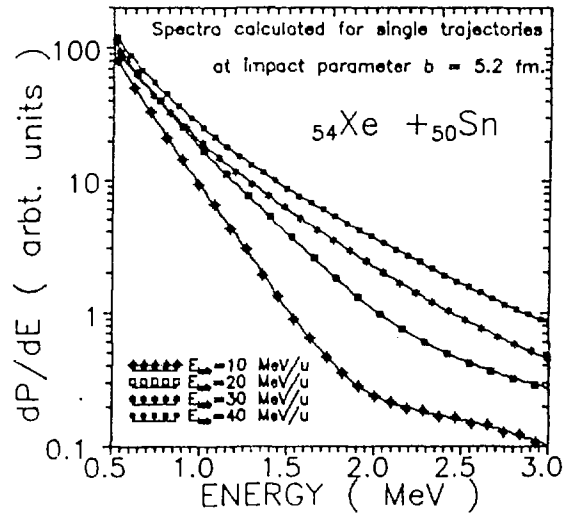

Fig.4

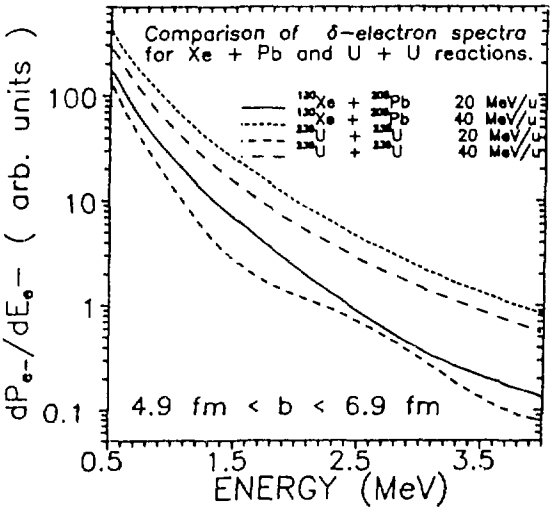

Fig.5

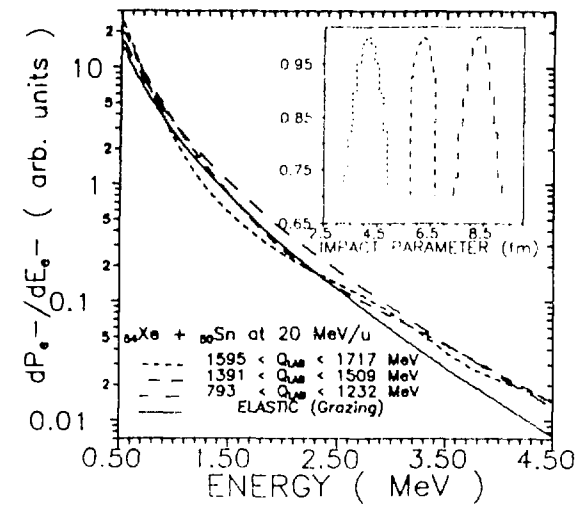

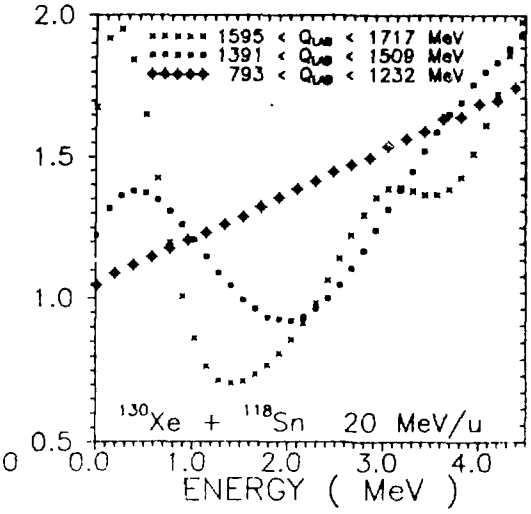

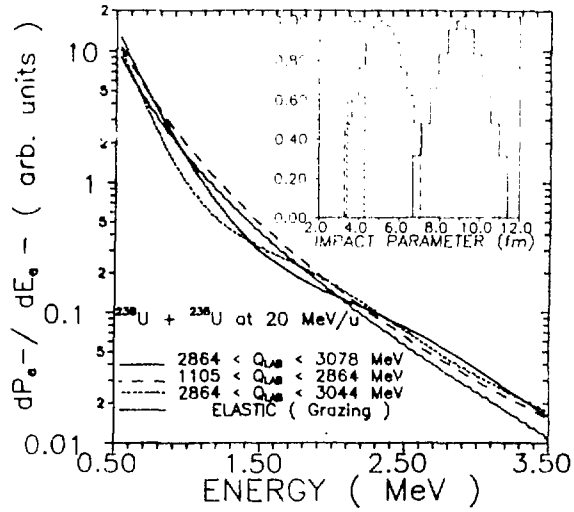

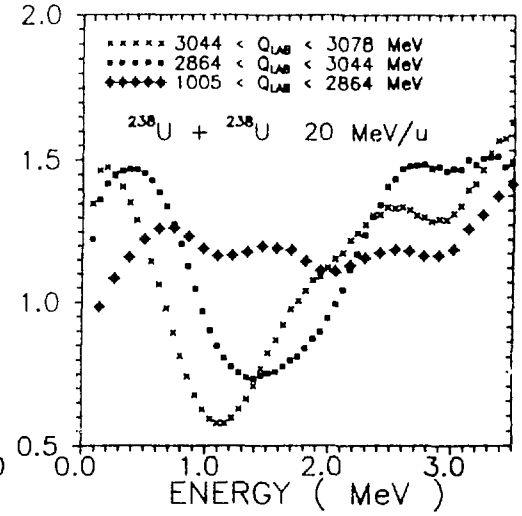

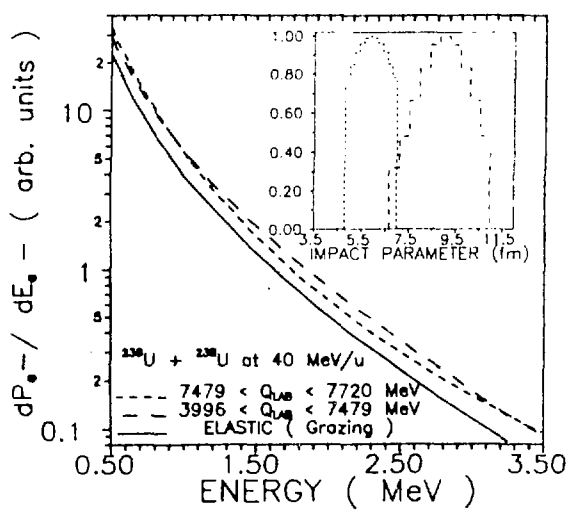

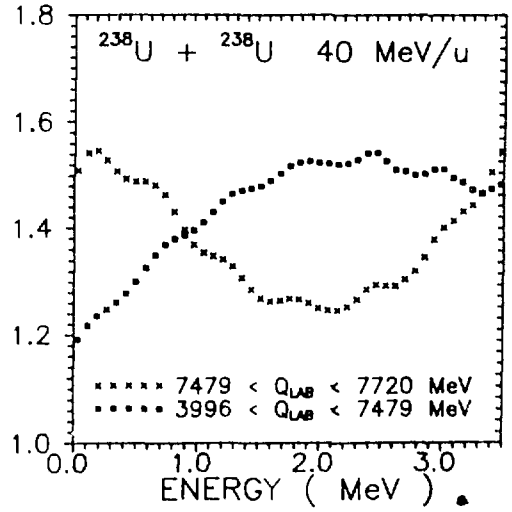

Fig.1 Delta electron spectra

Fig.2 Ratio of inelastic to elastic dP/dE

3. CONCLUSIONS

To summarize, within the applied model delta electron spectral shapes can be used to deduce the nuclear reaction time for beam energies up to 20 MeV/u and systems with Z_{UNITED} greater than 110. There is a need for new model calculations and experiments for asymmetric systems at intermediate energies, where observables such as angular distributions and absolute emission probabilities of δ-electrons should be investigated.

APPENDIX

LIMITS OF APPLICABILITY OF THE MODEL

The use of many approximations makes the estimation of the applicability of eq. (2.1) difficult. We employ the semiclassical theory, where the nuclear motion is described classicaly. As long as we use the molecular model and neglect relativistic kinematics, the results are valid for energies $E \leq 100$ MeV/u. The adiabaticity condition requires, that the collision should not be too fast. The Coulomb potential should vary sufficiently slowly, so that electrons can relax adiabatically to the nuclear motion. A rough criterion when the quasi-atomic state can be formed is obtained comparing the velocities of electronic and nuclear motion.

Quasi-atoms are formed within the condition [o]:

$$0.02 < \frac{V_{ION}}{V_{elektr}^{U.A.}} < 0.16$$

Also the monopole approximation restricts the validity of the model to nuclear charges

$$Z_{proj.} + Z_{target} > 110^{(!)},$$

but this condition depends strongly on the impinging heavy ion energy. In addition this approximation is limited to near symmetric systems :

$$\frac{Z_{proj}}{Z_{Target}} < 0.6$$

In order to obtain information about the accuracy of the monopole approximation, one can measure the angular distribution of delta electrons. Measurments performed for systems not fulfilling condition[!] like Br + Pb or I +Pb show, that monopole condition is valid even for $Z_p + Z_t < 0.4$ [He84].

REFERENCES

[Re79] J.Reinhardt, B.Müller, W.Greiner, G.Soff, Z.Phys.A292(1979)211.

[Fr90] P.Fröbrich, J.Stroth, Phys.Rev.Lett.64(1990)629.

[Kr88] M.Krämer et al., Phys.Lett.B201(1988)215.

[Be78] F.Beck, J.Błocki, M.Dworzecka, G.Wolschin, Phys.Lett.76B(1978)35.

[Bl77] J.Błocki, J.Randrup, W.J.Swiatecki & C.Tsang, Ann.Phys. 105(1977)427

[Ra77] J.Randrup, in: Proc.Intern. Workshop V on Gross Properties of Nuclei and Nuclear Excitations, Hirschegg, Austria, 1977, AED-Conf. 77-017-001.

[Mo78] P.H. Mokler, X-Ray Production in Heavy Ion-Atom Collision in I.A. Sellin Structure and Collision of Ions and Atoms

[He84] M.A.Herath-Banda et al., Phys.Rev.A29 (1984) 2429.

THE K X-RAY SPECTRA OF TA AND U FOLLOWING THE COLLISIONS WITH ENERGETIC IONS

D.F. Anagnostopoulos, G.L. Borchert, and D. Gotta
Institut für Kernphysik, Forschungszentrum, 5170 Jülich

K. Rashid
Informatics Complex, Sector H-8, P.O.Box 2191, Islamabad

ABSTRACT

We have performed a high resolution study of the satellite structure of K X-rays in Ta and U produced by energetic heavy ion bombardment. The experimental results are compared with theoretical predictions based on the Semiclassical Approximation. We discuss the importance of L subshell coupling, charge transfer from the L shell of the target to the K shell of the projectile, vacancy redistribution during the life time of the K hole and the holes' angular momentum coupling with the open shells. We find very good agreement between theory and experiment, nevertheless a small discrepancy in the vicinity of the diagram lines remains.

INTRODUCTION

In the last years the X-ray spectroscopy of energetic ion-atom collisions has proven to be a fruitful field for new insight in the atomic reaction and relaxation mechanisms [1-7]. In the energetic ion-atom collision the target atom experiences a violent Coulomb shock which leaves the atom in a multiply ionised state, where the electrons have been promoted to empty shells, to the continuum and even to atomic shells in the projectile. The probabilities for these processes depend sensitively on the velocity and charge of the projectile, the nuclear charge of the target atoms, and on the state of the involved electrons. While the Coulomb ionisation cross section can be described satisfactorily within the frame of the semiclassical approximation (SCA) [8-11], the theoretical prediction of the charge transfer process from target atom to projectile [12-13] and subshell coupling [14] only yields qualitative estimates.

After the collision the highly excited target atom decays through a variety of competing processes: radiative deexcitation by emission of characteristic X-rays, where the transition energy contains the information about the relevant vacancy configuration, and Auger and Coster-Kronig transitions which shift the vacancy distribution from the inner shells to the outer shells.

Due to the very short lifetime of the K–hole, the K X–ray spectrum will reflect the vacancy distribution close to the statu nascendi. In contrast, because the lifetime of the L hole is almost an order of magnitude larger, the L X–ray spectrum is significantly modified by the competing decay processes.

The complexity of the X–ray satellite spectra requires an investigation at ultimate resolution, which can only be achieved by the use of focussing crystal spectrometers.

Recently, several experiments [6,7] have been carried out with rather light atomic systems. As expected from the scaling relations of SCA [8,11] very complex X–ray spectra have been found, where in addition the $K\alpha_1$ and $K\alpha_2$ satellite structures overlap.

Therefore we decided to perform experiments with heavy targets: We use a projectile beam, having the ion velocity in the vicinity of the Bohr velocity of the L electrons. We performed the study of the K X–ray spectra of Ta bombarded with 350 MeV N^{6+} ions and of U bombarded with 500 MeV Ne^{8+} ions.

THE EXPERIMENT

We used our high resolution crystal spectrometer [15] which is installed online at the Jülich Cyclotron JULIC. The experimental details and the measuring

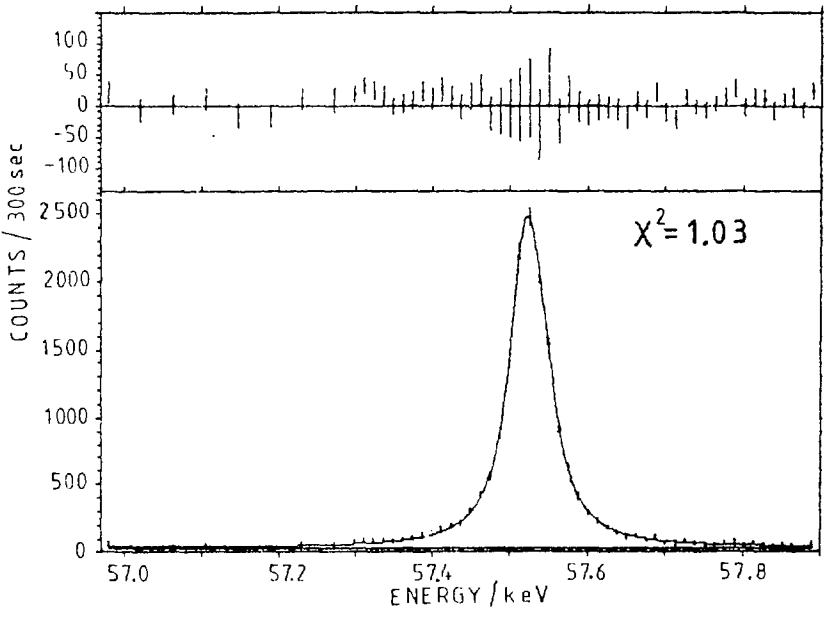

Fig.1: The second order reflection of the $K\alpha_1$ transition in Ta excited by bombardment with 25 MeV protons.
The solid line represents the fit from which we extract the geometrical target response function parameters. The differences between fit and experiment data are displayed in the upper part of the figure.

strategy is described elsewhere [16]. We measured the $K\alpha_1$, $K\beta_{1,3}$ X–ray lines in second and third order reflection at negative and positive Bragg angles, scanning across the region of the reflection, point by point. Simultaneously a Ge(Li) detector is used to monitor intensity changes due to beam intensity and positioning fluctuations, which in this way are corrected. For calibration purposes and line shape studies, in either case the target, was bombarded with 25 MeV p. As an example we show in Fig. 1 the $K\alpha_1$ line of Ta in second order reflection excited by proton bombardment.

THEORETICAL CALCULATION

For the interpretation of the experimental data we use the same procedure as outlined elsewhere [16,17]. The calculations of the ionisation probabilities, the corrections due to L subshell coupling and due to the charge transfer of an electron from the L shell of the target to the K shell of the projectile (other transitions have been estimated to be negligible) have been provided by Jakubassa [18]. From these, we determined the intensity of all satellite lines with up to 3 spectator holes in the L and M shells, whereas the satellites with N,O, ... holes, are treated as inclusive. We take into account the slight rearrangement which occurs during the lifetime of the K hole due to radiative, Coster–Kronig and Auger transitions.

The energy shifts of the satellites have been obtained with the use of the relativistic Dirac Fock program of Desclaux [19]. Here we also took into account the multiplet structure of the L satellites.

For the $K\alpha_1$ transition we obtain here 286 satellites. The 60 strongest already carry away 70% of the total intensity. For the $K\beta_{1,3}$ transitions, which we treat as one data set, because of their small energy distance, we handle a total of 321 satellites.

COMPARISON BETWEEN EXPERIMENT AND THEORY

The intensity of the satellites is normalised with respect to the diagram line. Each of them is provided with a line shape corresponding to the natural line width of the diagram line. By a fitting procedure, we adjust the peak intensity of the diagram line in the theoretical spectrum, which consists of all superimposed satellites, to that of the experimental spectrum.

We include in the theoretical spectrum the above discussed effects, one after the other, and judge its importance from the agreement with the experimental data

via a χ^2–test.

The I subshell coupling tends to decrease the intensity of the satellites where L spectator holes are involved. For Ta the effect is in the order of 10% on the average and increases in the case U to 30%.

The electron transfer process from the L shell of the target to the K shell of the projectile leads to an increased probability for L shell vacancies. Its trend is therefore opposite to that of the L shell coupling. If we include this effect in the predicted spectrum as calculated, a significant discrepancy to the experimental data remains. From an earlier experiment [20] it was found that the strong potential Born approximation theory underestimates the effect by a factor of about 3. We also find best agreement for Ta with a factor of 3 (see Fig. 2b) and, as expected from relativistic considerations, for U with a factor of 5 [17] (see Fig. 3).

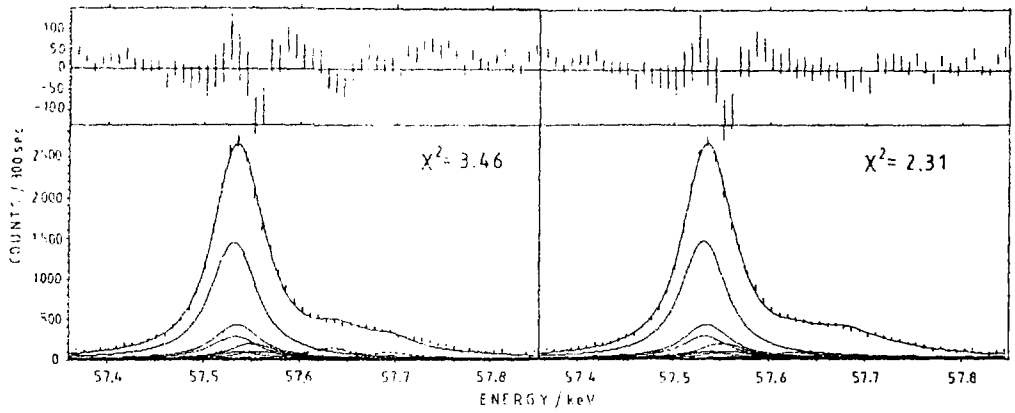

Fig.2: a) The second order reflection of the $K\alpha_1$ in Ta produced during collisions with 350 MeV N^{6+} ions. With solid lines are given the complete fit, the diagram line as the largest component and some of the strongest satellites. The residue is shown in the upper part of the figure. Without taking the multiplet splitting into account there remains a clear discrepancy between experimental data and theory in the region of the L satellites.

b) We include now the angular momentum coupling of the K and L_{III} holes of the transition, with the L spectator holes.

To demonstrate the effect of the angular momentum coupling of the holes in open shells we calculated the splitting and the intensity spread for the $K\alpha_1$ transition in the presence of one L spectator hole. The resulting 9 lines extend over a region of 64 eV to 375 eV in U with respect to the diagram line. In the case of Ta they cover a region of 36 eV to 200 eV. The corresponding shape of the spectrum agrees

considerably better with the experimental data as can be seen from a comparison of Fig. 2a and Fig. 2b.

In the $K\alpha_1$ Ta spectrum, there is a clear discrepancy in the vicinity of the diagram line in the region of M spectator holes. We have to emphasize that in the present calculation, we did not include M subshell coupling, electron capture from the M shell of the target to the shells of the projectile and the M multiplet coupling, partly because the relevant theories do not exist or the calculations are expected to be extremly complicated. From the structure of the discrepancy, we assume some redistribution of the M vacancies, that might be accounted for by the M multiplet splitting analogous to the L multiplet splitting.

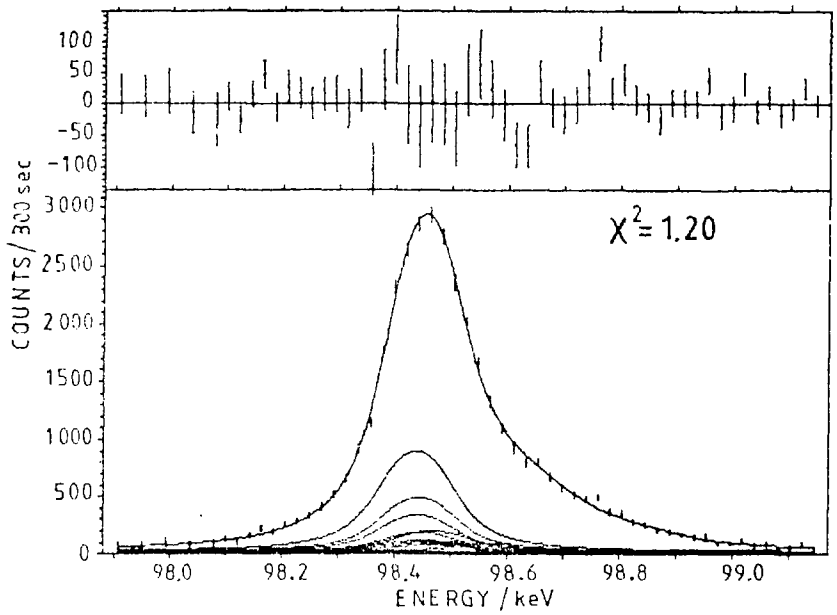

Fig.3: The second order of the $K\alpha_1$ line in U produced in collisions with 500 MeV Ne^{8+} projectiles. Due to the larger natural line width and the enhanced capture effect the agreement between experiment and theory is very good.

To check the validity of these calculations we use the corresponding predictions to construct the $K\beta_{1,3}$ spectrum. As the relevant energy shifts of the satellites are larger, the structure is more sensitive to the presence of M spectator holes. In Fig. 4 we compare the $K\beta_{1,3}$ spectrum of Ta with the theoretical one. The general agreement is rather good. Small deviations may be due to the fact, that we have not included the above mentioned effects concerning the treatment of the M shell, and also the L spectator hole angular momentum coupling.

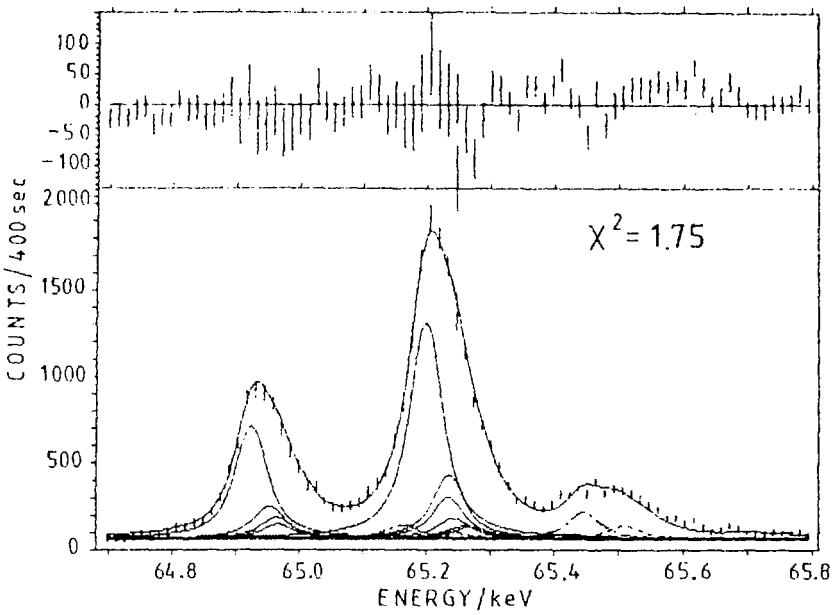

Fig.4: The $K\beta_{1\,3}$ complex of Ta measured in second order reflection is compared to the theoretical prediction. The diagram lines and some intense satellites are also shown indicating the overlap of the satellite structure of $K\beta_1$ and $K\beta_3$.

CONCLUSION

We have investigated the K X–ray satellite spectra produced in the energetic collisions of 350 MeV N^{+6}→Ta and 500 MeV Ne^{+8}→U. The experimental data have been compared with the results of vacancy production in semiclassical theory. For the occurance of L shell vacancies, corrections to the SCA theory from L subshell coupling, electron capture and multiplet splitting of the L_I, L_{II} and L_{III} satellites have been included.

The production of L shell vacancies can be quite well explained if the capture cross–sections from L shell of the target into the K shell of the projectile, which are calculated in non–relativistic approximation, are scaled up by a factor of 3 for the case of Ta and by a factor of 5 for the case of U. This indicates that the theoretical non–relativistic capture cross–sections underestimate the experimental results, which has also been found for the systems ^{3}He→Au and ^{3}He→Sn at 72 MeV [20]. In some cases we see a small deviation between theory and experiment in the region of multiple M shell vacancies. Possible explanations are being investigated, but, we like to point out, that better theoretical predictions for other but the L shells and relativistic calculations for the capture process are highly desirable.

REFERENCES

[1] Watson R.L., Jenson F.E., and Chiao T., 1974, Phys. Rev. A10, 1230

[2] Kauffman R.L., McGuire J.H., Richard P., and Moore C.F., 1973, Phys. Rev. A8, 1233

[3] Knudson A.R., Burkhalter P.G., and Nagel D.J., 1974, Phys. Rev. A10, 2118

[4] Vane C.R., Källne E., Källne J., Morford G., Raman S., and Smith M.S., 1985, Nucl. Instrum. Methods B10/11

[5] Awaya Y., Kambara T., Kase M., Shibata H., Kumagai H., Mizogawa T., Kanai Y., and Shima K., 1985, Riken Accelerator Program Report 19, p. 70

[6] Perny B., Dousse J.–Cl., Gasser M., Kern J., Rheme Ch., Rymuza P., and Sujkowski Z., 1987, Phys. Rev. A36, 2120

[7] Rymuza R., Sujkowski Z., Carlen M., Dousse J.–Cl., Gasser M., Kern J., Perny B., and Rheme Ch., Z. Phys. D14, 37 (1989)

[8] Bang J., and Hansteen J.M., 1959, Mat. Fys. Meddr. 31, No. 13

[9] Hansteen J.M., Mosebekk O.P., 1972, Phys. Rev. Lett. 29, 1361

[10] Kocbach L., Hansteen J.M., and Gundersey R., 1980, Nucl. Instrum. Methods 169, 281

[11] Hansteen J.M., Johnsen O.M., and Kocbach L., 1975, At. Data Nucl. Data Tables 15, 305

[12] Jakubassa–Amundsen D.H., 1989, International Journal of Modern Physics A4, 769

[13] Jakubassa–Amundsen D.H., 1983, Z. Phys. A316, 161

[14] Amundsen P.A., and Jakubassa–Amundsen D.H., 1988, J. Phys. B: At. Mol. Opt. Phys. 21 L99 and references therein

[15] Borchert G.L., Bojowald J., Ercan A., Labus H., Rose Th., and Schult O.W.B., 1986, Nucl. Instrum. Methods A245, 393

[16] Salziger R., Borchert G.L., Gotta D., Schult O.W.B., Jakubassa–Amundsen D.H., Amundsen P.A., Rashid K., J. Phys. B22, 821 (1989)

[17] Anagnostopoulos D.F., Borchert G.L., Rashid K., and Gotta D., to be published

[18] Jakubassa–Amundsen D.H., private communication

[19] Desclaux J.–P., Comp. Phys. Commun. 9, 31 (1975)

[20] Katayama, I., Fujiwara, M., Noro, T., Ikegami, H., Fukuzawa, F., Yoshida, K., Haruyama, Y., Aoki, A., Ogawa, H., Sugai, K., Proc. of ICAP–10, Tokyo, 75 (1986)

M-SHELL IONIZATION PROBABILITIES IN CENTRAL COLLISIONS WITH ENERGETIC α PROJECTILES

M. CARLEN(*), J. CL. DOUSSE(*), M. GASSER(*), J. KERN(*), CH. RHEME(*), P. RYMUZA(**), Z. SUJKOWSKI(**) and D. TRAUTMANN(***)

(*) *Physics Department, University of Fribourg, CH-1700 Fribourg, Switzerland*

(**) *Institute for Nuclear Studies, 05-400 Swierk, Poland*

(***) *Institut für theoretische Physik, University of Basel, CH-4056 Basel, Switzerland*

ABSTRACT

The Kβ x-ray spectra of Mo, Pd and La bombarded by 28 MeV ^{4}He ions were measured with a transmission curved crystal spectrometer. M-shell ionization probabilities in central collisions were deduced from the M satellite lines of the $K\beta_{2,5}$ transitions. A comparison of the values obtained for Mo, Pd, and La with theoretical (SCA) predictions demonstrates the importance of the recoil term.

INTRODUCTION

Single and multiply ionized atoms can be produced by bombarding target atoms with fast ions. These inner-shell ionization processes have been a subject of intensive research during the last two decades. They can be investigated by observing the x-ray or Auger electron spectra. Most of the studies deal with K- and L-shell ionization. For the M-shell ionization by light ions, only few experimental data exist [1, 2, and refs. therein], giving total M-shell or subshell ionization cross sections for heavy atoms. Discrepancies up to a factor of 2 are observed between the experimental data reported by different authors [1]. The main difficulties originate from the low x-ray energies, target contaminations and the complexity of the M-shell spectrum. In addition, to calculate the ionization cross sections from the observed x-ray yields, the fluorescence ratios, which have large uncertainties, are needed.

Further, total cross sections are not always the best quantities to test the theory, since due to the integration over the whole impact parameter range, oscillation effects are smeared out. A measurement of the differential M-shell ionization cross section has not yet been attempted in view of large experimental difficulties. In the following, we present a new method for determining the M-shell ionization probability in central collisions.

We report on the measurement of the M-shell ionization probabilities of mid-Z target elements, bombarded by 28 MeV α projectiles. The Kα and Kβ x-ray spectra of $_{42}$Mo, $_{46}$Pd, and $_{57}$La were recorded with a high resolution crystal spectrometer. Besides the diagram K x-ray lines, L and M satellite transitions were observed. Satellite lines are due to the presence of spectator vacancies in the atom when the x ray transition takes place. These holes modify the electron screening, resulting in net energy shifts of the x-rays, usually towards higher energies. In general, the energy shifts for satellite x-ray transitions due to an inner shell spectator vacancy increase with the principal quantum number characterizing the electron undergoing the transition. Therefore, the M satellites of the K$\beta_{1,3}$ transitions of Mo and Pd appear as resolved singulets, whereas for the Kγ transitions only a line broadening is observed. The notation KβM^m designates a Kβ x-ray with m additional vacancies in the M-shell. In the following, we will concentrate on the Kβ_2 spectra.

Since for a K transition an initial K-shell hole must be present, the collisions can be considered as central in the M-shell scale. From the intensity yields of the Kβ satellites the M-shell ionization probabilities in central collisions are deduced. The present results are compared with predictions of the semiclassical approximation [3]. It is shown that inclusion of the contribution of the recoil of the target nucleus in treating the M-shell ionization probability in central collisions is needed.

EXPERIMENT

The 28 MeV $^4He^+$ ion beam was obtained from the PSI variable energy cyclotron in Villigen, Switzerland. The experimental setup has been described in detail elsewhere. [4]. The x-ray spectra were recorded with an in-beam bent crystal spectrometer in a modified DuMond slit-geometry. The (110) reflecting planes of a 2.5 mm thick quartz crystal plate were used for the diffraction of the x-rays. he crystal bending radius was 3.15 m. The peak reflectivity of the crystal was enhanced by a factor of 3-4 by applying a high-frequency alternating electric field across the lamina [5]. The instrumental resolution, which depends mainly on the slit width and the AC voltage applied to the crystal, was chosen to match the natural line width of the Kβ diagram lines. Self supported metallic targets of natural molybdenum, palladium and lanthanum about 25 mg/cm^2 thick were used. Before impinging on the target, the $^4He^+$ ions were fully stripped by the entrance window of the target chamber (a 5 mg/cm^2 thick Havar foil). Beam intensities between 0.5 and 3 μA were used. Taking into account self-absorption and stopping power of the target and the energy dependence of the K-shell ionization cross sections, the effective beam energy for producing the observed x-rays was 6.7 MeV/nucleon. The Kβ spectra were mesured in first order of reflection.

RESULTS

The measured Kβ spectra are shown in fig. 1. The Kβ_2 satellite regions, measured with longer collecting times, are illustrated in fig. 1, too. Kβ_3, Kβ_1, Kβ_1M^1, K$\beta_{1,3}$L^1,

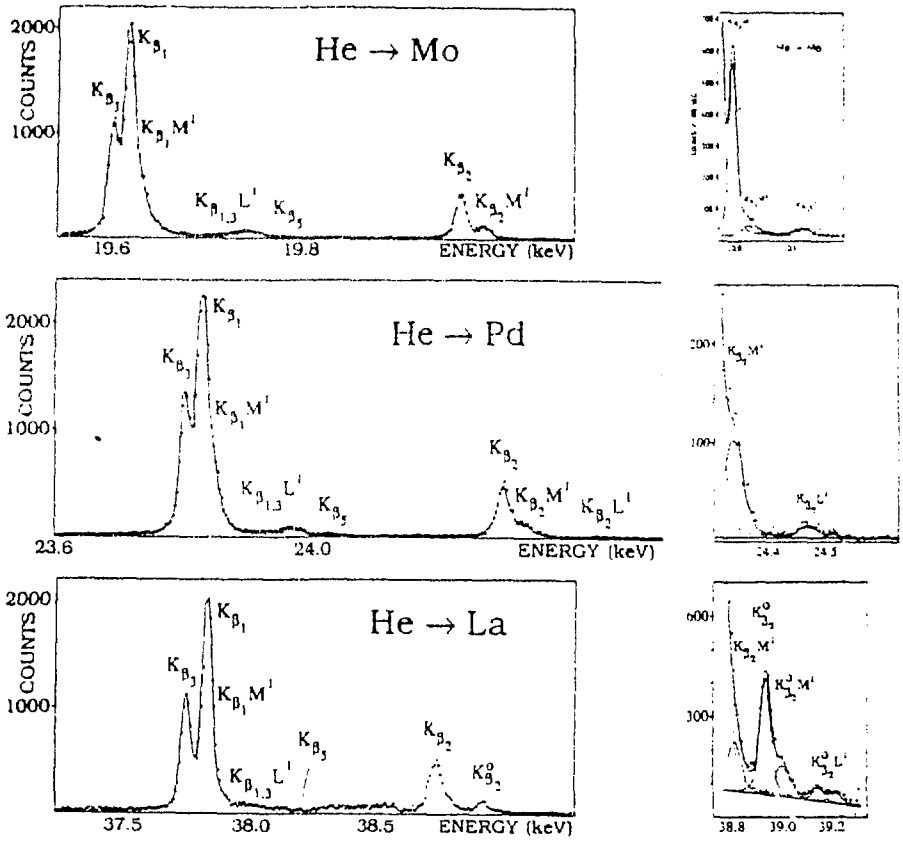

Fig. 1: Crystal spectrometer spectra of Mo, Pd, and La Kβ x-rays induced by 6.7 MeV/u ^{4}He ions. The right parts of the figures show the $K\beta_2$ satellite regions.

$K\beta_5$, $K\beta_2'$, $K\beta_2'M^1$, $K\beta_2'M^2$, $K\beta_2'L^1$ and $K\beta_2'L^1M^1$ transitions were observed. In the La spectrum the O-K line ($K\beta_2^O$) was resolved. The energies of the observed transitions are compared for Pd and La with the results of relativistic Dirac-Fock calculations [6] in table I. The latter gives also Bearden standard energies of the diagram lines [7]. For Mo, the corresponding values are listed in [8].

	Pd			La		
Transition	E_{exp} (keV)	E_{MCDF}	$E_{Bearden}$	E_{exp} (keV)	E_{MCDF}	$E_{Bearden}$
$K\beta_3$	23.7928(16)	23.7936	23.7911	37.7215(6)	37.7371	37.7202
$K\beta_1$	23.8196(16)	23.8216	23.8187	37.8026(3)	37.8181	37.8010
$K\beta_1M^1$	23.8359(16)	23.8371	-	37.8282(13)	37.8426	-
$K\beta'_{1,3}L^1$	23.9485(22)	23.9468	-	37.9797(50)	37.9709	-
$K\beta_5$	24.0169(26)	24.0192	23.995	38.0924(12)	38.1055	38.086
$K\beta_2$	24.2985(17)	24.2998	24.2991	38.7258(4)	38.7351	38.7299
$K\beta_2M^1$	24.3331(19)	24.3307	-	38.7964(29)	38.7824	-
$K\beta_2L^1$	24.4637(34)	24.4592	-	-	38.9534	-

Tab. I: Measured, calculated and standard Pd and La Kβ X-ray energies.

The distribution of the x-ray satellite yields reflects the hole distribution at the x ray emission time. The originally induced hole distribution can be deduced by a statistical scaling procedure [9], taking into account the competition of other possible processes (the Auger, the Coster-Kronig and radiative transitions for the L and higher shells). The M satellite intensities are mainly modified by M and L Auger transitions, whose effects partly cancel each other: the L Auger transitions produce double M shell vacancies, while the M Auger effect transfers the M vacancies to the N shell. These corrections on the measured intensity yields are small so that the uncertainties on the primary distribution yields are only weakly increased by the uncertainties of the involved radiative and Auger values. The intensity yields of the $K\beta_2 M^m$ transitions and the corresponding hole distribution are shown in table II.

Configuration	Mo				Pd				La			
	X^m		I^m		X^m		I^m		X^m		I^m	
$K^1 M^0$	716	(9)	724	(10)	739	(19)	756	(19)	919	(10)	917	(10)
$K^1 M^1$	230	(6)	235	(7)	241	(20)	241	(21)	81	(25)	83	(26)
$K^1 M^2$	54	(21)	41	(22)	-		-		-		-	

Tab. II: Observed X^m and primary vacancy I^m distributions deduced from $K\beta_2$ transitions. The sum of the intensities is normalized to 1000. The correction for increased self-absorption for energies higher than the K-edge is included.

Assuming a binomial distribution of the primary relative vacancy yields we can obtain from the measured data the average M-shell ionization probability for collisions involving the K-shell ionization. They are for Mo: $p_M^{EXP} = 0.018 \pm 0.001$ [8], for Pd: $p_M^{EXP} = 0.017 \pm 0.002$, and for La $p_M^{EXP} = 0.0050 \pm 0.0015$ respectively.

DISCUSSION

The M-shell ionization probabilities for central collisions were calculated in the frame of the semiclassical approximation (SCA). The calculations were performed with relativistic hydrogenic wave functions of the united atom. Screening effects were taken into account by introducing an effective charge which reproduces the experimental binding energy. The results of the calculations performed without and with the inclusion of the recoil term are shown in Fig. 2.

The importance of the recoil term is obvious. Not only the interaction of the projectile with the target, but also the recoil of the target nucleus induced by the collision can give rise to ionization. The contribution of the nucleus recoil to the ionization of a specific shell depends on different physical quantities, like bombarding energy, mass and charge numbers of projectile and target and impact parameter. Depending on the values of these quantities, the inclusion of the recoil term can result in an increase or decrease of the ionization probability. In

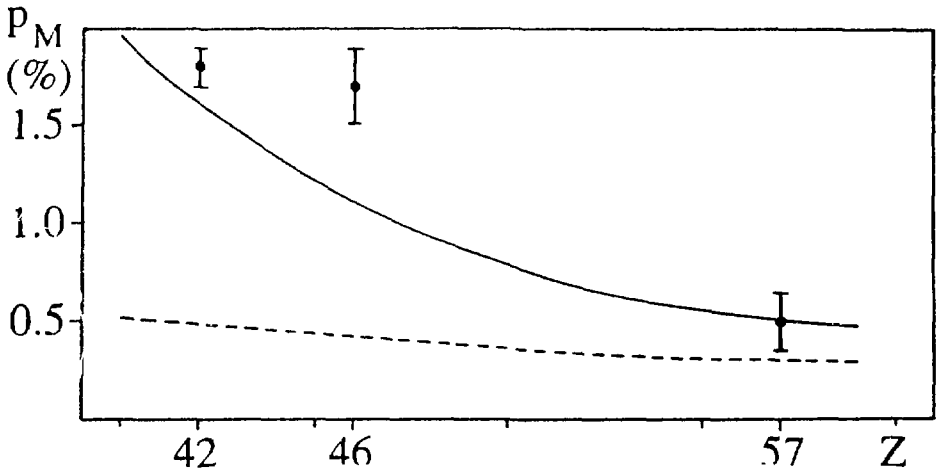

Fig. 2: Measured and calculated M-shell ionization probabilities in central collisions for mid-Z target elements, bombarded by 28 MeV α particles. SCA calculation ——— with recoil term, – – – without recoil term.

central collisions with α particles, the M-shell ionization probability of Mo, Pd, and La targets is increased for bombarding energies higher than 4 MeV, 5 MeV, and 7.5 MeV respectively.

Since the screening of the nuclear charge by the other electrons is for M-shell electrons an important fact, the proper choice of the effective charge, when using hydrogenic wave functions, is of great importance. If the Slater rule is applied the ionization probabilities including the recoil term are up to 50% smaller, but using the single atom model they are about 10% higher. The best way to handle this problem is to use a Hartree-Fock calculation. This will be done in the near future.

REFERENCES

[1] PAJEK M., KOBZEV A.P., LAPICKI G., Nucl. Instrum. Methods B, **48** (1990) 87, BIENKOWSKI A., BRAZIEWICZ J., CZYZEWSKI T., GLOWACKA L., JASKOLA M., LAPICKI G., PAJEK M., Nucl. Instrum. Methods B, **49** (1990) 19.

[2] JESUS A.P., RIBEIRO J.P., Nucl. Instrum. Methods A, **280** (1989) 370.

[3] BANG J., HANSTEEN J.M., Kgl. Danske Videnskab Selskab, Mat.-Fys. Medd., **31**, No 13 (1959), TRAUTMANN D., RÖSEL F., Nucl. Instrum. Methods, **169** (1980) 259.

[4] PERNY B., DOUSSE J.-CL., GASSER M., KERN J., LANNERS R., RHEME CH., SCHWITZ W., Nucl. Instrum. Methods A, **267** (1988) 120.

[5] DOUSSE J.-CL. and KERN J., Acta Cryst. A, **36** (1980) 966.

[6] DESCLAUX J. P., Comput. Phys. Commun., **9** (1975) 31.

[7] BEARDEN J. A., Rev. Mod. Phys., **39** (1967) 78.

[8] CARLEN M., DOUSSE J.-CL., GASSER M., KERN J., RHEME CH. RYMUZA P., SUJKOWSKI Z., TRAUTMANN D., to be published in Europhys. Lett.

[9] RYMUZA P., SUJKOWSKI Z., CARLEN M., DOUSSE J.-CL., GASSER M., KERN J., RHEME CH., Z. Phys. D, **14** (1989) 37.

THE CLUSTER COUNTER AS A PART OF THE 4 -FACILITY AT SIS/ESR

R. TEZKRATT, C. CERRUTI, J.P. COFFIN, P. FINTZ, G. GUILLAUME,
F. JUNDT, C.F. MAGUIRE*, F. RAMI and P. WAGNER
Centre de Recherches Nucléaires, IN2P3-CNRS/Université Louis Pasteur
B.P. 20, F-67037 STRASBOURG CEDEX, France

ABSTRACT
A cluster detector composed of ionisation chambers and thin plastic scintillators has been developed as part of the large 4π-detector at SIS/ESR.

Multifragmentation of the nuclear system is a dominant process in violent nuclear collisions [1]. As a consequence several fragments are observed in the final state of these reactions. It turns out that the entropy (S) can be reliably extracted from fragment yields. Therefore, S carries interesting information about the early hot and dense stage of the collision and it should help in the derivation of the nuclear equation of state.

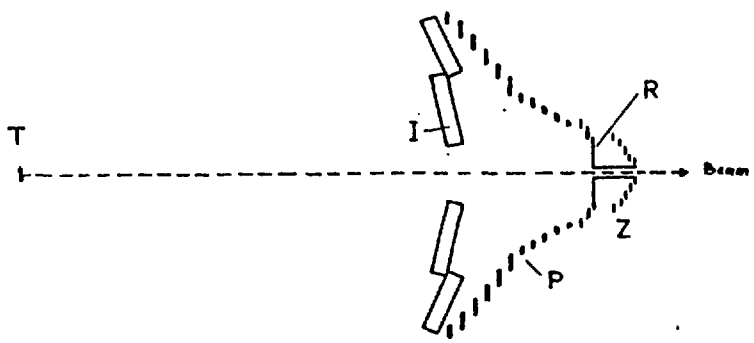

Fig. 1. Set up of Detector modules. I. Gas cluster detector ("Parabola"); P. External plastic wall ; Z. Internal plastic wall ; R. Scintillator cluster detector ("Rosace"). The distance between the "Rosace" and the target T is ≈ 4.5 m.

---

* Present address : Dept of Physics, Vanderbilt University, Nashville, TN 37235 (U.S.A.)

We describe here a project for determining the entropy and temperature reached in heavy-ion collisions at 100 MeV/nucleon and higher from the study of complex fragments. The nuclear matter concept is now reexamined on the light of recent works in the perspective of a first experiment at SIS/ESR at Darmstadt (Germany) [2].

Fig. 1 shows a schematic layout of the detector modules which we shall briefly describe here. The system is composed of two main parts : The plastic wall and the ionisation chamber shell.

The plastic wall is composed of an external part (7° to 30°) and an internal part (1° to 7°), which are respectively constructed and assembled by GSI of Darmstadt and the LPC of Clermont Ferrand (France) groups.

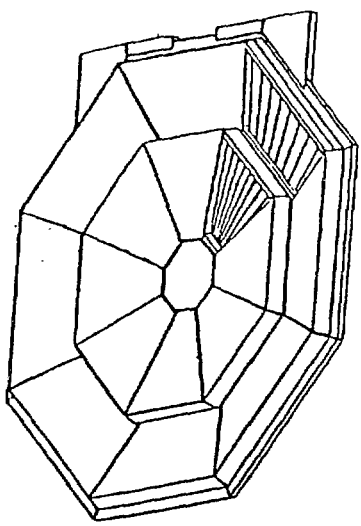

Fig. 2. Gas cluster detector "Parabola". The total size of the detector is Ä 3.5 m.

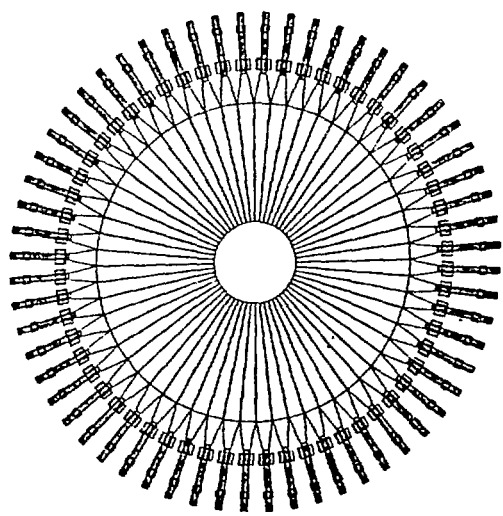

Fig. 3. The Rosace ; the sixty NE102A scintillator detectors subtent an angular domain of 1° to 6° from the target.

The ionisation chamber part (The "Parabola") which is assembled by us stands in front of the plastic wall and measures the energy loss of the heavy fragments $Z \geq 3$ in the angular range 6° to 30°, the shell is filled with an Ar (90 %) + CF_4 (10 %) mixture at atmospheric pressure, and is formed of 8 sectors divided into an inner and outer part (Fig. 2). Each module is subdivided

into 8 radial submodules consisting of a double ionisation chamber. The resulting granularity of 128 elements is expected to be adequate in view of the multiplicity measurements of heavier fragments. At smaller angles (1.3 to 6°) the cluster detector will be supplemented by 60 NE102A scintillators 2 mm thick arranged as the petals of a flower (The "Rosace" Fig. 3), each petal subtending 6° in azimuth.

The fragments will be identified by their atomic number Z by measuring the energy loss ΔE in the cluster detector and their time-of-flight τ between the target and the plastic wall, on a bidimensional plot (ΔE, τ).

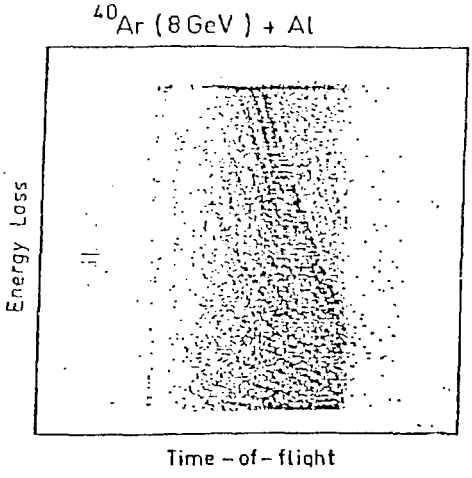

Fig. 4. Two-dimensional Z-identification spectrum obtained with an ionisation chamber module and a plastic scintillator strip (5 mm thick) disposed behind and giving the time-of-flight signal. The experiment was done at SIS/ESR.

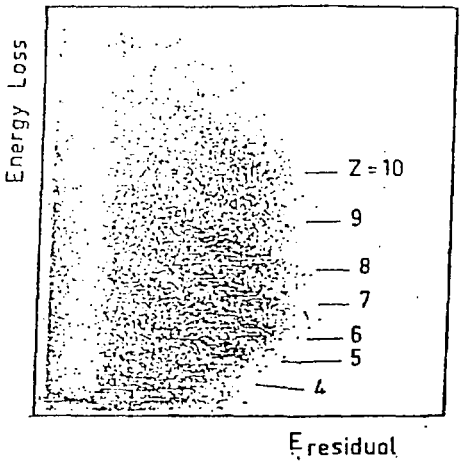

Fig. 5. Two-dimensional Z-identification plot (ΔE, E_{res}) obtained with one of the Rosace modules and silicon jonction (38 mm^2 section and 38 m thick). The beam was a ^{20}Ne (38 MeV/nucleon) empinging on a Carbon target at SARA.

The figures 4 and 5 displays the preliminary results of beam tests at SARA (France) and SIS at Darmstadt (Germany) of modules of each part of the cluster detector.

The expected response of the cluster detector/scintillator wall has been investigated with the use of the "Geant" detector program and the "Freesco" event generator code [3].

As a part of the 4π-detector at SIS/ESR, the Cluster Counter offers the following performances.

- Complete transparence for particles (the shadow effect is limited at 3 % only).
- A complete Z-identification of the clusters upto about 18
- An angular domain from 1° to 30°
- The possibility to measure the velocity vector by means of the position given by the plastic wall detector.

REFERENCES :

[1] G. Perlert, H. Stöcker and W. Greiner, Phys. Rev. C39 (1989) 1402 ; and references therein.

[2] R. Bock et *al.*, as submitted at the Spring General Meeting of the 4π–Detector, GSI Darmstadt (1989) ; see also, J.P. COFFIN et *al.*, Workshop on experiments and experimental facilities at SIS/ESR, GSI Darmstadt (1987).

[3] C.F. Maguire et *al.*, Strasbourg Report 1990, CRN/PN 90-04

TAPS - A TWO ARM PHOTON SPECTROMETER FOR THE DETECTION OF NEUTRAL MESONS AND SINGLE PHOTONS

M. Pfeiffer, II. Phys. Inst., Univ. of Giessen

and the TAPS-collaboration

(II. Phys. Inst., Univ. of Giessen, Germany; KVI, Groningen, Netherlands; Univ. of Münster, Germany; GSI, Darmstadt, Germany; GANIL, Caen, France)

ABSTRACT

A photon-spectrometer for the detection of neutral mesons and single photons has been built. It will be used at several facilities to study heavy ion (GSI and GANIL) and photon induced (MAMI B) reactions. The spectrometer consists at present of 4 blocks with 64 BaF_2-scintillation detectors each. The blocks are arranged in two movable towers to provide a flexible geometry. The spectrometer has been recently used for a first experiment (350 MeV/u ^{20}Ne on ^{27}Al) at GSI. Preliminary results from this run will be presented.

PHYSICS MOTIVATION

Heavy ion reactions in the energy regime from roughly 100 MeV/u to the order of 1 GeV/u offer the possibility to obtain information about the nuclear equation of state by producing hot, compressed nuclear matter. Besides the study of outgoing nucleons and fragments from the two colliding nuclei (transverse flow) a second possibility is to obtain information from particles produced in the reaction (photons and mesons). Due to their low absorption in nuclear matter, photons or dileptons are favourable candidates. Since the particles should be produced from a thermalized reaction zone, the production probability in the first nucleon-nucleon collisions should be small. For this reason, photons are only sensitive probes below energies of roughly 100 MeV/u. To reach a reasonable compression ($\rho = 2\text{–}3\ \rho_0$), energies of several 100 MeV/u up to the order of 1 GeV/u are needed. At these energies mesons become suitable probes. Neutral pions (m_{π^0}=135 MeV, $E^{NN}_{thres.} = 280$ MeV) can be used for the energies between 200 and 500 MeV/u while η– and K^+–mesons ($m_{\eta,K^+} = 549{,}494$ MeV, $E^{NN}_{thres.} = 1.3{,}1.6$ GeV) are the favoured probes in the most interesting energy regime around 1 GeV/u where significant compression is reached. All mesons show final state interaction which increases the absorption probability. η– and K^+–mesons have a lower absorption than pions due to their strange quark content. η–meons, however, are absorbed more than K^+-mesons due to the coupling to nucleonic resonances like $N^*(1535)$. The excitation of these subnucleonic degrees of freedom can be studied with photoproduction reactions of neutral mesons. For a detailed discussion of the theoretical aspects see also reference [1].

PHYSICS PROGRAMME

Heavy ion experiments with beam energies up to 100 MeV/u (hard photons, sub-threshold pion and dilepton production) will be carried out at GANIL. First runs were performed in February and March 1990 using an initial configuration of TAPS. Heavy ion experiments at beam-energies up to 2 GeV/u (neutral meson production, pion correlations and relativistic Coulomb excitation) will be done at GSI. Some of these experiments will be performed together with the 4π-Detector-System [2] to achieve a full event characterisation. A first run on neutral pion production was performed in May 1990 (see below and [3]). In addition, the photoproduction of neutral mesons in

cold nuclear matter at normal density (excitation of subnucleonic degrees of freedom, mean free path of neutral mesons) will be studied at MAMI B (Mainz, Germany) with incident photon energies up to 800 MeV.

DETECTOR SYSTEM

The TAPS-spectrometer is built to detect single photons and to measure coincidences of two photons from the decay of neutral mesons. Therefore, the detector-system has to meet the following requirements. The detector modules must provide a large dynamic range (5-1000 MeV). They should have a good intrinsic energy resolution and a sufficient size to register the electromagnetic shower at higher photon energies. Since TAPS will operate in an environment with high hadron-multiplicities, the granularity should be sufficient to allow for a high multi-hit capability. Furthermore, the detector-system has to provide a clean separation of hadrons (charged and neutral) from photons. The BaF_2-scintillators of the TAPS-spectrometer meet all these requirements. The energy resolution is quite good (e.g. $(\Delta E/E)_{FWHM} = 8$ % for 185 MeV electrons and better than 12.5 % for a 662 keV Cs-source). The detector modules have a sufficient size (length : 250 mm = 12 radiation lengths X_0, inscribed diameter : 59 mm = 0.7 $R_{Molière}$) to register high energy photons. On the other hand, the diameter is small enough to allow the shower to spread over more than one module which permits an increase in the spatial resolution. Using the two different scintillation components of the BaF_2-crystals, charged particles can be discriminated by the pulse-shape method. In addition, a plastic veto-detector (5 mm NE102A, 0.05 X_0) mounted in front of each module can be used to identify charged particles. Using the fast component for the timing ($(\Delta T/T)_{FWHM} < 200$ ps for 45 MeV electrons) neutrons can be separated from photons by the TOF-method. In the standard TAPS-configuration, the detector modules are arranged in blocks of 8 by 8 detectors. At present 4 of these blocks are mounted in two movable towers to provide a flexible geometry (see fig. 1) needed for measuring the complete angular and energy distribution of the produced particles and to optimize the set-up for various neutral meson detection. Typical efficiencies, which are strongly dependent on the geometrical set-up, are $\epsilon_\gamma \approx 8$ % and $\epsilon_{\pi,\eta} \approx 1$ %. The detector-system and the performance of the individual BaF_2-modules is described in [4]-[6].

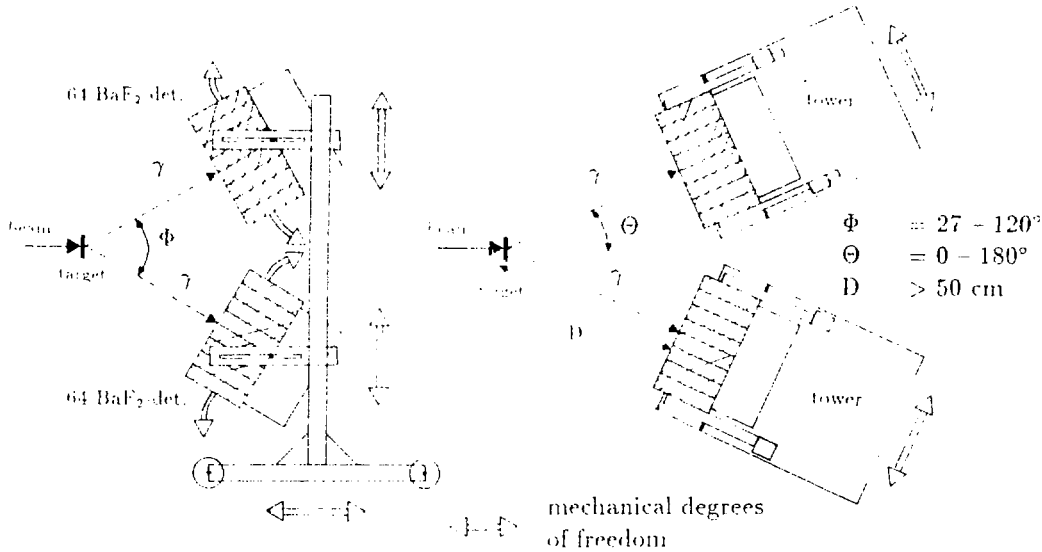

Fig. 1 : Schematic view of the TAPS-spectrometer showing the present status with 4 blocks of 64 BaF_2-detectors each arranged in 2 movable towers (**left** : side view of one tower, **right** : top view of the system)

FIRST EXPERIMENT AT GSI

For the first experiment [3] a beam of 350 MeV/u ^{20}Ne from the SIS-accelerator (10^4–10^5 particles per spill, one 300 ms spill each 3 s) was used in conjunction with a 4 mm ^{27}Al–target. The TAPS-spectrometer with two fully equipped blocks in the horizontal plane was positioned at ± 65 degrees with respect to the beam. In addition, a time-zero detector consisting of 5 small plastic-detectors close to the target was used. A run of 6 houres was analysed. In the first step charged particles were discriminated by using the veto-detector information. Neutrons were separated by the TOF-method. The BaF_2-detectors were calibrated with cosmic rays. The total energy of a photon was calculated by including the sum of the energies in the next neighbouring detectors (max. 6). Calculating the invariant mass, (150 ± 30) neutral pions were found (see fig. 2). Using the number of charged hits and coincidences which determined the number of reactions, a production probability for neutral pions per reaction of $(7 \pm 2) \cdot 10^{-3}$ was found to be in good agreement with the systematics describing known data at lower (< 100 MeV/u) [7] and higher (1–2 GeV/u) [8],[9] beam energies (see fig. 2).

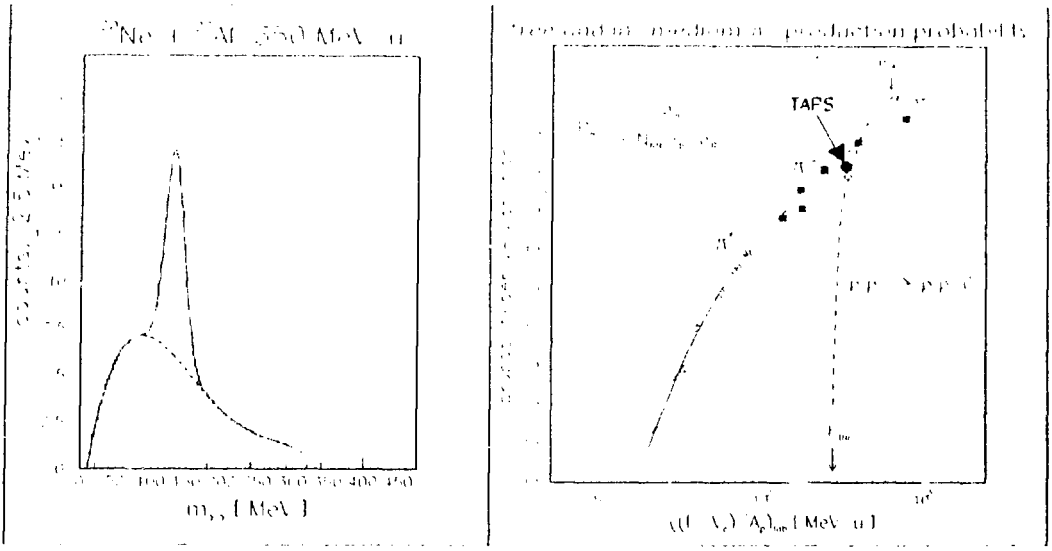

Fig. 2 : Invariant mass spectrum ($m_{\gamma\gamma} = \sqrt{2E_{\gamma_1}E_{\gamma_2}(1 - cos\Phi_{\gamma\gamma})}$) (**left**). Production probability per nucleon-nucleon collision for neutral pions as a function of the incident energy [7]-[9] (V_C = Coulomb barrier , $P_\pi = \sigma_\pi / (<N_{NN}>_b \cdot \sigma_R)$, $<N_{NN}>_b$ = number of first nucleon-nucleon collisions [10]) The ◘-points refer to data for negative pions [11]. In addition, the data point from the first TAPS-experiment is shown. (**right**).

[1] W. Cassing et al., Phys. Rep. 188(1990)363

[2] Technical Proposal of the 4π-Detector for SIS/ESR, GSI-Report 88-03

[3] F.D. Berg et al., to be published in Zeitschrift f. Physik

[4] Technical Proposal of a Two Arm Photon Spectrometer, GSI-Report 87-19

[5] R. Novotny et al. NIM A 262(1987)340

[6] O. Schwalb et al. NIM A (1990) in press

[7] P.Braun Munzinger et al., Ann. Rev. Nucl. Part. Sci. 37(1987)1

[8] T. Hallmann et al., Nucl. Phys. A 440(1985)697

[9] G. Roche et al., Nucl. Phys. A 439(1985)721

[10] H. Nifenecker et al., Nucl. Phys. A 442(1985)478

[11] J. Miller et al., Phys. Rev. Lett. 58(1987)2408

IN-BEAM ELECTRON SPECTROSCOPY WITH COLLINEAR GEOMETRY

J.S. Dionisio, Z. Méliani, C. Schück and Ch. Vieu

C.S.N.S.M., IN2P3-CNRS, Orsay, FRANCE

ABSTRACT

The basic relations for the Doppler shift and the Doppler broadening of an electron line given by an electron spectrometer oriented in the collinear geometry are discussed in detail. The main features of the in-beam e-γ spectrometer recently operated with direct collinear geometry (i.e. with $20 \geq \alpha \geq 10°$) at Orsay's MP Tandem accelerator are briefly described. The interesting performances of that instrument for the investigation of prompt and short delayed low energy transitions ($E_e \leq 200$ keV) deexciting nuclear high spin states are illustrated with a few typical examples. Further developments with reverse collinear geometry (i.e. with $170° \geq \alpha \geq 160°$) are also shortly discussed in the present context of nuclear structure studies involving in-beam nuclear spectroscopic measurements.

1. INTRODUCTION

The Doppler broadening is a serious drawback for the investigation of nuclear high spin states of compound nuclei deexciting in flight shortly after their production by fast heavy ion bombardement of thin targets. This energy spread is particularly unfavourable for the accurate study of high spin states of odd A and odd-odd A nuclei which generally have very complex level spectra. However, the Doppler broadening can be minimized by orienting a radiation detector in the same direction- or the reverse one- of an accelerated charged particle beam (i.e. the so-called collinear geometry). For that reason, we start this contribution with a brief discussion of the Doppler broadening basic relations for an electron spectrometer oriented in the collinear geometry (section 2). This led us to consider similar kind of measurements performed with different types of in-beam electron spectrometers (section 3) having wide angular openings either in the direct (i.e forward) orientation (with $90° > \alpha \geq 25$) or in reverse (i.e.backward) orientation (with $125° \geq \alpha > 90°$). After this broad comparison of the available instrumental capabilities operating with that geometry we illustrate the main possibilities of the Siegbahn-Kleinheinz magnetic lens oriented in the same direction (section 4) by a few results of recent studies performed in such conditions and a broad description of an extensive project using the reverse orientation. Finally, we conclude (section 5) by a brief discussion of the present status of the relationship between these devices and multi-gamma ray spectrometers.

2 - DOPPLER BROADENING OF AN AXIAL ELECTRON SPECTROMETER

The *Doppler shift* of an electron line emitted in flight by a recoil nucleus and the same nucleus deexciting at rest in given by the relativistic transformation law of its linear momentum :

$$\vec{p}' = \vec{p} - (\vec{p}.\hat{V})\hat{V} + \frac{(\vec{p}.\hat{V})\hat{V} - \vec{V}E/c}{\sqrt{(1 - (V^2/c^2)}} \qquad (1)$$

where V is the unit vector in the direction of V [1]. This relation can be rather complicated in the general case due to the p'-p dependence on the angles between the recoil ion direction and the symmetry axis (of the electron spectrometer) as well as the electron emission direction. However, there are two special cases corresponding to simple solutions which will be considered in the following subsections (2.1 and 2.2).

2.1 - Recoil ion emission collinear with the symmetry axis

The *Doppler shift* of an electron line corresponding to a recoil ion with reduced speed, β_r, (collinear with the electron spectrometer axis), and a reduced electron speed, β_e, (making an angle θ, measured in the LAB system with the same axis) is given by the following formulae :

$$p_e(\theta)c - p_o c = p_o c \left(\frac{\beta_r^2}{2} + \left(\frac{\beta_r}{\beta_e} \right) \cos\theta - \frac{1}{2} \left(\frac{\beta_r}{\beta_e} \right)^2 (1+\beta_e^2) \sin^2\theta + \ldots \right) \quad (2)$$

(restricted to the second order in β_r, like in ref. [2]).

The corresponding *Doppler width*, $(\Delta p/p)_e(\theta)$, is related to the solid angle ($T = \Delta\Omega/4\pi = \sin\theta d\theta/2$) of the spectrometer by the similar formulae :

$$\left(\frac{\Delta p}{p} \right)_e (\theta) \simeq 2 \left(\frac{p_o}{p_e(\theta)} \right) \left(\frac{\beta_r}{\beta_e} + \left(\frac{\beta_r}{\beta_e} \right)^2 (1 + \beta_e^2) \cos\theta \right) T \quad (3)$$

where p_o and $p_e(\theta)$ are the electron momentum in the CM and LAB-systems respectively. Replacing in this formulae $p_o/p_e(\theta)$ by its value deduced from the relation (2) one gets the following Doppler width expression :

$$\left(\frac{\Delta p}{p} \right)_e (\theta) \propto \frac{\left(\frac{\beta_r}{\beta_e} + \left(\frac{\beta_r}{\beta_e} \right)^2 (1 + \beta_e^2) \cos\theta \right) \sin\theta \, d\theta}{\left[1 - \frac{1}{2} \left(\frac{\beta_r}{\beta_e} \right)^2 (1-\beta_e^2) \right] + \frac{\beta_r}{\beta_e} \cos\theta - \frac{1}{2} \left(\frac{\beta_r}{\beta_e} \right)^2 (1+\beta_e)^2 \cos\theta^2} \quad (4)$$

valid under the same assumptions and approximations as (2) and (3). The reduced recoil ion speed, β_r, is deduced from the linear momentum conservation in the collision between the accelerated particle p, and the bombarded nucleus according to the classical relation :

$$\beta_r = (A_p/A_r)\,\beta_p = \frac{A_p}{A_r} \sqrt{\frac{2E_p}{M_p c^2}} = \frac{1}{A_r} \sqrt{\frac{E_p(\mathrm{MeV}) A_p}{470}} \quad (5)$$

where A_p and A_r are the accelerated particle and compound nucleus recoil mass numbers, E_p is the kinetic energy of the accelerated ion. Similarly, the reduced electron speed, β_e, is related to the electron energy, ε, and momentum, η ($= p_o/\mu_o c$) by the relativistic formulae :

$$\beta_e = \frac{\eta}{\varepsilon} = \frac{\sqrt{\eta^2 + 1} - 1}{\varepsilon} = (1 + 1/\eta^2)^{-1/2} \quad ; \text{ with } \eta = \frac{B\rho(\text{gauss xcm})}{1704.4} \qquad (6)$$

The squared term (β_r/β_e) in the relations (2-4) can be neglected in the usual range of in-beam electron spectroscopy measurements [$\beta_e = 23.10^{-2}$ for E_e = 13.88 keV and $\beta_e = 80.10^{-2}$ for E_e = 347.2 keV leading to $(1/23) \geq \beta_r/\beta_e \geq (1/80)$] corresponding to very small recoil ion velocities ($\beta_r \simeq 10^{-2}$). For higher recoil velocities (such as $\beta_r \geq 5.10^{-2}$) the contribution of the second term increases (up to 4.10^{-2}) but remains negligeable (i.e. at least five times smaller than the first term). Consequently the *Doppler shift* given by (2) depends essentially on the initial electron momentum, p_o, as well as on the ratio between the recoil ion speed and the electron speed and the angle between them :

$$p_e(\theta) - p_0 \simeq p_0 \frac{\beta_r}{\beta_e} < \cos \vec{v}_r \vec{v}_e > = (\eta \mu_0 c) \frac{\beta_r}{\beta_e} < \cos \theta > \qquad (2')$$

Similarly, relations (3) and (4) corresponding to the *Doppler width* become :

$$\left(\frac{\Delta p}{p}\right)_e (\theta) \simeq 2 \left(\frac{p_0}{p_e(\theta)}\right) \left(\frac{\beta_r}{\beta_e}\right) T \simeq \frac{\beta_r}{\beta_e} \sin \theta d\theta \qquad (3';\ 4')$$

The relations (3) and (3') show that the Doppler width varies linearly with the overall transmission of the electron spectrometer. In particular, the mean value of the Doppler broadening for measurements performed with the Siegbahn-Kleinheinz magnetic lens ($<\theta> = 15°$, $T = 2.5\ 10^{-2}$) is roughly ten times smaller than the corresponding broadening for an iron free toroidal spectrometer ($<\theta> = 50°$, $T = 2.5\ 10^{-1}$). Instead, the mean value of the *Doppler shift* given by that lens (deduced from 2 or 2') is roughly fifty percent larger than in the latter spectrometer (i.e. $(\cos 15°)/(\cos 50°) \simeq 1.503$).

The same relations (2, 2', 3, 3', 4, 4') correspond to definite values of the recoil ion speed and electron speed. However, in all practical cases these values are not unique and spread out within a certain interval. Indeed, the energy losses of the accelerated ions and the compound nuclei within the target contribute to a recoil ion velocity spread, $\Delta\beta_r/\beta_r$, which must be introduced in such relations. For instance, the mean value of the *electron line broadening* due to the relative recoil ion velocity spread, $\Delta\beta_r/\beta_r$, resulting from the ion collisions within the target is given by the following relation :

$$\left(\frac{\Delta p}{p}\right)\left(\frac{\Delta\beta_r}{\beta_r}\right) = \int_{\theta_1}^{\theta_2} (\Delta p/p)_e\ (\theta)\ \sin\theta d\theta \Big/ \int_{\theta_1}^{\theta_2} \sin\theta d\theta$$

$$\left(\frac{\Delta p}{p}\right)\left(\frac{\Delta\beta_r}{\beta_r}\right) = - \frac{\left[\, b \int_{x_1}^{x_2} \frac{dx}{X} - 2a \int_{x_1}^{x_2} \frac{x dx}{X} \,\right] \left(\frac{\Delta\beta_r}{\beta_r}\right)}{(\cos\theta_1 - \cos\theta_2)}$$

$$= \frac{(\log|X_1| - \log|X_2|)}{(\cos\theta_1 - \cos\theta_2)} \left(\frac{\overline{\Delta\beta}_r}{\beta_r}\right) \qquad (6)$$

where $X = ax^2 + bx + c = \frac{1}{2}\left(\frac{\beta_r}{\beta_e}\right)^2 (1+\beta_e^2)\, x^2 + \frac{\beta_r}{\beta_e} x + \left[1-\frac{1}{2}\left(\frac{\beta_r}{\beta_e}\right)^2 (1-\beta_e^2)\right]$;

$x = \cos\theta$; $x_1 = \cos\theta_1$; $x_2 = \cos\theta_2$

θ_1 θ_2 being the lower and upper limits of the angular aperture of the electron spectrometer. In the practical cases $ax^2 << bx$ and $c \simeq 1$. In such condition the previous relation (5) becomes :

$$\left(\frac{\Delta p}{p} \quad \frac{\Delta\beta_r}{\beta_r}\right) = \frac{\log\left(1 + \frac{\beta_r}{\beta_e}\cos\theta_1\right) - \log\left(1 + \frac{\beta_r}{\beta_e}\cos\theta_2\right)}{\cos\theta_1 - \cos\theta_2} \left(\frac{\overline{\Delta\beta}_r}{\beta_r}\right)$$

$$= \frac{\frac{\beta_r}{\beta_e}\left(\cos\theta_1 - \cos\theta_2\right) - \frac{1}{2}\left(\frac{\beta_r}{\beta_e}\right)^2\left(\cos^2\theta_1 - \cos^2\theta_2\right)}{\cos\theta_1 - \cos\theta_2} \left(\frac{\overline{\Delta\beta}_r}{\beta_r}\right)$$

$$= \frac{\beta_r}{\beta_e}\left(\frac{\overline{\Delta\beta}_r}{\beta_r}\right) \qquad (6')$$

The mean value of the recoil velocity spread, $\left(\frac{\overline{\Delta\beta}_r}{\beta_r}\right)$, can be evaluated from the formulae :

$$\langle\Delta\beta_r/\beta_r\rangle = 1/4\ (\Delta E_p + \Delta E_r)/E_r \qquad (7)$$

where ΔE_p and ΔE_r are the total energy losses of the accelerated ion and compound nucleus inside the target. This contribution to the electron line broadening depends mostly on the target thickness which contributes both to the accelerated ions and recoil nuclei energy loss. Indead the influence of the electron spectrometer angular opening on that broadening is ruther small.

The *electron line broadening* due to the reduced electron velocity spread, $\Delta\beta_e/\beta_e$, resulting from the electron collisions within a thin target placed perpendicularly to the electron spectrometer axis is given by the approximate relation :

$$\left(\frac{\Delta p}{p}\right)_e \left(\frac{\Delta\beta_e}{\beta_e}\right)_{\theta_1\theta_2} \simeq \frac{d\ (\sec\theta_2 - \sec\theta_1)}{2\left(1 + \frac{\mu}{\mu+E}\right) E} \left(\frac{dE}{dx}\right)_e \qquad (8)$$

assuming an isotropic electron emission from the middle of a thin, homogeneous, target (having a uniform thickness, d, and a stopping power for electrons $\frac{dE}{dx}$) within the angular aperture (θ_1 θ_2) of the electron beam. Finally, the relativistic factor in the denominator arises from the general electron energy-momentum relation :

$$\left(\frac{\Delta E}{E}\right) = \left(1 + \frac{\mu}{\mu+E}\right) \frac{\Delta(B\rho)}{B\rho} \simeq \left(1 + \frac{\mu}{\mu+E}\right) \frac{\Delta\beta_e}{\beta_e} \qquad (9)$$

This contribution to the mean electron line broadening given by the relation (8) depends essentially on the electron spectrometer angular aperture as well as on the electron kinetic energy, E, and stopping power, dE/dx. Consequently its relative importance increases for lower electron energy and spectrometers with large transmission.

The mean velocity spread of the electrons due to electron straggling within the target is given by a quite similar relation to (8) :

$$\left(\frac{\Delta p}{p}\right)_e \left(\frac{\Delta\beta_e}{\beta_e}\right)_{\bar\theta} \simeq \frac{0,61\rho d\ (\sec\theta_1 + \sec\theta_2)\ Z}{4\left(1 + \frac{\mu}{\mu+E}\right)\beta_e EA} \qquad (10)$$

where ρd is the areal density of the target characterized by the atomic number Z and mass number A. β_e and E are the reduced electron speed and kinetic energy respectively. Finally this relation is deduced from the formulae (9) combined to the mean value of the electron energy distribution given by Landau theory [3] :

$$\Gamma(\Delta E) = 0.61 \left(\frac{Z}{A}\right) (\rho x)/\beta_e \qquad (\Gamma : \text{keV} ; \rho x : \text{mg/cm}^2)$$

where x is the mean value of the effective target thickness $\bar{x} = d \sec\bar\theta$ and $\bar\theta = (\theta_1 + \theta_2)/2$ is the mean value of the electron emission angle.

This contribution to the electron line broadening depends essentially on the target properties and increases factor for lower electron kinetic energies.

2.2 - Recoil ion emission around the symmetry axis

The recoil ion collinear assumption is a rather convenient one but does not take into acount several physical effets occurring during (or after) the interaction between the accelerated ions and the target atoms. Among such effects the following are quoted : angular spread of the incoming particle beam, kinematic effects related to the nuclear reaction (including neutron evaporation from the compound nuclei and recoil ion angular distribution) as well as those effects arising in recoil ion angular spread due to the interaction between the recoil ions and the target atoms. The assumption of a recoil ion emission within a cone around the symmetry axis of the spectrometer is a better approximation than the collinear one.

The *Doppler broadening* of an electron line corresponding to a recoil ion motion within a small cone of mean angular aperture $\bar\alpha$ (relatively to the electron spectrometer axis) and the axial recoil motion is given by the expression (taken from [2]) :

$$(\Delta p/p)_e(\vartheta,\phi,\alpha) = [p_e(\vartheta,\phi,\alpha) - p_e(\vartheta,\phi,0)]/\ p_e(\vartheta,\phi,0)$$

$$= p_e(\cos\vartheta + \alpha\sin\vartheta\cos\phi) - p_e(\cos\vartheta)/\ p_e(\cos\vartheta) \qquad (11)$$

under the assumption $\sin\alpha \simeq \alpha$ and $\cos\alpha \simeq \sqrt{1-\alpha^2} \simeq 1$.

The relative contribution to the electron line broadening due to this non-collinear recoil motion can be obtained by integrating the relation (11) within the electron spectrometer angular apperture $(\vartheta_1, \vartheta_2)$ and the azimuthal

angular interval $(\phi_1, \phi_2) = (-\pi/2, \pi/2)$:

$$\left(\frac{\Delta p}{p}\right)_{\alpha} = \frac{\iint \left(\frac{\Delta p}{p}\right)_{o}(\vartheta,\phi,\alpha)\,\sin\vartheta\,d\vartheta\,d\phi}{\iint \sin\vartheta\,d\vartheta\,d\phi}$$

$$\propto \int_{x_1}^{x_2} \frac{2\bar{\alpha}a\sqrt{1-x^2}\,dx}{X} \int_{-\pi/2}^{+\pi/2} \cos\phi_1 \Big/ \pi(x_1-x_2)$$

$$\propto 4\bar{\alpha}a\left[\int_{x_1}^{x_2}\frac{dx}{X} - \frac{1}{2}\int_{x_1}^{x_2}\frac{x^2dx}{X}\right]\Big/\pi(x_1-x_2)$$

$$\propto 4\alpha a\left[\frac{x_1-x_2}{2a} + \frac{b}{4a^2}\log\left|\frac{X_2}{X_1}\right| + \left(1-\frac{b^2-2ac}{4a^2}\right)\int_{x_1}^{x_2}\frac{x^2dx}{X}\right]\Big/\pi(x_1-x_2) \qquad (12)$$

where the variable $x = \cos\vartheta$, the function $X = ax^2 + bx + c$ and the x power coefficients a, b, c, have a similar meaning as in the relation (5). The relation (12) can be further simplified according to the relative values of b^2, 2ac and 4ac. Indeed, if $b^2 = 2ac \propto 2a << 1$, one has :

$$\left(\frac{\Delta p}{p}\right)_{o} \alpha\simeq 2\bar{\alpha}\left[(x_1-x_2)+\frac{1}{b}\log\left|\frac{1+bx_2}{1+bx_1}\right| + \frac{1}{\sqrt{2ac}}\left(\tan^{-1}\frac{2ax_2+b}{\sqrt{2ac}} - \tan^{-1}\frac{2ax_1+b}{\sqrt{2ac}}\right)\Big/\pi(x_1-x_2)\right. \qquad (13)$$

Instead when $b^2 = 4ac \propto 4a << 1$.

$$\left(\frac{\Delta p}{p}\right)_{o} \alpha\simeq 2\bar{\alpha}\left[(x_1-x_2)+\frac{1}{b}\log\left|\frac{1+bx_2}{1+bx_1}\right| + \left(1-\frac{c}{2a}\right)\left(\frac{2}{2ax_1+b} - \frac{2}{2ax_2+b}\right)\right]\Big/\pi(x_1-x_2$$

$$\propto \frac{2\alpha}{\pi}\left(1 + \frac{1}{2b}\,\frac{b(x_2-x_1) - b^2(x_2^2-x_1^2)/2}{(x_1-x_2)}\right) \propto \frac{2\alpha}{\pi}\left(1 - \frac{1}{2} + \frac{b}{4}(x_1+x_2)\right)$$

$$\propto \frac{\alpha}{\pi}\left(1 + \frac{1}{2}\,\frac{\beta_r}{\beta_e}(\cos\vartheta_1 + \cos\vartheta_2)\right) \qquad (14)$$

Consequently, the mean value of the Doppler broadening due to the non collinear motion of the recoil ions is rather small for electron spectrometers with small angular aperture around the symmetry axis [like the Siegbahn-Kleinheinz magnetic lens where $(\vartheta_1\ \vartheta_2) \simeq (10°, 20°)$]. This correction is more important for the intermediate image electron spectrometers with the same angular aperture than in the previous lens but

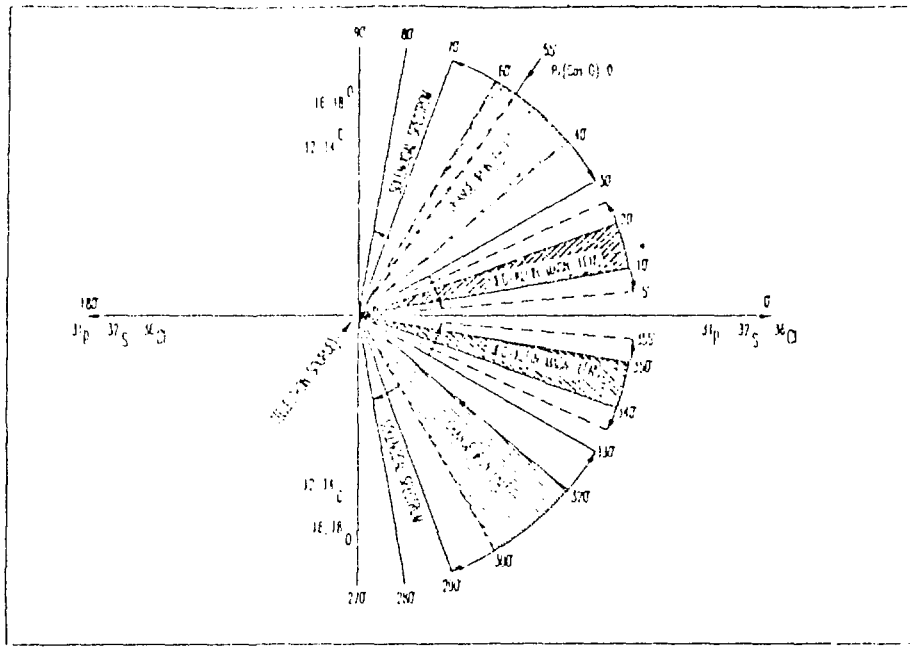

Fig. 1 - Angular openings and axial orientations of in-beam electron spectrometers (relatively to the accelerated ion-beam). The Doppler broadening of prompt transitions arising in compound nuclei produced by heavy ion (^{31}P, ^{32}S) induced reactions favours the collinear geometry.

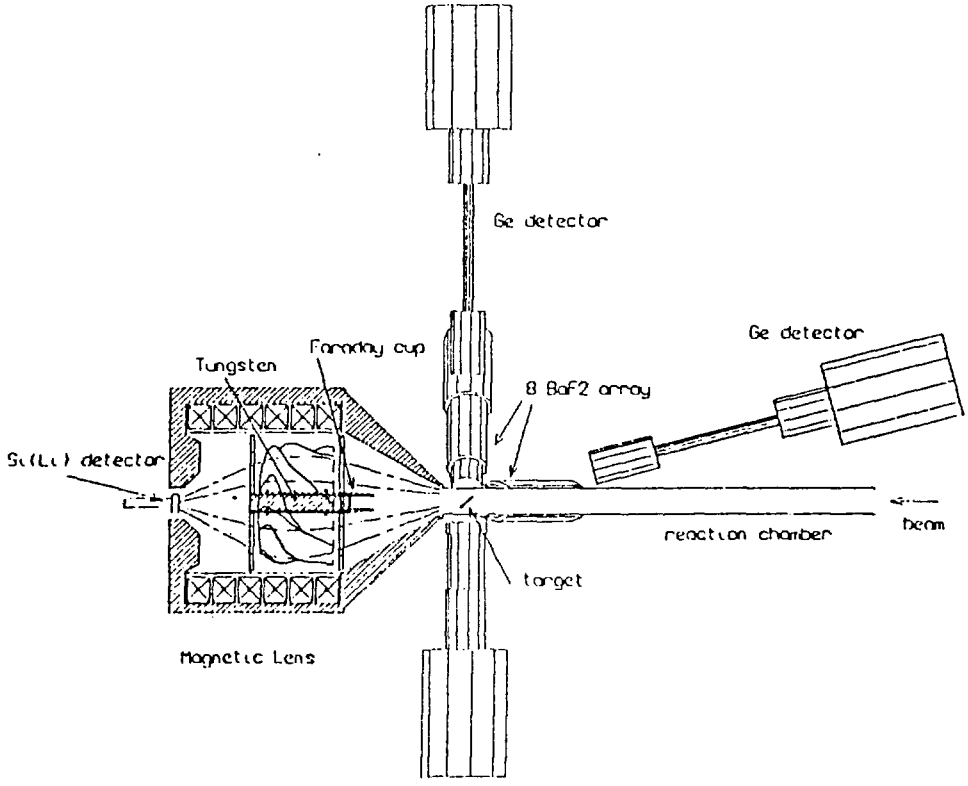

Fig. 2 - Schematic representation of the in-beam e-γ spectrometer operating at Orsay with the Siegbahn-Kleinheinz magnetic lens oriented in the direct collinear geometry.

remains small on account of the (β_r/β_e) ratio. The same is also true for the toroidal electron spectrometers in spite of their much larger angular aperture.

The recoil ion angular spread emerging from an irradiated target is the overall superposition of several angular deflections due to three main different physical effects : (i) finite angular spread of the accelerated ion beam hitting the target and its kinematical influence on the recoil ion angular deflection ; (ii) neutron evaporation influence on the compound nucleus recoil ion angular (and velocity) spread ; (iii) multiple ion scattering of the accelerated ions and recoil ions within the target. For each such effects there is a mean recoil ions angle, α, which must be introduced in the relation (14) in order to evaluate its effect on the electron Doppler broadening of an electron line requires an accurate evaluation of the electron line width given by the analyzing spectrometer as well as their electron optical properties (including spherical and chromatic aberrations). An example of such a detailed study is given in ref. [2].

3 - IN-BEAM ELECTRON SPECTROMETERS WITH COLLINEAR GEOMETRY AND THEIR USES

All in-beam electron spectrometers having a symmetry axis either geometrical (like in multi-gap toroidal spectrometers) or magnetical (like in axial symmetric magnetic spectrometers) can be operated with the collinear geometry. The fig. 1 illustrates schematically the geometrical arrangement of several in-beam electron spectrometers operated in the collinear geometry (and a few other orientations).

The iron core magnetic lenses and the iron free toroidal spectrometers are the most currently used electron spectrometers in the collinear geometry. In both cases the electron beam angular opening is rather large and the transmission quite high [i.e. $(\theta_1,\theta_2) \simeq (40°,50°)$, $(\theta_1,\theta_2) = (30°,70°)$, $T = 9\ 10^{-2}$, $T = 26\ 10^{-2}$ respectively]. The first type of instrument has been mostly applied to in-beam measurements with accelerated protons and light ions [4-6]. Instead, the second type has been used with a wide variety of in-beam experiments involving heavy ions [2,8-11]. The Doppler broadening in the former type of experiments is not very important but the collinear geometry is required for angular distribution considerations of electron-positron spectral measurements. The situation is quite different for nuclear reactions induced by heavy ions where the Doppler broadening is very important unless the transmission is considerably reduced or a wide transmission combined with a kinematic compensation [2,8]. On the other hand both types of electron spectrometers have rather large target- detector distances (i.e. d = 40-50 cm) allowing an efficient shielding for the radiations emitted by the Faraday cup stopping the accelerated ion-beam plus the recoil ions far away from the electron detector. Finally, the exclusion of small electron angular openings in both cases (i.e. $\theta > 30°$) restricts the amount of δ-electrons accepted in the collinear measurements performed with such instruments. In this respect the situation is unfavourable for the Siegbahn-Kleinheinz magnetic lens [where $(\theta_1,\theta_2) = (10°,20°)$; see fig. 1] due to the strong δ-rays focused forward by the magnetic field on the large Si(Li) detector. For that reason, it is essential to operate this combined magnetic-Si(Li) spectrometer with several background suppression devices (as briefly reported in the section 4).

A similar situation occurs for solenoidal spectrometers operated in this geometry [12-13]. A possible way to avoid such a drawback is to place the Si(Li) detectors off-axis in order to avoid the concentration on their surface of δ-electrons propagating along that direction. This method was already used in non-collinear measurements performed with the double solenoidal spectrometers operating with recoil ion shadow method [13].

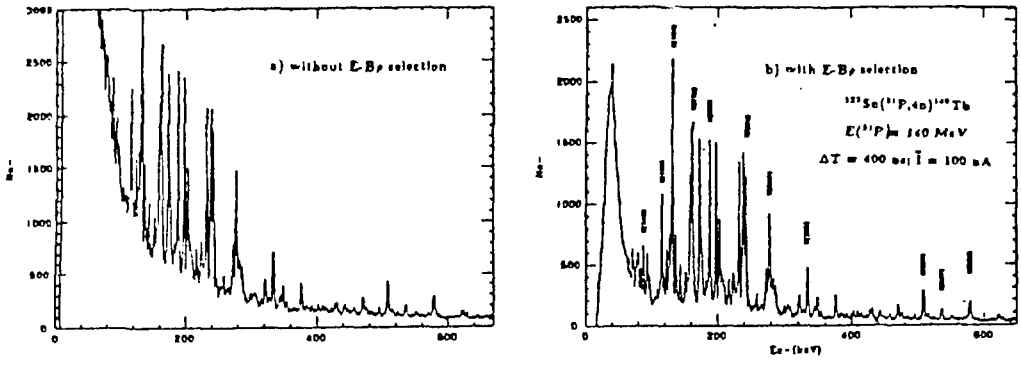

Fig. 3 - Time filtered spectrum in prompt coincidence with at least one BaF_2 (ΔT = 33 ns).

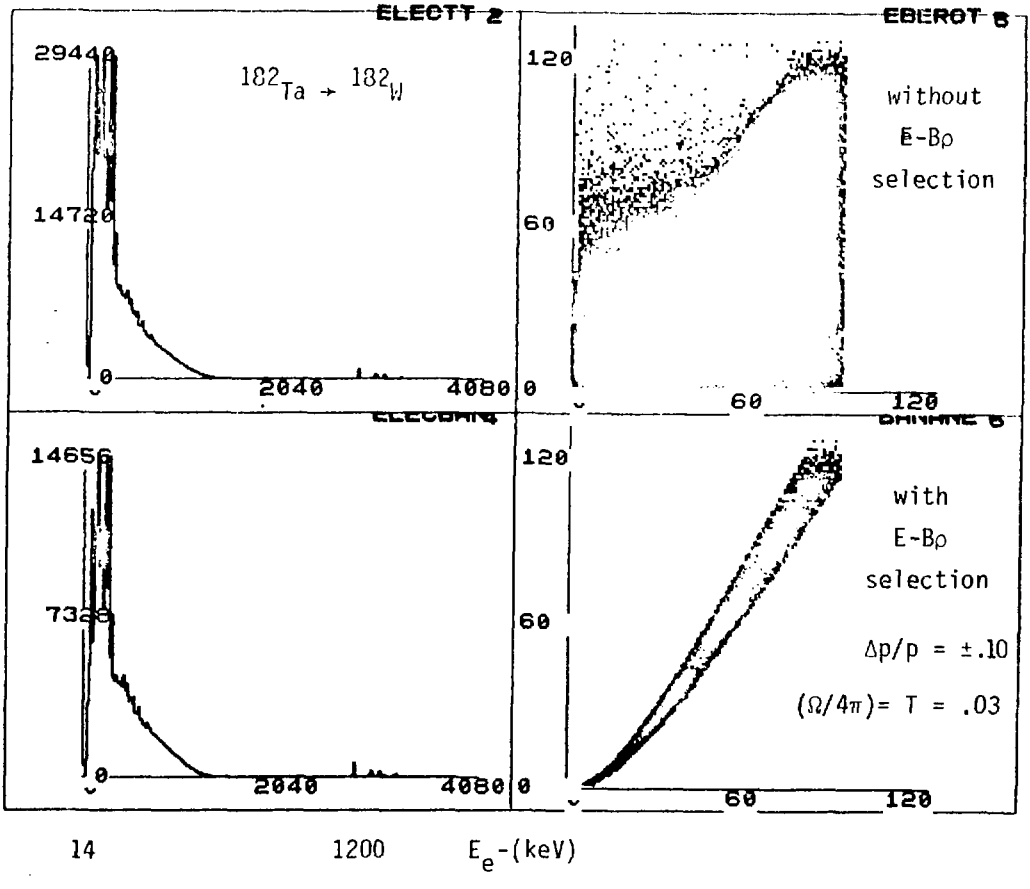

Fig. 4 - Internal conversion electron spectrum of a thin radioactive source (tantalum-182) obtained with the Orsay's e-γ spectrometer operated with and without E-Bρ selection during the magnetic field sweep.

Another procedure to reduce the δ-ray background in solenoidal electron spectrometers is to measure the electrons in the backward collinear geometry (see ref. [14]). The main features of a similar set-up designed for the Siegbahn-Kleinheinz magnetic lens is briefly discussed in the section 5.

4 - THE SIEGBAHN-KLEINHEINZ MAGNETIC LENS

This magnetic lens, combined to a Si(Li) detector, has been used previously for a wide variety of in-beam measurements either oriented at 90° or at 125° of the accelerated ion-beam [15-18]. A few results obtained with the same e-γ spectrometer oriented in the forward collinear geometry are described in subsection 4.1 and the main features of a similar set up aligned in the backward direction are briefly reported in section 4.2.

4.1 - Forward collinear geometry

The figure 2 illustrates a schematic representation of the in-beam e-γ spectrometer operated in the forward collinear geometry at the experimental area of Orsay's MP Tandem accelerator. This geometry allows internal conversion measurements of prompt (and short delayed) transitions emitted by fast compound nuclei ($\beta_r = 3\ 10^{-2}$) produced by heavy ion bombardment of thin foils. Moreover, this electron spectrometer has several devices [15-18] for reducing a continuous background -or spurious discrete lines- overlapped with internal conversion lines. The most important devices are the following ones :

i) an electron-positron discriminator made of a twisted baffle;

ii) an electronic time filter selecting prompt and delayed time intervals between two consecutive bursts of the accelerated particle beam ;

iii) a simultaneous electron energy-momentum analyzer operating for each electron detected by the Si(Li) crystal. Such detection occurs within the electron momentum interval focused at any instant by the magnetic lens on the effective area of the detector surface. Moreover, according to the required experimental purpose (like, for instance, to search very weak IC lines lying on a narrow momentum interval or instead to explore a wide momentum interval looking for medium intensity IC lines) that momentum window ($\Delta p/p = 0.2$) is fixed around a given momentum value, p, or swept within a momentum interval (p_1, p_2) ;

iv) a detection device for the instant of production of the compound nucleus including an array of very fast γ-ray detectors (i.e. a set of eight BaF2 (2"x2") coupled to fast P.M. like XP2020Q), giving a time resolution of 250 ps at high counting rate (10^5 Hz).

v) a multiplicity selection of γ-rays deexciting high-spin states using the same array of fast scintillators.

Fig. 3 illustrates the electron background reduction in the low energy part ($E_e \leq 200$ keV) of the internal conversion spectrum of ^{149}Tb obtained with simultaneous electron energy and momentum selection plus special time filtering using a pulsed beam (∝ 33 ns width prompt time window) and multiplicity filtering (at least one BaF2 firing). This operating mode reduceds considerably the contribution of the scattered electrons (and photo-electrons) originated in the baffles and the magnetic lens wall to the detector counting rate. Furthermore the continuous background due to back-scattered electrons in the Si(Li) detector is drastically reduced. Finally all these features are well illustrated by the IC electron spectra of tantalum-182 (figs. 4a and 4b) obtained without (fig. 4a) and with (fig. 4b) simultaneous electron energy-momentum selection.

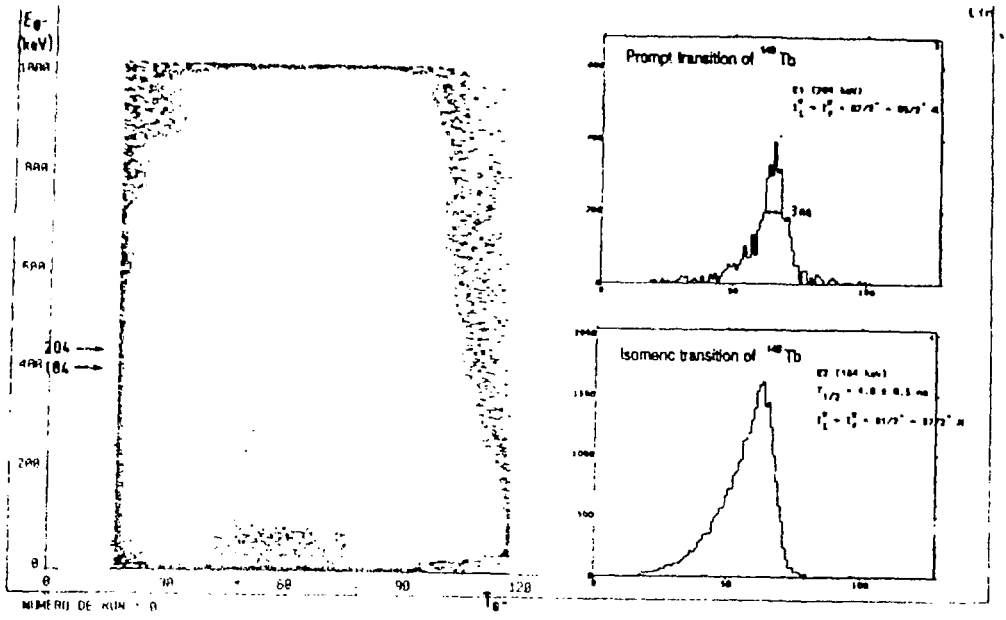

Fig. 5 - Bi-dimensional spectrum (E_{e^-}, T_{e^-}) of prompt transitions of Terbium 149. Time projections of prompt (E = 204 keV ; E1) and delayed (E = 184 keV ; E2) transitions are shown in fig. 5a and 5b.

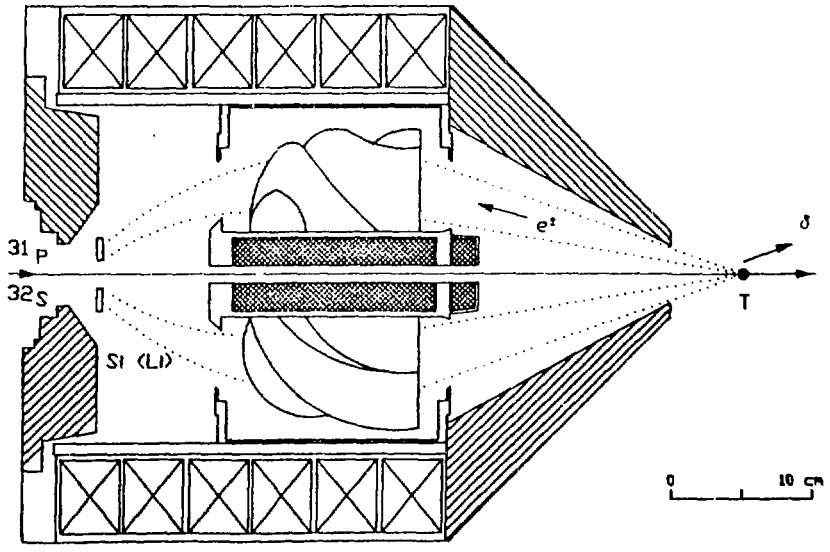

Fig. 6 - Longitudinal cross section of the Siegbahn-Kleinheinz magnetic lens oriented in the backward collinear geometry. The annular Si(Li) detector (without its holder and cryostat not shown in the figure) and the tubular heavy metal shielding (surrounded by the twisted baffle) are schematically represented.

Another interesting feature of the collinear geometry is the possibility of analysing internal conversion lines of EM transitions deexciting very high spin states. Indeed such states are usually populated by heavy ion induced reactions creating a considerable Doppler broadening. Therefore, the complementary study of γ-rays and internal conversion electrons corresponding to EM transitions deexciting very high spin states requires the use of in-beam electron spectrometers oriented in the collinear geometry.

A typical example of such studies is given by the half-life measurement of the 184 keV transition in ^{140}Tb performed with the electron-gamma spectrometer (represented in fig. 1) operating at Orsay. Fig. 5 shows the bidimensional spectrum (E_{e^-} T_{e^-}) of the prompt transitions in that nucleus. The time projections of the prompt (E=204 keV ; E1) and delayed (E=184 KeV ; E2) transitions are represented in fig. 5b and fig. 5c respectively).

This experiment confirmed the existence of the high spin isomer at 9.915 MeV, $I^{\pi} = 61/2^{+}$ state in ^{149}Tb. Indeed, the existence of that isomer was previously suggested by the γ-γ experimental data obtained with the Chateau de cristal and the corresponding IC data collected in the e^--γ spectrometer operated with a recoil catcher foil close to the target [20]. However, these preliminary investigations did not allowed an accurate determination of the corresponding half-life which was performed with the latter measurement ($T_{1/2}$ = 4 ± 0.5 ns).

Finally, the target qualities -like the performances of the accelerated ion-beam optics- are particularly important for in-beam measurements of low-energy (E ≤ 100 keV) internal conversion electrons [21-23].

4.2 - Backward collinear geometry

Figure 6 gives a schematic representation of this in-beam e-γ spectrometer designed for backward collinear measurements. Four major differences (i-iv) discriminate this experimental set up from the previous one (shown in fig. 2) :

i) The circular Si(Li) detector shown in fig. 2 is replaced by an annular Si(Li) detector (or two half-annular Si(Li) detectors) in fig. 6 ;

ii) The cylindrical (X+γ)-ray central absorber (made of a tungsten rod) and its Faraday cup are replaced by a tubular heavy metal absorber. Its inner diameter (Ø = 10mm) allows a free passage for the (nearly parallel) accelerated ion-beam and the corresponding outer diameter protects the Si(Li) detector from the (X+γ) rays emitted directly from the target towards that detector ;

iii) The Si(Li) cryostat allows not only axial displacements (under vacuum) of that detector (like in all other geometrical configurations), but also lateral displacements of the same detector in its position outside the magnetic lens. The latter possibility is intended to protect that detector during adjustements of the accelerated ion-beam optics .

iv) A miniaturised target vacuum lock allowing easy (and fast) target changes with a maximum amount of free space around the target needed for increasing the efficiency of the (X+γ)-ray detection.

This experimental set up is mainly intended for the study of low-energy prompt transitions (i.e. both (X+γ) rays as well as internal conversion electrons). For that purpose it is important that all electronic and other devices described earlier (section 4.1) will be operated also in the particular case. In particular, the δ-electrons background should be considerably reduced by its strongly anisotropic emission.

5. CONCLUSION AND PROSPECTS

The experimental results obtained at Orsay with a Siegbahn-Kleinheinz magnetic lens oriented in the forward collinear geometry are extremely encouraging for the planned measurements with a similar set up oriented in the reverse direction of the accelerated ion-beam. Consequently, in order to create new possibilities for simultaneous in-beam (X+γ) ray and electron measurements required by accurate (and extensive) nuclear spectroscopy measurements it seems necessary to investigate thoroughly how to combine electron spectrometers of different types to multi-gamma-ray detector arrangements.

The general requirements for such a combination as well as the main features of an electron goniometer associating a miniaturized axial magnetic lens (with triangular + uniform fieldshape) to a Si(Li) detecter were already discussed earlier [17]. Iron-core and iron-free mini-orange electron spectrometers were also specially designed for in-beam measurements coupled to γ-arrays [24-25] or other types of detectors [26]. These examples are good illustation of a wide research field of instrumental developments for nuclear (and atomic) structure investigations.

ACKNOWLEDGEMENTS

We are very grateful to Helmut BOKEMEYER, Peter BUTLER, Helmut FOLGER, Juhani KANTELE, Arto PASSOJA and Ziemowid SUJKOWSKI for their valuable help, advice and strong encouragements concerning this type of measurements. We thank also very much our colleagues Jean-Marie LAGRANGE, Michèle PAUTRAT and Jean VANHORENBEECK for their precious help on the development of the data acquisition system of this e-γ spectrometer as well as its successful application to many nuclear isomeric investigations.

REFERENCES

[1] Bohm D., *The special theory of Relativity* (Benjamin, NY 1965), p. 98
[2] Handschug L., Backe H., Bokemeyer H., Nucl. Instr. Meth. 161 (1979) 117
[3] Knop G. and Paul W., in *α, β and γ-ray Spectroscopy*, Vol. 1, ed. K. Siegbahn (North Holland, Amsterdam, 1968) p. 1
[4] Passoja A., Kantele J., Luontama M. and Julin R., Nucl. Instr. Meth. 157 (1978) 513 and 166 (1979) 203
[5] Luontama M., Kantele J., Julin R., Passoja A., Poikolainen T. and Pylvänainen M., Nucl. Instr. and Meth. 159 (1979) 339
[6] Julin R., Kantele J., Kumpulainen J., Luontama M., Nieminen V., Passoja A., Trzaska W. and Verho E., Nucl. Instr. Meth. A270 (1988) 74
[7] Backe H., Berdermann E., Bokemeyer H., Greenberg J.S., Handschug L., Hebberger F., Kankeleit E., Kienle P., Kozhuharov Ch., Nakayama Y., Richter L., Stettmeyer H., Vincent P., Weik F. and Willwater R., J. Phys. Soc. Japan 44 (1978) Suppl. 832-837
[8] Balanda A., Bokemeyer H., Grosse E., Matsuki S., Nakayama Y., Schwalm D., Backe H., Handschug L.,GSI Annual Report (1978) p. 50
[9] Kozhuharov Ch. in Proc. NATO Advanced Studies Institute, *Quantum Electrodynamics of Strong Fields*, Lahnstein 1981 (Plenum Press NY) 317
[10] Koenig W., Bosh F., Kienle P., Kozhnharovc, Tsertos H., Bedermann E., Huchler S. and Wagner W., Z. Physik A328 51978) 129
[11] Backe H., GSI-Nachrichten 01-87, Darmstadt (1987) p. 13
[12] Kantele J., Kumpulainen J., Nieminen, Pesonen J., Julin R., Passoja A. and Verho E., J.Y.F.L. Annual Report 1987, p. 30
[13] Backe H., Weik F., Butler P.A., Metag V., Wilhelmy J.B., Habs D., Himmeleb-Specht H.J., Phys. Rev. Lett. 43 (1979) 1077
[14] Backe H., Senger P., Bonin W., Kankeleit E., Kramer M., Krieg R., Metag

V., Trautman N., Wilhelmy J.B., Phys. Rev. Lett. 50 (1983) 1838
[15] Bokemeyer H., GSI-Nachrichten 01-87, Darmstadt (1987) p. 13 and GSI 90-11 Report
[16] Butler P., Daresbury Annual Report 1987-88
[17] Dionisio J.S., Vieu Ch. and Passoja A., Proc. 22nd Int. Winter Meeting on Nuclear Physics, ed. I. Iori, Milano University, 1984, p. 167
[18] Dionisio J.S., Vieu Ch., Lagrange J.M., Pautrat M., Vanhorenbeeck J. and Passoja A., Proc. 23rd Int. Winter Meeting on Nuclear Physics, ed. I. Iori, Milano University, 1985, p. 214
[19] Dionisio J.S., Vieu Ch., Lagrange J.M., Pautrat M., Vanhorenbeeck J. and Passoja A., Proc. 26th Int. Winter Meeting on Nuclear Physics, ed. I. Iori, Milano University, 1988, p. 596
[20] Schück C., Bendjaballah N., Dionisio J.S., Meliani Z., Vieu Ch., Beck F.A., Byrski T., Curien D., Duchêne G., Merdinger J.C., Rouabah S., Fallon P., Howe D., Sharpey-Schafer J.F., Twin P., Proceed. 26th Int. Winter Meeting on Nuclear Physics, ed. I. Iori, Milano University, 1988, p. 619
[21] Méliani Z., Dionisio J.S., Schück C., Vieu Ch., Beck F.A., Byrski T., Curien D., Duchêne G., Roberts J., and Sharpey-Schafer J.F., Nucl. Phys. Spring Meeting, Strasbourg, March 1990
[22] Méliani Z., Dionisio J.S., Schück C., Vieu Ch., Beck F.A., Byrski T., Curien D., Duchêne G., Roberts J., and Sharpey-Schafer J.F., Int. Conf. on Nuclear Structure in the Nineties, Oak-Ridge (April 1990)
[23] Lagrange J.M., Pautrat M., Dionisio J.S., Vieu Ch., Vanhorenbeeck J. Nucl. Instr. and Meth. A271 (1988) 527
[24] Dionisio J.S., Vieu Ch., Lagrange J.M., Pautrat M., Vanhorenbeeck J. Nucl. Instr. and Meth. A288 (1989) 10
[25] Dionisio J.S., Méliani Z., Schück C., Vieu Ch. and Folger H. to be published.
[26] Steenberger T., KVI Internal Report (Groningen 1989)
[27] Bacelar J.C., private communication
[28] Bokemeyer H., private communication.

MICROPHYSICS EVOLUTION AND METHODOLOGY

A few remembrances and reflections on F. Joliot's conceptions on Nuclear Research

J.S. DIONISIO

C.S.N.S.M. (I N2 P3), Orsay, FRANCE

Abstract

A few general features of *Microphysics evolution* and their relationship with *Microphysics methodology* are briefly surveyed. Several pluri-disciplinary and interdisciplinary aspects of *Microphysics research* are also discussed in the present scientific context. The need for an equilibrium between individual tendencies and collective constraints required by team work, already formulated thirty years ago by Frédéric Joliot, is particularly stressed in the present conjuncture of *Nuclear Research* favouring very large team projects and discouraging individual initiatives. The increasing importance of the *Science of Science* (due to their multiple social, economical, political, ecological aspects) and the stronger competition between national and international tendencies of scientific (and technical) cooperation are also discussed.

1. Introduction

More than twenty five years after the publication of "*The Science of Science*" [1], following the same trend of the well-known book of J.D. Bernal dealing with "*The Social function of Science*" [2] published half a century ago, it seems interesting to review a few important problems of Microphysics Research (including Nuclear Physics) which strongly influence its present development and probably its future as well.

Many epistemological problems of that kind -like, for instance, the nature of the physical theories [3], their relationship with physical experiments [4] or the characters of the physical laws [5]- were extensively investigated in the past [see, for instance, the ref. 3-5 and many others quoted therein] and are still important topics of reflection and discussion. The same occurs with a few more specific topics of very wide interest, like "Simultaneity and Relativity" [6,7] "Continuum and discontinuum" [8] "Particle and wave " [9,11] "Determinism and Indeterminism" [12-17] "symmetry and asymmetry" [18,19] "order and chaos" [20-21], which are essential for the development of all Natural Sciences. [see, for instance, ref. 6-21 for a broad view on the extensive literature concerning these topics).

There are also other general problems dealing with the relationship between Physics, Philosophy (Epistemology, Metaphysics, Ethics, Religion) as well as Economical, Social and Political Sciences. These problems were also thoroughly investigated in the past and are still analyzed nowadays on account of their importance in our everyday life and its evolution [see, references 1-2 and 12-21].

At first sight the methodological problems of Microphysics Research look less fundamental than the previous problems for the development of

Science. Nevertheless, their practical importance for the development of Microphysics Research is rather crucial. Consequently, the main purpose of this work is to evoke a few remembrances and reflections on Frédéric Joliot's conceptions on Nuclear Research collected at Orsay more than thirty years ago [22-24]. Such reflections were progressively developed on other occasions [25-26] and recently extended to similar discussions held earlier in other European countries [27-29].

We start this contribution with a broad discussion of *the general features of Microphysics Research* (section 2). Afterwards we consider a few *pluridisciplinary and interdisciplinary aspects of Microphysics Research* (section 3) before discussing the important questions of *individual tendencies and team work constraints* (section 4) as well as *planned and unplanned scientific work* (section 5). Before concluding, we make a brief discussion concerning the need for a deep -and close- *national and international scientific cooperation* (section 6) within this important research field. Indeed, such a cooperation is particularly urgent on a European Scale due to the scientific, social and political context prevailing in this continent at present as well as its world impact. However, the increasing number of very large and expensive projects plus the international character of the scientific development (far beyond national and political barriers !) makes World wide Nuclear Science Cooperation also indispensable. Finally, we conclude stressing the actual importance of Microphysics Research and showing the superficial nature of many frequent criticisms made against Nuclear Physics (section 7).

2. General features of Microphysics Research

The large amount and wide variety of scientific knowledge accumulated in Microphysics during this century has led to the development of many different concepts within three main scientific branches : Atomic and Molecular Physics, Nuclear Physics and Elementary Particle Physics.

The present status of development of these different branches is characterised by a *good theoretical description of most atomic and molecular phenomena* and *less accurate theoretical predictions of nuclear and elementary particle effects.*

In the earlier phases of development of these different branches of Microphysics their experimental methods were often quite similar and had generally comparable complexity. However, the proliferation of specific problems dealing with atomic and nuclear structure led to the requirement of very different experimental methods and tools for their investigation. In particular, very complex and expensive experimental facilities (like particle accelerators, nuclear reactors and large powerful radiation analysers) were designed, built and used for a wide variety of nuclear investigations. Moreover, the expansion of elementary particle physics research led to the development of still larger experimental facilities (including gigantic particle accelerators !) which differentiated quite sharply the methods used in the investigation of such branches of Microphysics.

The present status of development of these experimental methods is characterised by a general tendency prevailing nowadays in the orientation of their evolution : The experimental projects (and experimental tools) motivated (or suggested) by the theoretical description of the different branches of Microphysics are usually very different and employed exclusively within a single branch. Sometimes their use is still more restricted to a

particular research topic or a special branch of Microphysics research. Only very rarely one can find experimental methods used alternately (and sometimes uncorrelated) by several Microphysics branches.

This general feature of Microphysics Research has the following major drawback : Whenever the specific topic chosen for that investigation becomes less scientifically important (and attractive) or new technological developments make that tool obsolete for that particular purpose (without excluding other potentially interesting applications for other purposes not considered in the original purpose -or application- of that instrument) there is usually a tendency to stop the operation of that facility. Later the same is often dismantled -and sometimes destroyed- invoking either economical reasons or the need to recover valuable free space within the laboratory as well as to release scientific and technical manpower needed for other experimental projects. Of course, to the extent where such facilities still remain unique -or scientifically useful- their extinction (or destruction) is basically anti-scientific and anti-economical (in the sense of reducing the actual scientific capabilities and possibilities of development). However, considering the limited budget and manpower capabilities for scientific development there is a unique solution to avoid (or reduced the importance of) such drawbacks : Any new large project should be fully investigated considering the main features of its primary aim as well as other important features of related topics. Indeed, the potential experimental possibilities of any new instrument -or facility- for a *different purpose* of its original aim, may contribute to very important unpredicted experimental discoveries of other scientific branches. Consequently, it might be advisable (whenever possible !) to investigate the potential possibilities of alternative use (either correlated or uncorrelated) of large experimental facilities. In other words a *scientific instrument for general purpose* should never be considered "in competition" with a *single purpose instrument* even when this is considered very important for the scientific progress. In such a case, it should be taken as an extra development not a replacement of an indispensable tool !

3. Pluridisciplinary and interdisciplinary aspects of Microphysics Research

There are many different aspects to be considered in each branch of Microphysics research. Such pluridisciplinary aspects may be very important for the solution of a particular problem of a given branch and less important for the solution of similar problems of another branch. Consequently there is no hope in the present status of our knowledge to *unify* the experimental and theoretical description as well as the research methodology of all Microphysics branches. Instead, there is hope of finding a better correlation between their descriptions and exploration methods for all interdisciplinary aspects of such branches.

In our opinion, the interdisciplinary problems of Microphysics are very important provided they are considered in detail and without making too rough approximations. Indeed, the interdisciplinary investigations, apart *from their* inherent complexity due to the overlap of multiple physical effects and interactions, are potentially very rich exploration fields of scientific knowledge. Furthermore, they often stimulate new scientific developments in different interacting fields. Last but not least they require -and stimulate- a broad view of the scientists working on interdisciplinary topics. Nevertheless, this requirement must be fulfilled at a high level of scientific knowledge and needs technical qualifications within a wide -and complex- research domain. Consequently, this limitation is a major drawback for the development of this type of investigations.

Spectroscopy, for instance, is one of the most typical inter-disciplinary topics covering all branches of Microphysics through a wide variety of special spectroscopic methods and techniques [30]. Among these methods the following should be quoted : Nuclear magnetic and quadrupole resonance spectroscopy, electron spin resonance and Mossbauer spectroscopy, microwave, infra-red and Raman spectroscopy, electronic spectroscopy of atoms and molecules, photoluminescence spectroscopy, optical rotatory dispersion, maser and laser spectroscopy, photoelectron spectroscopy, etc.. All these spectroscopic branches deal essentially with atomic and molecular structure (apart from the influence of nuclear moments in the first mentioned spectroscopic branches). More generally, the nuclear spectroscopic methods cover a wide portion of the nuclear structure research field. Furthermore, the low energy γ-ray spectroscopy as well as the low energy electron spectroscopy (i.e. internal conversion electrons and β-rays) are partially overlapped with discrete atomic transitions (like X-rays and Auger electrons respectively). Consequently, there is a considerable overlap of atomic and nuclear effects for all available nuclides (i.e. $Z \leq 110$) in the low energy photon and electron spectroscopy domain (i.e. E_γ, $E_e \leq 120$ keV). Moreover, there is a similar overlap of atomic and molecular effects for very high resolution low energy electron spectroscopy (i.e. $E_e \leq 2\text{-}5$ keV) studies. These spectroscopic methods led to a wide field of analytical studies and practical applications. More recently several new mechanisms of atomic de-excitation were also discovered in these very low energy investigations. In such conditions, it would not be surprising to find new important facts concerning atomic and nuclear de-excitation mechanisms when the instrumental features (as well as the radiation source and detection techniques) increase considerably the overall resolving power of the low energy radiations (E_γ, $E_e \leq 120$ keV). In other words, one can expect important unpredictable discoveries in atomic physics by improving the present available spectroscopic tools or by creating new ones grounded on new materials and (or) technical developments [31]. Similar previsions concerning the nuclear structure progress seem more uncertain due to the present inaccuracy of theoretical nuclear predictions. However, from an empirical point of view one can expect the discovery of interesting spectral regularities by improving the analysis of low energy nuclear transitions.

These general arguments are in favour of *small sized -but highly sophisticated- instrumental developments* in order to improve the exploration of the Microphysics world. Indeed, the multiparametric features of a given experiment must be kept in mind. The energy of an accelerated particle beam (or its beam intensity) is not *a priori* the unique feature -or even the most important one for a given in-beam experiment. For instance, the beam time structure and its spatial distributions are also essential features for the application of important spectroscopic methods (like those using recoil ions).

4. Individual tendencies and team work constraints

The working conditions within a nuclear reseach laboratory before the last World War were quite different from those of post-war scientific laboratories. The main differences occurring in French laboratories of that scientific research branch were well described earlier by Frédéric Joliot (quoted in ref. [24]): "The (classical) research workers -who, in my opinion, should sometimes have an artistic temperament- felt very close to the phenomenon under investigation. Furthermore, the observation of such a phenomenon looked straightforward and the experimenter felt quite free to

follow his creative imagination doing quite different, unpredicted, trial experiments. Often he reached an unexpected result leading to a new scientific discovery (like a poet writing a poem by following his inspiration) without very expensive scientific equipment or creating too many risks for his own working mates". In other words, "fundamental research in the earlier phase of development of Nuclear Physics had an artisanal character rather favourable to the development of the nuclear scientist's personality" [loc. cit. 24].

Instead, "a modern centre of nuclear research has apparently an industrial character". Consequently, "there is a risk of crashing the scientist's mind with quite impressive, large, complex and very expensive instruments (like reactors and particle accelerators) which are rather costly and difficult to operate". In such conditions -set by the experimental requirements and our technological development- "the research worker no longer feels free to experiment by multiple trials but instead he forces himself to reduce as much as possible the number of exploratory attempts before starting a new research work". Consequently, "it is rather difficult nowadays to a make an experiment involving an expensive instrument -or material- with a small chance of success supported essentially by the simple motivation of scientific curiosity. However, isn't it a fact that scientific discoveries are sometimes unpredictable and quite surprising ?" [see ref.24]

According to this broad description of such quite different experimental conditions, Frédéric Joliot gave the important advice : "In this transition from scientific work on an artisanal scale to the same work on an industrial scale it seems to me that it is indispensable to evaluate all drawbacks of such transition and to find the best experimental uses of modern experimental equipment which do not attenuate -or even suppress- the personality of the scientist. In any case, there is no hope of making an original masterpiece with chain work !" [see loc. cit. 24].

The increasing complexity of theoretical and experimental scientific problems as well as the fast expansion of so many scientific branches induced several important consequences in those research fields -like Microphysics- where such evolution was very fast and deep. In particular, the individual research work become progressively less frequent and is gradually replaced by team work of research groups specially devoted to a particular project or an experiment dealing with very complex, bulky and expensive instruments.

The same point of view was stressed by P.M.S. Blackett [28] and C.F. Powell [29] in their E. Rutherford's and H. Bhabha's memorial lectures. For instance, talking about the great success of the CERN, Powell claims that "such institutions serve to demonstrate the immense power in human resources on which international science can call in well-directed and well-managed institutions". However, like F. Joliot, Powell sees also several drawbacks of such research institutions : "But this great increase in our powers of investigation has also a negative aspect. The change is reminiscent of the transformation from handicraft to machine and industrial production, but it has been much more rapid. In place of individual investigation there is now research by large teams of people in institutions where good management and an effective bureaucracy are indispensable and where an individual has to find satisfaction in this work in a new way". Nevertheless, Powells looks confident in the solution of this problem : "It seems, however, that we can indeed so organise the work in such institutions that the young people continue to find deep satisfaction in it. It is important to be alive to the problems and to make sure that all members know the significance of their

contribution and feel that good efforts are respected. We are here meeting what is becoming a very general problem : how to ensure the creative participation of people in the affairs of large enterprises at a time when an elaborate hierarchy seems to be an essential element in effective organisation". [cf. ref. 29].

5. Planned and unplanned scientific work

The team work requires for its success a detailed planning and an effective coordination of all efforts of different participants. This looks easy in theory but it is not always in practice. Furthermore, in order to take the maximum benefit of the creative possibilities of the different members of such teams, it is indispensable that the planning should not be too rigid. In other words, it is advisable to adopt a relative adaptability in the application of such planning making a compromise between the old tradition of unpredicted (or unplanned) work and the modern tendency towards planned scientific constructions (or experiments). This point of view is strongly emphasised by H.S.W. Massey in a presidential address to the (British) Physical Society [27] : "It is also most important that the research programme of a team should not be over planned. The surest way to miss the unexpected is to plan the programme so that only what is predictable is observed. This is, of course, obvious but, in practice, it is only too easy to make this mistake".

"Original scientific work" arises either as the result of an unpredicted *new scientific result* or from a *new synthesis* condensing previous experimental results and new theoretical interpretations. This type of scientific work is the main characteristic feature of pure research work.

"Routine scientific work" is the daily activity of most scientists in their analytical, gradual investigation of different theoretical and technical problems involved in their investigations. "In spite of the fact that this kind of scientific activity has a lower merit than the original scientific investigations one should not neglect such an activity for that reason. Instead, one should support it as a valuable and indispensable activity for scientific progress. In any case original and routine scientific works should be considered as complementary research activities" [24]. Indeed, the division of research work between "original" attempts and "routine" activities is usually made according to the personal tendencies and aptitudes of the scientists as well as their surrounding media (i.e., material and instrumental means for the experimentalists ; scientific background and computational means for the theorists). However, "any excess of one kind of such activities is dangerous for the scientist and may have bad consequences for his scientific career" [24].

More generally, according to Frédéric Joliot, "it is advisable not to make a clear sweep of the scientific heritage in the organisation of scientific teaching and research work. On the contrary, in the organisation of pedagogical and research plans suitable to the modern tools required by such activities, the past knowledge and experience should be taken into account and an attempt should be made to fit these plans with the best features of the classical mind" [24].

F. Joliot completed this advice with a personal judgment of the limitations of large scale Microphysics research work in the late fifties : "If large nuclear research teams obtained spectacular results in the U.S.A. and U.S.S.R. using more or less strict planning, the average efficiency of their scientists looks inferior to the French ones. Furthermore, France has

not the same material and human means to compete with those super-powers" [see ref. 24].

6. National and International Scientific Cooperation

The same reasons that led to the increasing development of team research work (and reduced instead the scientific contributions of individual research workers) enhanced also the national (and international) scientific collaborations extending (or replacing) local -or regional- scientific projects. Indeed, the very large increase in the material and the qualified scientific (and technical) manpower required by the construction (and operation) of large experimental facilities used in Microphysics Research make such cooperation advisable for large countries and indispensable for smaller ones. However, what looks reasonably advisable in general is not necessarily adopted due to the fear of unknown situations, prejudices against foreigners, or simply preference for the routine instead of novelty. Consequently, one can imagine that international collaboration is necessarily more difficult to promote (and to develop) than a national collaboration while a local -or regional- collaboration should be much easier to handle due to closer contact, common background and surroundings. This rule is certainly true in many cases but not when scientists from very different origins sympathise and enjoy their work together.

In general, one should try to organise first the local and regional collaborations before extending them to the national and international frames. Indeed, "like the human organism, every country is in a very special sense unique, and its problems can only be resolved by its own people who alone knows its strengths and weaknesses intimately, and its problems at first hand" [29]. Nevertheless, a country -like an individual- is not free from interferences from other countries -or individuals- and consequently the solution of their problems is not completely uncorrelated and in a few cases may be closely related. In other words, international cooperations cannot solve completely all national problems (including the scientific ones) but may help to find their solutions.

The scientific cooperation in High Energy Nuclear Physics -and Elementary Particle Physics- on a European Scale has been considerably developed since the Last World War at the CERN laboratories installed at Geneva. Other collaborations concerning Nuclear Spectroscopy of Nuclei far from Stability were also developed in the same laboratories using an on-line Isotope Separator (ISOLDE) coupled to a medium energy particle accelerator.

Similar research activities were performed at the JINR operated at Dubna by nuclear scientists from several Eastern European Countries. Apart from these Fundamental Research Institutions there are a few European laboratories for Nuclear Applications like those of EURATOM and NUCLEAR FUSION Projects (such as the JOINT EUROPEAN TORUS (JET) (see ref. [32]).

The large amount and w'de variety of Nuclear Research facilities now existing -or actually in project- within European Countries are not coordinated by any of the previously quoted institutions. A first step for that purpose has been the recent creation of NUPECC (Nuclear Physics European Collaboration Committee) which plans to make a complete inventory of the main scientific experimental facilities -and corresponding scientific responsibles- existing now within Europe (see Ref. [33]).

Finally, considering the great importance of such a coordination not only for strictly scientific purposes but also as a valuable guide for other

kinds of International Cooperation let us to hope that such initiative and the already existing international institutions will develop first on an European scale and later be extended to a World Wide frame (like IAEA). For that purpose, it is indispensable that the will of scientific cooperation prevails over the tendency towards the national competitions as illustrated in the recent analysis of the international position of U.S. Physics [34] : "For 40 years, the United States has been the world leader in physics research, but the situation is changing rapidly. During the past decade, both the Western European nations and Japan have fully recovered from World War II and have reassumed an aggressive role in science. In many areas where previously we were clearly ahead, these nations are now fully competitive. Their re-emergence in the field of physics benefits science as a whole, but the United States can and must retain a competitive edge. Without it an essential factor in maintaining our economic well-being will be lost". Indeed, two interesting remarks can be made about this analysis : First the so-called aggressive role of Western European nations and Japan ; second the priority of economical well-being as a major justification for Fundamental Research. It is doubtful that these remarks correspond to our scientific aims and certainly not to our traditions.

7. Conclusion

The evolution of Microphysics is permanently changing with the introduction of new scientific and technical developments. Consequently, Microphysics research is potentially full of unpredictable discoveries within its very wide research field. Moreover, the relationship between Microphysics and Macrophysics (in our scale) research becomes closer and more familiar everyday through multiple Microphysics concepts (and devices ! guiding or helping us. Finally the increasing development of Inner (and Outer) Space exploration and research as well as the renewed interest in fundamental cosmological problems make the relationship between Astrophysics and Microphysics more and more important. In such conditions, it is hard to believe -and even less to understand- a "requiem" for Nuclear Physics or any other branch of Microphysics. On the contrary fascinating discoveries may be expected provided the physicists remain enthusiastic and "enjoy" their hard research work looking for a better and deeper understanding of the Physical World instead of their own social -or scientific- promotion. This prospect seems to us the main answer to the question : Quo Vadis Nuclear Physics ?

Acknowledgements

We are grateful to Ziemek SUJKOWSKI for suggesting and warmly supporting this contribution, extending our previous work on Frédéric Joliot's scientific conceptions on Nuclear Research, to this International Summer School on Nuclear Physics.

References

[1] *The Science of Science* (ed.M. Goldsmith, A. Mackay, Pergam. London 1966)
[2] Bernal J.D., *The Social Function of Science*, (Routledge, London 1939).
[3] Bridgman P.W., *The nature of Physical Theory*, (Princeton Univ. 1936).
[4] Born M., *Experimental and Theory in Physics*, (Dover N.Y., 1956).
[5] Feynman R.P., *The character of Physical law*, (MIT Press, 1967).
[6] Born M., *Einstein's Theory of Relativity*, (Dover N.Y., 1962).
[7] Pauli W., *Theory of Relativity*, (Pergamon Press London, 1958).
[8] Broglie L. de, *Continu et discontinu en Physique moderne*, (Albin Michel, Paris 1950).
[9] Broglie L. de, *Matter and Light, The New Physics*, (Dover, N.Y. 1950).
[10] Broglie L. de, *Ondes, corpuscules, Mécanique ondulatoire*, Albin Michel.
[11] Feynman R.P., *QED, the strange theory of light and matter*, (Princeton Sc. Libra, 1985).
[12] Planck M., *Initiations à la Physique* (trad.; Flammarion, Paris 1941).
[13] *Sources of Quantum Mechanics*, ed. B.L. Van der Waerden (Dover NY 1967)
[14] *Niels Bohr and the Development of Physics*, ed. W. Pauli (London, Pergamon Press, 1955).
[15] Bohr N., *Essays 1958-1962 on Atomic Physics and Human Knowledge*, (J. Willey, N.Y. 1963).
[16] Selerì, Franco, *Le grand débat de la théorie quantique*, (Flammarion, Paris 1986).
[17] Proceed. of Conf. on *Microphysical Reality and Quantum Formalism* at Urbino 1985 (ed. Kluwer, 1988).
[18] Lindsay R.B. and Margenau H., *Foundations of Physics*, (Dover, N.Y., 2nd ed. 1957) and references quoted therein.
[19] Weyl H., *The theory of Groups and Quantum Mechanics*, Dover, N.Y. 1931.
[20] Gleik J., *Chaos, Making a new Science*, (Pergamon Books, N.Y. 1987).
[21] Swiatecki W.J., *Contribution to this Summer School.*
[22] Joliot F., *Discours de l'ouverture du Congrès International de Physique Nucléaire* (ed. Mm P. Gugenberger, Dunod, Paris 1959).
[23] Joliot F., *Le nouveau Centre de Recherches Fondamentales en Physique Nucléaire à Orsay et la formation des chercheurs*, in F. Joliot-Curie, *Textes choisis*, (ed. Sociales, Mars 1959).
[24] Dionisio J., *Frédéric Joliot e a investigaçao cientifica* (Lisboa, 1958)
[25] Dionisio J.S., *A reforma das Faculdades de Ciencias* (Lisboa, 1961).
[26] Dionisio J.S., *Electron Spectroscopy and Nuclear Structure*, to be published in Fizika (1990).
[27] Massey H.S.W., *Progress and Problems in Physics To-day* in Year Book of the Physical Society, 1955, p. 1.
[28] Blackett P.M.S., *The Rutherford Memorial Lecture 1954*, in Year Book of the Physical Society, 1955, p. 13.
[29] *Selected Papers of Cecil Frank Powell* (ed. E.H.S. Burhop, W.O. Lock, and M.G.K. Menon, NHPC, Amsterdam, 1972).
[30] Chang R., *Basic Principles of Spectroscopy* (Mc Graw Hill NY, 1971).
[31] *Physics of the 20th Century. History and Outlook*, Y.P. Velikhov et al. (Mir. Publ. Moscow, 1987).
[32] *European Communities World Nuclear Directory* (ed. C.W.D. Wilson, Longman 1985).
[33] *NUPECC Handbook (International access to Nuclear Physics facilities in Europe)* (ed. C. Détraz, Strasbourg, 1990).
[34] *Physics through the 1990's, An overview*, (ed. Physics Survey Committee, National Research Council, W. Brinkman Chairman, National Academy Press Washington 1990), Summary, p. 5.